PART I.

MATERIAL TRANSFER IN TURBULENT GAS STREAMS

INFLUENCE OF SHAPE ON EVAPORATION OF DROPS OF *n*-HEPTANE

PART II.

THERMAL AND MATERIAL TRANSPORT FROM SPHERES

INTO A TURBULENTLY FLOWING AIR STREAM

PART III.

TEMPERATURE GRADIENTS IN TURBULENT GAS STREAMS

RECOVERY FACTORS IN STEADY, UNIFORM FLOW

Thesis by

Kazuhiko Sato

In Partial Fulfillment of the Requirements

For the Degree of

Doctor of Philosophy

California Institute of Technology

Pasadena, California

1955

ACKNOWLEDGEMENT

The constant encouragement and guidance of Dr. B. H. Sage, who served as technical advisor for the project, is gratefully acknowledged.

The operation of the apparatus described in this thesis would have been impossible without the untiring efforts of N. T. Hsu. The assistance of L. T. Carmichael, W. M. DeWitt, G. A. Griffith, H. E. Smith and H. H. Reamer has contributed to the progress of the program.

The author is indebted to Dr. W. N. Lacey and Dr. W. H. Corcoran for their helpful suggestions regarding the preparation of the thesis.

The assistance of A. Miller who typed the manuscript, and V. Berry who prepared many of the figures is appreciated.

ABSTRACT

I.

Measurements of the rate of evaporation of drops of varying shapes are required in order to determine the influence of such a variable on this important industrial transport process. Few data, if any, are available concerning the evaporation of drops of hydrocarbons.

Measurements were made of the evaporation of drops of n-heptane at air velocities from 2 to 8 feet per second, corresponding to Reynolds numbers as high as 200. The transport rate was established for drops under approximately 30 different conditions, and for each drop the shape, surface area, and volume were determined in detail. The measurements were made at an air temperature of 100° F. and at a low level of turbulence, with negligible radiant transfer to the drop. The temperature of the evaporating drop was measured with small thermocouples.

The results indicate a marked influence of the shape of the drop on its evaporating rate, and the Sherwood number was found to increase by as much as 30 percent for drops which deviate significantly from spherical forms. The present results, when reduced to the behavior of spheres, are in excellent agreement with the early measurements of Frossling and in fair agreement with those of Ranz and Marshall.

II.

An investigation was made on the effect of turbulence level on the thermal and material transport from spherical surfaces in a turbulently flowing air stream. A high level of turbulence was produced at the location of the test sphere by inserting a perforated plate in the flowing air stream.

Measurements were made of the rate of heat flow from a polished silver sphere, 0.500 inch in diameter, at air velocities from 4 to 32 feet per second. The measurements were made at a bulk air temperature of 100° F.

Measurements were made of the rate of evaporation of n-hexane and n-heptane from a porous sphere, 0.500 inch in diameter, at air velocities from 2 to 35 feet per second. The measurements were made at bulk air temperatures of 85° F., 100° F., and 115° F.

The results indicate that the turbulence level in the flowing air stream has a marked influence on the magnitude of the transfer coefficients. It was found that, in an air stream flowing at a bulk velocity of 16 feet per second with a turbulence level of 13 per cent, the Nusselt number increased by 11 per cent over the value obtained in the undisturbed air stream. The Sherwood number was found to increase by 14 per cent under the same flow condition.

The data obtained in this investigation were compared where possible with published information of similar nature.

III.

At high velocities the temperature variation across a flowing stream is appreciable under steady conditions for fluids having a high Prandtl number. A knowledge of such temperature distributions within steady, uniform streams is needed in certain thermal transport calculations. This information is not readily available in the literature.

By utilizing available information concerning the dissipation of kinetic energy and the thermal transport in laminar turbulently flowing streams, expressions were derived for the temperature distribution in fluids flowing between infinite parallel plates and in circular conduits. The calculations included both adiabatic and isothermal conditions at the wall.

These expressions differ somewhat from the relationships which have been derived for the temperature distribution in fluids flowing along a plate in an infinite stream under isobaric conditions. Recovery factors are directly proportional to the Prandtl number and not to the square root of the Prandtl number as found for the case of isobaric flow. Only the value of the Prandtl number is required in order to establish the temperature distribution under known conditions of laminar flow, whereas supplemental information is required in order to determine the behavior in turbulent flow.

TABLE OF CONTENTS

PART I.

MATERIAL TRANSFER IN TURBULENT GAS STREAMS

INFLUENCE OF SHAPE ON EVAPORATION OF DROPS OF n-HEPTANE

Effect of Shape on Evaporation of Drops

I&EC—May 1954

Measurements of the rate of evaporation of drops of varying shapes are required in order to determine the influence of such a variable on this important industrial transport process. Little, if any, data are available concerning the evaporation of drops of hydrocarbons.

Measurements were made of the evaporation of drops of *n*-heptane at air velocities from 2 to 8 feet per second, corresponding to Reynolds numbers as high as 200. The transport rate was established for drops under approximately 30 different conditions, and for each drop the shape, surface area, and volume were determined in detail. The measurements were made at an air temperature of 100° F. and at a low level of turbulence with negligible radiant transfer to the drop. The temperature of the evaporating drop was measured with small thermocouples.

The results indicate a marked influence of the shape of the drop on its evaporating rate, and the Sherwood number was found to increase by as much as 30% for drops which deviate significantly from spherical forms. The present results, when reduced to the behavior of spheres, are in excellent agreement with the early measurements of Frössling and in fair agreement with those of Ranz and Marshall.

MATERIAL TRANSFER IN TURBULENT GAS STREAMS

N. T. Hsu, K. Sato, and B. H. Sage.....870
California Institute of Technology, Pasadena, Calif.

Reprinted from **INDUSTRIAL AND ENGINEERING CHEMISTRY**, Vol. 46, Page 870, May 1954

Material Transfer in Turbulent Gas Streams

INFLUENCE OF SHAPE ON EVAPORATION OF DROPS OF *n*-HEPTANE

N. T. HSU, K. SATO, AND B. H. SAGE
California Institute of Technology, Pasadena, Calif.

LITTLE information is available concerning the effects of the shape of a drop or the level of turbulence of the approaching stream on the rate of evaporation from drops (*7*, *20*, *22*). Maisel and Sherwood (*22*) reviewed available data concerning the evaporation of drops in turbulent streams and presented some new information on material transfer from spheres. These results did not yield a simple analogy with available correlations of thermal transfer (*14*, *21*). Powell (*27*), Frössling (*6*, *7*), Ranz and Marshall (*28*), Takahashi (*39*), and Whitman (*40*) investigated the behavior of drops in turbulent air streams. Such data served as a limited basis for predicting material transfer from spherical drops (*35*). Since a more extensive review of the experimental background is available (*33*), no further discussion of earlier work is required.

As a result of the absence of data concerning the effect of the shape of the drop, an experimental investigation was made of drops of *n*-heptane for a number of configurations. Primary emphasis was placed on measurement of the rate of material transport rather than on the interrelation of thermal and material transfer. The experimental information obtained will, nevertheless, permit a limited comparison of the mechanism of the two transport processes to be made.

Measurements of the rate of evaporation of drops of *n*-heptane in an air jet at a free stream temperature of 100° F. were carried out for nominal velocities of 2, 4, 6, and 8 feet per second. At each air velocity measurements of the dimensions of the drop and its temperature were made for a series of different rates of evaporation. For each rate of evaporation and air velocity, the dimensions of three independently formed drops were established (*9*). These independent measurements on three different drops aided in establishing the reproducibility of the investigation.

The analysis of the evaporation of drops has been considered by many investigators. Hughes and Gilliland (*10*) reviewed the mechanics of drops. Langmuir (*18*) set forth the basic relationships for the evaporation of spherical drops into quiescent air, whereas Fuchs (*8*) extended the work to include the behavior of much smaller drops. Frössling (*6*) developed from established simple boundary layer theory that the weight rate of evaporation of a drop in a turbulent stream could be established.

$$\mathring{m}_k = 4\pi r_d D_{v,k}(\sigma_{k,i} - \sigma_{k,s})(1 + K\mathrm{Sc}^{1/3}\mathrm{Re}^{1/2}) \qquad (1)$$

Ingebo (*11*, *12*) followed Frössling's analysis and developed an empirical expression of the same general form. More recently, Ranz and Marshall (*28*) considered the evaporation of drops and confirmed the earlier work of Bedingfield and Drew (*1*) concerning the relative independence of the wet bulb temperature with respect to the Reynolds number of the flow around the drop. All earlier work appears to consider the gas phase as a perfect gas. A somewhat more complete review of the analysis of the evaporation of drops is available (*33*) which considers the gas phase to be an ideal solution. In order to take into account deviations from the perfect gas law, fugacity was considered as the potential. Under these circumstances the Maxwell hypothesis may be written for spherical coordinates in the following way (*33*):

$$f_k^\circ \left(\frac{\partial n_k}{\partial r}\right)_T + C_k \sigma_j \sigma_k u_k = f_i^\circ \left(\frac{\partial n_j}{\partial r}\right)_T - C_j \sigma_j \sigma_k u_k = 0 \qquad (2)$$

Equation 2 may be combined with the normal definition of the Maxwell diffusion coefficient to yield

$$\mathring{m}_k = \frac{ZD_{M,k}}{b_k T} \frac{f_k^\circ}{P} \left(\frac{\partial \ln n_j}{\partial r}\right)_T \qquad (3)$$

Equation 3 describes the weight rate of transport per unit area

from a sphere for the components of an ideal solution in accordance with the Maxwell hypothesis, with fugacity as a potential. Equation 3 does not take into account the effect of temperature gradients or other fields on the transport process (*17, 36, 37*). The Maxwell hypothesis yields expressions which are simpler to integrate than does the Fick diffusion coefficient when the hydrodynamic velocity resulting from the counterdiffusion of the stagnant component is taken into account. These matters have been discussed by Bedingfield and Drew (*1*) and reviewed recently (*25*). The integration of Equation 3 results in

$$\underline{\dot{m}}_k = -4\pi r_d \frac{D_{M,k}Z}{b_k T} \frac{f_k^\circ}{P} \ln (n_{j,i}/n_{j,s}) \qquad (4)$$

Equation 4 may be extended to other than stagnant conditions, following the analysis of Frössling, to give

$$\underline{\dot{m}}_k = -4\pi r_d \frac{D_{M,k}Z}{b_k T} \frac{f_k^\circ}{P} \ln \left(\frac{n_{j,i}}{n_{j,s}}\right) (1 + K\,\mathrm{Re}^\beta \mathrm{Sc}^{1/3}) \qquad (5)$$

Equation 5 is similar to the equations developed by Frössling (*6*) and Ranz and Marshall (*28*). It differs primarily in the use of a logarithmic expression to describe the effects of the composition differences and in the use of fugacity as the potential. Furthermore, the exponent of the Reynolds number has not been indicated as 0.5 since deviations from this value may be experienced at Reynolds numbers as low as 2. Rubesin (*31*) and Seban (*34*) indicate the thermal transport across a turbulent boundary layer should be proportional to $\mathrm{Re}^{0.8}$. For this reason, a gradual increase in the exponent may be expected with increasing Reynolds numbers (*33*).

Following methods which have been described (*33*), the Sherwood number may be established from the experimental measurements. If it is assumed that Equation 5 is applicable and that the shape of the drop may be described in terms of the sphericity and the height-diameter ratio, the Sherwood number may be established (*33*) from

$$\mathrm{Sh} = 2[1 + K\,\mathrm{Re}^\beta \mathrm{Sc}^{1/3}\phi_2(\zeta)]\phi_3(\lambda)\phi_4(h/d_d)$$

$$= \frac{-6\underline{\dot{m}}_k \alpha^2 b_k T}{V_d D_{M,k} Z (f_k^\circ/P) \ln (n_{j,i}/n_{j,s})} \underset{n_j \to 1}{\approx} \frac{6\underline{\dot{m}}_k \alpha^2 b_k T}{V_d D_{v,k}(p_{k,i} - p_{k,s})}$$

$$= \frac{-6\dot{m}_k^* \alpha b_k T}{D_{M,k} Z (f_k^\circ/P) \ln (n_{j,i}/n_{j,s})} \underset{n_j \to 1}{\approx} \frac{6\dot{m}_k^* \alpha b_k T}{D_{v,k}(p_{k,i} - p_{k,s})} \qquad (6)$$

In Equation 6 the linear dimension describing the size of the drop has been taken as the dimensional quantity, α. It is the purpose of the following experimental work to establish the effect of the shape of the drop on the value of the Sherwood number, thus determining ϕ_3 and ϕ_4 of Equation 6. The present measurements were all made at nearly a single level of turbulence so that the data do not shed any information on ϕ_2 of Equation 6. The exponent of the Reynolds number was established on the basis of the value which yielded the smallest standard error of estimate from the experimental data. The foregoing represents an abridged discussion of the interrelation of the factors influencing the rate of evaporation of drops. A more complete discussion of these matters is available (*25, 33*).

Experiments Are Based on Detailed Measurements of Drop Size and Shape and Transport Rate

In order to investigate the effect of the size and shape of drops on their rate of evaporation, a method of steady-state measurement was developed. In some respects, the approach was similar to that used by Ranz and Marshall (*28*) and Ingebo (*11, 12*). The drop was supported by means of a small glass tube, and the rate of introduction of the evaporating component necessary to maintain the drop at a given size in the flowing stream was determined for a variety of conditions. Details of the equipment employed, together with a critical analysis of the uncertainties of the measurements of the several variables, are available (*9*). In principle, it involved an injector which was driven at an accurately known rate (*29*) to supply *n*-heptane to the evaporating surface at the required rate. The drops were photographed with transmitted light using a high intensity mercury vapor lamp actuated by a condenser discharge, giving an exposure time of about 0.1 millisecond. Records were taken at a magnification of 4 on fine grain film, and the dimensions of the drops were determined with a probable error of 0.00013 inch.

A platinum-constantan thermocouple, 1 mil in diameter, was employed to measure the difference in temperature between the undisturbed air stream and the drop. It is believed that the temperature of the junction within the drop was known relative to that of the air stream with a probable error of not more than 0.1° F. Suitable corrections for the thermal conductivity of the platinum and constantan wire were made in interpreting the temperature of the interior of the drop in terms of the temperature of the thermocouple junction.

The air stream was supplied from a converging duct which produced nearly potential flow over a range of velocities from 2 to 20 feet per second. After a careful study of the fluctuating and steady-state characteristics of the air flow (*9*), it was found, for air speeds of 2 feet per second, that variations in temperature with time of as much as 0.09° F. were encountered. At the higher velocities the variations were relatively small.

The total volume and evaporating area of the drop were determined from measurements with a comparator and it was found (*9*) that the surface of a drop was known with a probable error of 0.3×10^{-6} square feet and the volume within 0.45×10^{-9} cubic feet. These quantities correspond to relative probable errors of 0.23 and 0.28%, respectively, as compared to the average area and volume of the drops. It was found (*9*) that the average standard deviation of the evaporation rate from the mean value for the groups investigated at a given velocity and evaporation rate was 0.83%, corresponding to a probable error of 0.097 in the Sherwood number. Table I records the variables of interest in determining the macroscopic behavior of evaporating drops, together with the ranges of variables encountered in the present investigation and the uncertainty associated with the measurement of each. These probable errors allow an estimation of the over-all accuracy if each of their effects on the transport process may be isolated. In the present instance the analyses of Frössling (*6*) and of Ranz and Marshall (*28*) were employed for this purpose.

n-Heptane Is Purified and Free Stream Properties Are Predicted from Physical Measurements

The *n*-heptane used in these studies was obtained from the Phillips Petroleum Co. and was reported to contain less than 0.01 mole fraction of material other than *n*-heptane. The material was subjected to fractionation in a glass column containing 16 plates at a pressure of approximately 4 pounds per square inch absolute. The fractionation was carried out a reflux ratio of approximately 40 to 1. Initial and final 10% fractions of the overhead were discarded. Portions of the partially purified *n*-heptane were passed through a column of activated alumina, approximately 7 feet in length, at ambient pressures and temperatures. The purified, air-free material exhibited a specific weight of 42.429 pounds per cubic foot at 77° F. and an index of refraction relative to the D-lines of sodium at 68° F. of 1.3877. These values may be compared with a specific weight of 42.417 pounds per cubic foot and an index of refraction of 1.384 reported by Rossini (*30*) for air-saturated *n*-heptane at the same state.

The absolute humidity, temperature, and pressure of the air stream were determined periodically so that the properties of the free stream could be predicted with accuracy. The physical properties of air were taken from a recent review (*26*) for the particular pressure and temperature of the jet. Suitable corrections

Table I. Experimental Results for Evaporation of Drops of *n*-Heptane

Specific gas constant of *n*-heptane = 15.4228 ft./° R.
Temperature of air stream = 100.0° F.
Compressibility factor of air = 0.9998
Kinematic viscosity of air = 1.8062×10^{-4} sq. ft./sec.
Maxwell diffusion constant for *n*-heptane = 0.1773 lb./sec.

	Air Stream			Drop							*n*-Heptane		
											Fugacity, lb./sq. ft.		
Drop No.	Pressure, lb./sq. ft. abs. P	Humidity, wt. fraction n	Velocity, ft./sec. u	Temp., ° F. t	Height, ft. $h \times 10^3$	Max. diam., ft. $d_d \times 10^3$	Surface area, sq. ft. $A \times 10^3$	Volume, cu. ft. $V \times 10^9$	Shape factor, ft. $\alpha \times 10^3$	Total transport rate, lb./sec. $\overset{\circ}{m}_k \times 10^6$	Gas $\overset{\circ}{f}_{k,g}$	Liquid $\overset{\circ}{f}_{k,l}$	Mole fraction $x_{j,i}$
24 A	2067.6	0.00625	3.899	64.15	5.140	5.855	0.0950	106.5	1.121	0.15378	1833.9	87.6	0.9523
25 A	2071.7	0.00540	3.939	64.33	4.232	5.359	0.0693	69.7	1.007	0.13220	1837.6	87.8	0.9522
26 A	2072.2	0.00540	3.951	62.33	6.690	5.570	0.1050	101.9	0.971	0.15378	1838.0	83.2	0.9548
27 A	2064.8	0.00498	3.878	65.12	6.334	6.545	0.1281	155.8	1.216	0.18377	1833.6	90.0	0.9509
28 A	2065.2	0.00611	3.884	66.07	4.325	5.306	0.0707	71.0	1.005	0.13220	1833.9	92.6	0.9495
30 A	2048.1	0.00242	5.935	61.88	9.448	6.642	0.1631	188.7	1.157	0.24301	1810.5	81.9	0.9548
31 A	2049.0	0.00228	5.949	61.92	10.202	6.937	0.1793	219.6	1.225	0.25976	1811.3	82.0	0.9547
32 A	2051.6	0.00271	5.967	61.63	7.378	6.174	0.1315	141.3	1.075	0.21525	1813.6	81.2	0.9552
32 B	2051.6	0.00271	5.957	61.63	7.522	6.227	0.1325	144.2	1.089	0.21525	1813.6	81.2	0.9552
32 C	2051.6	0.00271	5.967	61.63	7.611	6.338	0.1355	150.4	1.111	0.21525	1813.6	81.2	0.9552
34 A	2074.2	0.00313	6.008	63.16	4.962	5.788	0.0907	99.4	1.096	0.18377	1835.6	85.3	0.9536
36 A	2077.9	0.00413	6.022	62.73	5.522	6.177	0.1061	122.4	1.154	0.20362	1836.9	83.7	0.9544
37 A	2078.9	0.00398	6.027	63.27	9.009	7.016	0.1735	211.9	1.221	0.24301	1837.8	85.3	0.9536
38 A	2066.6	0.00498	2.054	63.60	7.404	5.971	0.1232	129.2	1.048	0.13220	1829.0	86.1	0.9529
39 A	2066.1	0.00441	2.059	62.65	8.414	6.470	0.1498	170.7	1.140	0.15378	1826.4	83.6	0.9542
39 B	2066.1	0.00441	2.059	62.65	8.390	6.450	0.1496	170.1	1.137	0.15378	1826.4	83.6	0.9542
39 C	2066.1	0.00441	2.059	62.65	8.352	6 537	0.1524	175.4	1.151	0.15378	1826.4	83.6	0.9542
40 A	2061.9	0.00610	2.050	65.14	7.493	5.999	0.1264	133.6	1.058	0.13220	1826.9	90.0	0.9507
41 A	2063.0	0.00596	2.055	63.70	8.880	6.652	0.1616	190.1	1.177	0.15378	1825.7	86.2	0.9528
42 A	2063.2	0.00596	2.059	65.35	5.307	5.810	0.0947	105.3	1.112	0.13220	1828.0	89.6	0.9510
43 A	2064.2	0.00596	2.060	65.00	6.575	6.536	0.1308	162.6	1.244	0.15378	1828.9	89.5	0.9510
44 A	2065.8	0.00596	2.044	62.66	10.037	7.159	0.1950	248.3	1.273	0.18377	1828.2	83.7	0.9542
45 A	2066.3	0.00582	2.044	65.32	5.714	6.143	0.1089	127.2	1.168	0.13220	1830.7	89.6	0.9511
46 A	2069.3	0.00596	2.046	64.78	6.624	6 600	0.1337	168.2	1 257	0.15378	1833.4	89.0	0.9515
47 A	2069.9	0.00596	2.049	64.35	7.980	7.215	0.1724	236.7	1.373	0.18377	1833.9	88 0	0.9520
48 A	2065.9	0.00568	8.007	62.26	7.339	6 316	0 1198	142.5	1.190	0.24301	1826.2	82.8	0.9547
49 A	2067.5	0.00483	8.041	62.22	8.451	6.804	0 1613	191.9	1.190	0.27899	1827.7	82.7	0.9548
50 A	2067.2	0.00483	8.051	62.20	6.201	7.218	0.1537	204.9	1.332	0.27899	1827.4	82.6	0.9548
50 B	2067.2	0.00483	8.051	62.20	6.872	7.078	0.1488	195.2	1 312	0.27899	1827.4	82.6	0.9548
50 C	2067.2	0.00483	8.051	62.20	6.874	7.149	0 1502	199.8	1.330	0.27899	1827.4	82.6	0.9548
51 A	2068.6	0.00526	8.072	62.64	5.998	6.526	0.1211	146.0	1.206	0.24301	1828.6	83.7	0.9542
55 A	2070.8	0.00681	8.071	64.26	6.824	7.104	0.1490	195.0	1.309	0.27899	1834.8	87.8	0.9522

for the effect of humidity were made by the methods described by Chapman and Cowling (*5*), using values of the viscosity for dry air previously discussed (*26*). Available information concerning the effects of humidity on the viscosity of air is contradictory (*23*, *38*), a fact which accounts for the need for recourse to the theoretical methods of Chapman and Cowling. The influence of composition on specific volume of the free stream was determined on the assumption of ideal solutions (*19*) and information concerning the specific weight of air (*13*, *15*) and gaseous water (*16*). Negligible excess quantities of carbon dioxide were found in the air stream, which was drawn through a filter of activated charcoal from outside the laboratory.

The thermodynamic properties of the gas phase adjacent to the interface of the drop were obtained by application of the Benedict equation of state (*3*) to the prediction of the specific volume and the fugacity of *n*-heptane. For present purposes the system was considered as binary. Coefficients for the Benedict equation for *n*-heptane were recently made available (*2*) and were employed (*32*). It is believed that the probable error in the prediction of the fugacity and the concentration of *n*-heptane was less than 1% for all the conditions covered in this investigation. The gas phase was assumed to be an ideal solution in the absence of experimental data as to its equilibrium volumetric behavior.

Sherwood Number Increases Substantially with Deviation from Spherical Drop Form

Experimental data obtained for the evaporation of drops of *n*-heptane under 26 different conditions are recorded in Table I. For nearly all of the conditions investigated the dimensions of three independently grown drops were measured, and the data recorded represent average values of the total volume and evaporating area of the drops. In three cases the characteristics of each of the three drops have been included in Table I. The shapes of the drops studied are shown in Figure 1. They vary from pendant contours with a large value of the height-diameter ratio to oblate spheroids with small values of this ratio. The drops depicted in Figure 1 are numbered and correspond to each of the conditions recorded in Table I. The detailed dimensions of each of the drops investigated are available (*32*).

From the information of Table I it is possible to compute the Sherwood number for each drop from the following expressions (*9*):

$$\mathrm{Sh} = \frac{6\alpha^2 \overset{\circ}{m}_k b_k T}{V_d Z D_{M,k} (f^\circ_k/P) \ln (n_{j,s}/n_{j,i})} = \frac{6 \overset{\circ}{m}^*_k \alpha b_k T}{D_{M,k} Z (f^\circ_k/P) \ln (n_{j,s}/n_{j,i})} \tag{7}$$

$$\mathrm{Sh} = \frac{6\alpha^2 \overset{\circ}{m}_k b_k T}{V_d D_{v,k} (p_{k,i} - p_{k,s})} = \frac{6 \overset{\circ}{m}^*_k \alpha b_k T}{D_{v,k} (p_{k,i} - p_{k,s})} \tag{8}$$

Equation 7 applies to an ideal solution, whereas Equation 8 as-

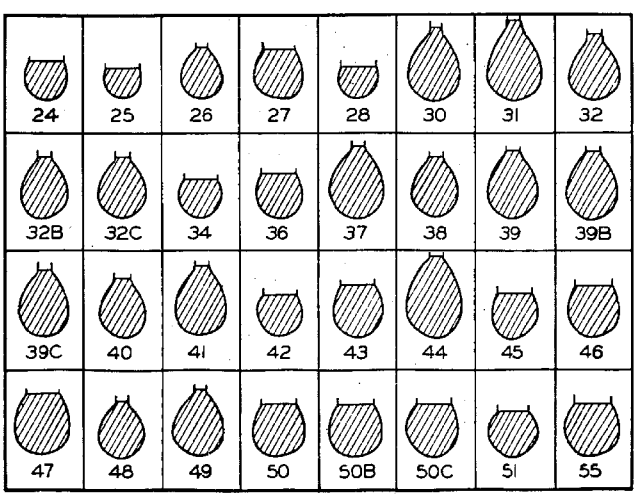

Figure 1. Shape of Drops

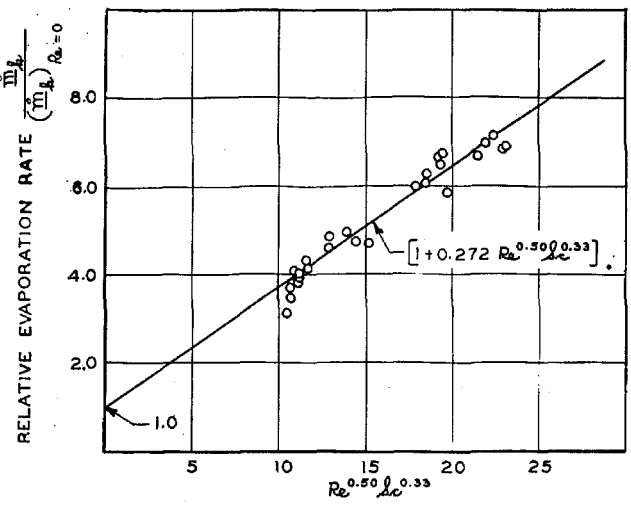

Figure 2. Effect of Reynolds Number on Evaporation Rate

sumes the equation of state to be that of a perfect gas. Values of the Reynolds number were computed and are recorded in Table II. The Reynolds number was defined from the following equations:

$$Re_\alpha = \frac{6\alpha(u_d - u_s)}{\nu_s} = \frac{6\alpha U}{\nu_s} = \frac{6_d VU}{A_d \nu_s} \quad (9)$$

$$Re = \frac{d_d(u_d - u_s)}{\nu_s} = \frac{d_d U}{\nu_s} \quad (10)$$

In the case of Equation 9 this number utilized a linear dimension, α, which was the ratio of the volume to the area of the drop. The same number, when defined by Equation 10, is based on the maximum linear dimension normal to the direction of flow. Equations 9 and 10 yield identical values of the Reynolds numbers for spheres. The kinematic viscosity of the free stream was employed in Equations 9 and 10 in order to establish the Reynolds number used in the correlation, and it appears to be satisfactory. For possible interest the Reynolds number based on Equation 9 was included in part of Table II. Macroscopic treatments suffer from the lack of uniformity in the Reynolds number and other dimensionless quantities throughout the region of transport.

The Schmidt number was established from the following expression:

$$Sc = \frac{\nu}{D_{F,k}} \approx \frac{\nu_s}{D_{v,k}} = \frac{\nu_s P}{D_{M,k}} \quad (11)$$

The kinematic viscosity of the free stream also was employed in Equation 11. Much of the transport resistance occurred in conditions where the kinematic viscosity was somewhat different from this value, but the behavior of the drop can be described satisfactorily from the properties of the free stream. In evaluating the Reynolds and Schmidt numbers reported in Table II the properties of air were taken from a recent critical review (*26*).

Assuming local equilibrium, the Reynolds and Schmidt numbers for the conditions existing at the interface were computed. The viscosity of the gaseous mixture at the interface was estimated from that of the components by the methods outlined by Chapman and Cowling (*5*). The uncertainty in the viscosity of *n*-heptane in the gas phase made the corresponding values of the Reynolds and Schmidt numbers for conditions at the interface sufficiently uncertain as to render the values based on the free stream properties preferable.

Table II records the Sherwood, Reynolds, and Schmidt numbers, together with the sphericity and the ratio of height to diameter for each of the drops investigated. From these data it is possible to prepare simple semiempirical correlations for the rate of evaporation of drops in a turbulent stream with particular emphasis on the effect of shape for conditions of a low level of turbulence.

Measurements of the level of turbulence in the jet were made (*9*) and indicated that the flow was nearly potential, with the root mean square of the fluctuating velocities only 1.3% of the gross stream velocity. The level of turbulence did not change significantly with the gross velocity. On the assumption of a constant level of turbulence, it appears feasible to correlate the Sherwood number with the characteristics of the stream and the shape of the drop on the basis of the following expression (*7*):

$$Sh = 2[1 + K_{Re}Re\beta Sc^{1/3}][1 + K\lambda(1 - \lambda)][1 - K_{h/d}(1 - h/d_d)] \quad (12)$$

Equation 12 assumes that the Sherwood number is a linear function of the sphericity and of the height-diameter ratio. The effect of the Reynolds and Schmidt numbers is of the same functional form as was proposed by Frössling (*7*). Equation 12 is sufficiently complex that it was desirable to employ statistical methods (*4, 24*) in order to predict the three coefficients from the experimental data. The application of such techniques to the data of Table II results in the following empirical expression if the exponent of the Reynolds number is taken as 0.5:

$$Sh = 2[1 + 0.272Re^{0.50}Sc^{0.33}][1 + 1.147(1 - \lambda)][1 - 0.371\ (1 - h/d_d)] \quad (13)$$

The effect of the quantity, $Re^{0.50}Sc^{0.33}$, on the evaporation rate is shown in Figure 2. Equation 13 yielded a standard error of estimate, with respect to the experimental data, of 4.87% in the Sherwood number. The linear terms of Equation 13 did not describe the effect of sphericity and of the height-diameter ratio on the evaporation rate in detail but were a first approximation.

The effect of Reynolds number as indicated in Equation 13 was based on the assumption of a laminar boundary layer (*7*). It is to be expected that the distribution of the thickness of the boundary layer will change with velocity, and a slightly higher exponent than 0.5 should yield a more accurate description of the experimental data in this range of Reynolds numbers. Using an exponent of 0.6 in Equation 12 and the same statistical methods (*4, 24*) the following expression was obtained:

$$Sh = 2[1 + 0.136Re^{0.60}Sc^{0.33}][1 + 2.913(1 - \lambda)][1 - 0.185\ (1 - h/d_d)] \quad (14)$$

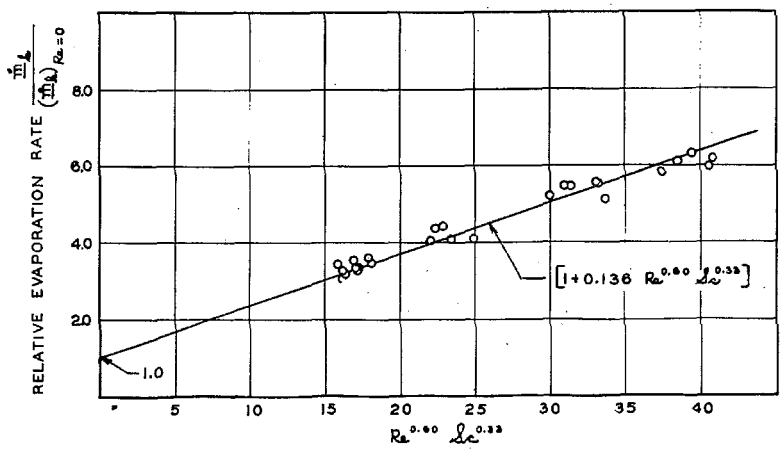

Figure 3. Behavior with Modified Reynolds Number Function

Table II. Evaporation Rate for Drops of *n*-Heptane

Drop No.	Drop: Height-diameter ratio, $\frac{h}{d_d}$	Drop: Sphericity, λ	Flow Conditions: Re[a]	Sc	$Re^{0.56}Sc^{0.33}$	$Re^{0.56}Sc^{0.33}$	$Re^{0.56}Sc^{0.33}$	Re[b]	Sherwood Number: Exptl. Drop	Exptl. Sphere[c]	Calcd. Drop
24 A	0.878	0.872	126.6	2.107	14.43	19.29	23.41	145.14	11.43	8.57	10.63
25 A	0.790	0.887	116.8	2.111	13.94	18.45	22.30	131.76	12.12	9.13	10.44
26 A	1.201	0.961	122.4	2.111	12.91	18.94	22.96	127.42	9.46	9.16	8.45
27 A	0.968	0.896	140.4	2.104	15.18	20.45	24.89	156.65	10.69	8.56	10.51
28 A	0.815	0.884	114.6	2.104	12.90	18.23	22.04	137.30	11.20	8.44	10.28
30 A	1.422	0.960	227.9	2.087	19.29	26.72	33.20	228.04	11.47	11.78	10.16
31 A	1.471	0.944	228.5	2.088	19.32	26.76	33.26	242.04	11.80	11.90	10.12
32 A	1.196	0.958	204.0	2.090	18.26	25.12	31.08	213.04	11.89	11.35	10 64
32 B	1.208	0.953	205.7	2.090	18.34	25.24	31.25	215.77	11.86	11.35	10.68
32 C	1.201	0.951	209.4	2.090	18.50	25.49	31.57	220.14	11.83	11.25	10.82
34 A	0.857	0.881	192.6	2.113	17.82	24.42	30.14	218.71	14.40	10.91	12.80
36 A	0.894	0.892	206.0	2.117	18.43	25.37	31.39	230.81	14.64	11.43	12.88
37 A	1.284	0.955	233.4	2.118	19.62	27.21	33.85	244.48	11.00	10.75	11.00
38 A	1.240	0.950	68.0	2.106	10.57	13.60	16.11	71.53	7.20	6.88	13.18
39 A	1.299	0.946	73.8	2.105	11.01	14.24	16.92	77.95	7.70	7.42	6.68
39 B	1.301	0.945	73.5	2.105	10.99	14.22	16.89	77.77	7.70	7.42	6.67
39 C	1.278	0.948	74.5	2.105	11.06	14.33	17.02	78.71	7 64	7.33	6.76
40 A	1.249	0.943	67.9	2.101	10.55	13.59	16.09	72.02	6.77	6.39	6.62
41 A	1.335	0.943	75.7	2.102	11.15	14.45	17.18	80.32	7.15	6.19	6.67
42 A	0.914	0.871	66.2	2.102	10.43	13.41	15.86	76.07	9.57	7.22	8.03
43 A	1.006	0.878	74.7	2.103	11.07	14.35	17.05	85.09	9.01	7.05	8.09
44 A	1.402	0.937	81.0	2.105	11.52	15.01	17.90	86.46	7.89	7.68	6.70
45 A	0.930	0.875	69.4	2.105	10.67	13.77	16.31	79.30	8.76	6.69	7.91
46 A	1.004	0.876	74.9	2.108	11.10	14.38	17.08	85.46	8.98	7.02	8.10
47 A	1.106	0.876	81.8	2.109	11.60	15.11	18.02	93.45	9.19	7.35	8.10
48 A	1.162	0.884	279.7	2.105	21.43	30.05	37.65	316.50	16.04	12.16	15.25
49 A	1.242	0.953	302.8	2.106	22.30	31.43	39.49	317.80	13.70	13.19	12.65
50 A	0.859	0.903	321.7	2.106	22.99	32.51	40.92	351.60	16.10	12.76	15.87
50 B	0.971	0.899	315.5	2.106	22.77	32.15	40.48	350.82	16.39	13.19	15.18
50 C	0.962	0.896	318.7	2.106	22.88	32.34	40.72	355.84	16.50	13.18	15.35
51 A	0.919	0.901	291.5	2.108	21.89	30.77	38.61	323.36	15.93	12.73	14.85
55 A	0.961	0.903	316.9	2.117	22.86	32.29	40.65	351.04	15.44	12.50	15.22

[a] Equation 4.
[b] Equation 3, not used in correlation.
[c] Calculated for sphere of same diameter from data for drop.

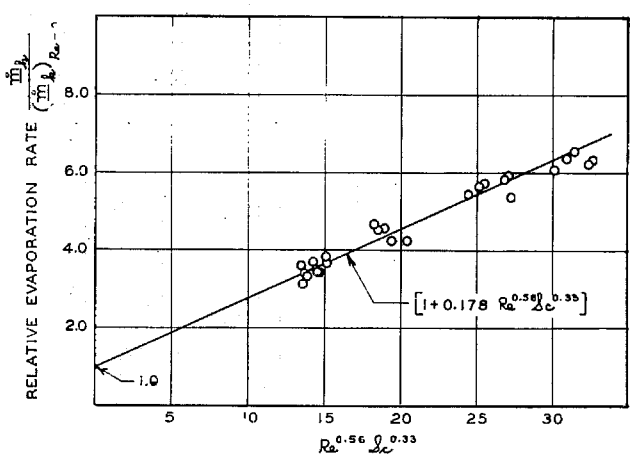

Figure 4. Behavior with Modified Reynolds Number Function

The experimental data represented as a linear function of the quantity, $Re^{0.60}\,Sc^{0.33}$, are shown in Figure 3. As in Figure 2, the data are expressed in terms of the evaporation rate compared to that under stagnant conditions. The relative standard error of estimate in the Sherwood number from Equation 14 was 4.61%.

By a trial-and-error procedure it was found that an exponent of 0.56 yielded a minimum standard error of estimate in the Sherwood number of 4.36%. Under these circumstances Equation 12 assumes the form

$$h = 2[1 + 0.178Re^{0.56}Sc^{0.33}][1 + 2.292(1 - \lambda)][1 - 0.257\,(1 - h/d_d)] \quad (15)$$

The relative evaporation rate as a function of the variable, $Re^{0.56}\,Sc^{0.33}$, is shown in Figure 4. The data of Figures 2, 3, and 4 were obtained by establishing from Equations 13, 14, and 15 the Sherwood number under quiescent conditions for each of the drops. The ratio of the experimental to the calculated Sherwood number is given in the ordinate for each of these figures.

Results Indicate Marked Influence of Shape of Drop on Evaporation Rate

As a result of the smaller deviation of Equation 15 from the experimental data it has been employed in all subsequent correlations except in connection with direct comparison with the measurements of Ranz and Marshall (*28*) and Frössling (*7*). The influence of sphericity on the evaporation rate is shown in Figure 5. The information presented in this figure was computed by application of Equation 16 to the experimental data.

$$\frac{\dot{m}_k}{(\dot{m}_k)_{\lambda=1}} = \left[\frac{Sh_e}{Sh_{\lambda=1}}\right] = \frac{Sh_e}{2[1 + 0.178Re^{0.56}Sc^{0.33}][1 - 0.257(1 - h/d_d)]} \quad (16)$$

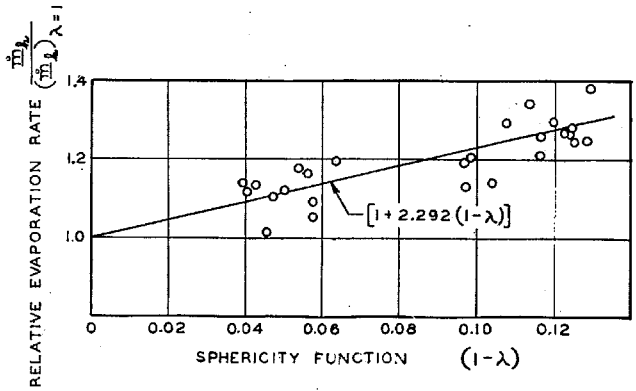

Figure 5. Effect of Sphericity on Evaporation Rate

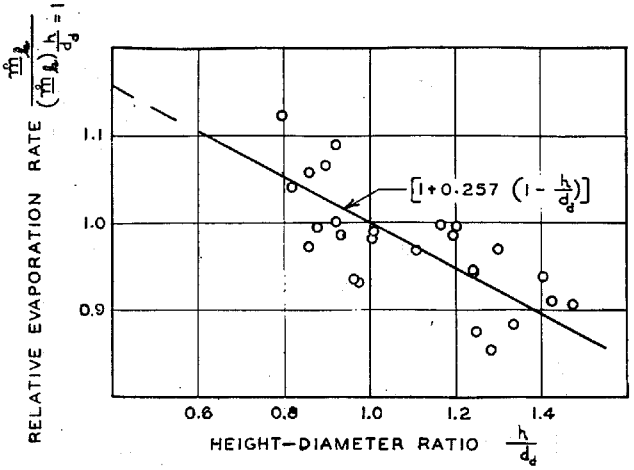

Figure 6. Effect of Shape of Drop on Evaporation Rate

The evaporation rate as measured by the Sherwood number increases rapidly with deviations from a sphere. The effect of the height-diameter ratio on the relative evaporation rate is shown in Figure 6. The oblate spheroids yield higher evaporation rates than the pendant drops. The data of Figure 6 were obtained by application of the following expression to the experimental values of the Sherwood number:

$$\frac{\dot{m}_k}{(\dot{m}_k)_{h/d_d=1}} = \left[\frac{\mathrm{Sh}_e}{\mathrm{Sh}_{h/d_d=1}}\right] = \frac{\mathrm{Sh}_e}{2[1+0.178\mathrm{Re}^{0.56}\mathrm{Sc}^{0.33}][1+2.292(1-\lambda)]} \quad (17)$$

It is emphasized that Figures 5 and 6 only attempt to segregate the variables in accordance with the empirical relationships set forth in Equation 15. For this reason they should be considered as empirically defined trends rather than as descriptions of the actual influences of the height-diameter ratio and sphericity on the evaporation rates.

A comparison of the present data, reduced to an equivalent sphere by Equation 13, with the measurements of Ranz and Marshall (*28*) and Frössling (*7*) is shown in Figure 7. The Ranz and Marshall data give a slightly higher value of the Sherwood number than was found in the present investigation, whereas Frössling's and the authors' data are similar. No information was reported by Frössling or Ranz and Marshall as to the shape of their drops. Some deviations from sphericity undoubtedly were experienced, and such behavior would tend to increase the Sherwood number, as indicated by Equation 15. Measurements of the level of turbulence of the gas stream were not reported by either Frössling or Ranz and Marshall. Since the present investigation was carried out under conditions of nearly potential flow, it is not surprising that some differences between the several sets of measurements occurred.

Many investigators have compared the material and thermal transport associated with the evaporation of drops. Ranz and Marshall (*28*) found a close similarity between the Nusselt and Sherwood numbers which was confirmed for small flux rates by Bedingfield and Drew (*1*). As was indicated in the description of the equipment (*9*), relatively large injection tubes were used to support the drops. For this reason the thermal transport along the tube to the drop was significant. The general energy equation for steady conditions describing the energy transport in the injection tube may be expressed as

$$(A_t k_t + A_k k_{k,l})\frac{d^2T}{dy^2} + (A_k C_{p,k,l}\sigma_{k,l}U_y)\frac{dT}{dy} + \pi d_t h'(T_s - T) = 0 \quad (18)$$

This differential equation may be solved to yield an expression of the following form:

$$T = T_s - (T_s - T_d)e^{-xy} \quad (19)$$

The coefficient, χ, of the exponent may be established from

$$x = \frac{1}{2}\left\{\frac{A_k C_{p,k,l}\sigma_{k,l}U_y}{(A_t k_t + A_k k_{k,l})} + \sqrt{\left(\frac{A_k C_{p,k,l}\sigma_{k,l}U_y}{A_t k_t + A_k k_{k,l}}\right)^2 + \frac{4\pi d_t h'}{A_t k_t + A_k k_{k,l}}}\right\} \quad (20)$$

Evaluation of Equation 20 indicates that the thermal flux through the injection tube and the differences in the enthalpy of the liquid entering the drop from that in the drop varied from 13.2 to 13.8% of the total thermal transport from the drop. For this reason it is to be expected that the temperature of the liquid would be influenced by the Reynolds number and by the shape of the drop to such an extent as to render correlation of the thermal transport measurements unprofitable. It was found that within the uncertainty with which the thermal transport could be predicted the Nusselt number was similar to the Sherwood number. The effect of the presence of the drop on the convective thermal transfer to the injection tube could not be evaluated conveniently. For this reason the uncertainty in the prediction of the thermal flux across the evaporating surface was of the order of 3%, making detailed evaluation of the behavior of little value. Sufficient information is recorded in Table I to permit the Nusselt number to be calculated if the corrections for the energy transfer by the injection tube to the drop were made with sufficient accuracy.

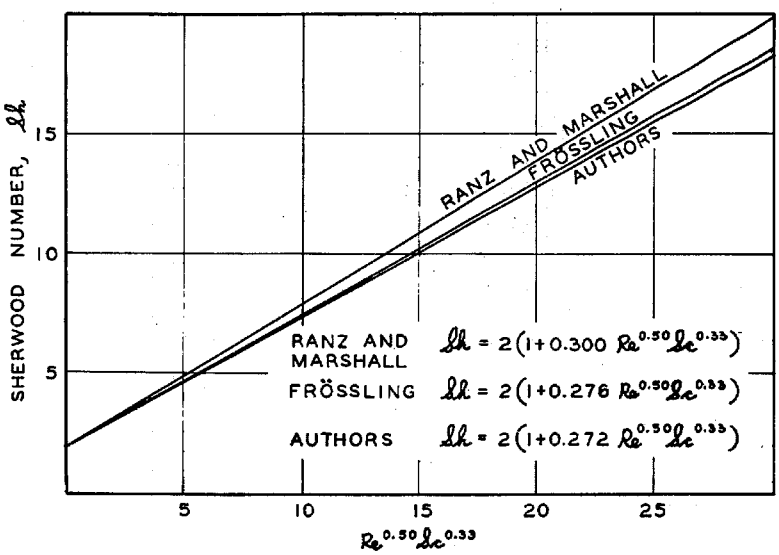

Figure 7. Comparison of Results with Other Investigators

Acknowledgment

Nan-Teh Hsu was a Peter E. Fluor Fellow, and the authors wish to express their appreciation to the Fluor Corp. for contributing financial support to this program. Betty Kendall assisted with the measurement of the dimensions of the drop and with the preparation of the data in a form suitable for publication.

Elizabeth McLaughlin and John Opfell contributed to the preparation of the manuscript and W. H. Corcoran reviewed it.

Nomenclature

A = area, sq. ft.
b_k = specific gas constant of component k, ft./° R.
C_p = isobaric heat capacity, B.t.u./(lb.)(° F.), ft./° F.
C_k = Maxwell coefficient of component k, (lb.) (sec.) (sq. ft.)/mole²
d = differential operator
d_d = maximum diameter of horizontal trace of drop, ft.
d_t = outside diameter of injection tube, ft.
$D_{F,k}$ = Fick diffusion coefficient of component k, sq. ft./sec.
$D_{M,k}$ = Maxwell diffusion coefficient of component k, lb./sec.
$D_{v,k}$ = volumetric diffusion coefficient of component k, $D_{M,k}/P$; $D_{F,k}(n_k/\dot{n}_k)$, sq. ft./sec.
e = base of natural logarithm
f_k° = fugacity of pure component k, lb./sq. ft.
h = height of drop, ft.
h' = local thermal transfer coefficient, B.t.u./(sec.) (sq. ft.) (° F.)
k_k = thermal conductivity of component k, B.t.u./(sec.) (sq. ft.) (° R./ft.)
K = constant of proportionality
l = characteristic length, ft.
ln = natural logarithm
m_c = material transfer coefficient, ft./sec.
$\dot{m}_k$ = transport rate of component k, lb./(sq. ft.) (sec.)
$\dot{m}_k^*$ = average weight rate of transport of component k, lb./-(sec.) (sq. ft.)
$\dot{m}_k$ = total transport rate of component k, lb./sec.
n_k = weight fraction of component k
n_k = mole fraction of component k
P = pressure, lb./sq. ft. abs.
p_k = partial pressure of component k, (Pn_k), lb./sq. ft.
r = radius, ft.
r_d = radius of horizontal trace of drop, ft.
Re = Reynolds number based on maximum diameter of drop
Re_α = Reynolds number based on shape factor
Sc = Schmidt number, $\nu_s/D_{F,k} \approx P\nu_s/D_{M,k}$
Sh = Sherwood number, $m_c l P/D_{M,k}$
t = temperature, ° F.
T = thermodynamic temperature, ° R.
u = local velocity, ft./sec.
u_k = transport velocity of component k, ft./sec.
U = relative velocity of stream and drop, ft./sec.
U_y = average velocity in y direction, ft./sec.
V = total volume, cu. ft.
y = vertical distance, ft.
Z = compressibility factor
α = shape factor, V_d/A_d, ft.
ζ = level of turbulence
λ = sphericity, $\dfrac{\alpha}{\alpha_o} = \dfrac{6V_d}{A_d d_d}$
ν = kinematic viscosity, sq. ft./sec.
σ_k = concentration of component k, lb./cu. ft.
ς_k = concentration of component k, mole/cu. ft.
$\phi_i(\ )$ = special functions of
χ = dimensional quantity (Equations 19 and 20), 1/ft.
∂ = partial differential operator

Superscripts

* = average value of
β = constant exponent

Subscripts

d = drop
e = experimental
g = gas phase
$\frac{h}{d}$ = height-diameter coefficient
i = interface
j = component in stream
k = diffusing component
l = liquid phase
o = sphere
Re = Reynolds number coefficient
s = free stream, at a distance from the drop
t = injection tube
λ = sphericity coefficient

Literature Cited

(1) Bedingfield, C. H., Jr., and Drew, T. B., IND. ENG. CHEM., **42**, 1164 (1950).
(2) Benedict, M., Webb, G. B., and Rubin, L. C., *Chem. Eng. Progr.*, **47**, 419 (1951).
(3) Benedict, M., Webb, G. B., and Rubin, L. C., *J. Chem. Phys.*, **8**, 334 (1940).
(4) Brough, H. W., Schlinger, W. G., and Sage, B. H., IND. ENG CHEM., **43**, 2442 (1951).
(5) Chapman, S., and Cowling, T. G., "Mathematical Theory of Non-uniform Gases," Cambridge, University Press, 1939.
(6) Frössling, N., *Gerlands Beitr. Geophys.*, **51**, 167 (1937).
(7) *Ibid.*, **52**, 170 (1938).
(8) Fuchs, N., *Physik. Z. Sowjetunion*, **6**, 234 (1934).
(9) Hsu, N. T., Reamer, H. H., and Sage, B. H., Am. Doc. Inst., Washington 25, D. C., *Doc.* **4219** (1954).
(10) Hughes, R. R., and Gilliland, E. R., *Chem. Eng. Progr.*, **48**, 497 (1952).
(11) Ingebo, R. D., Nat. Advisory Comm. Aeronaut., *Tech. Note* **2368** (1951).
(12) *Ibid.*, **2850** (1953).
(13) International Critical Tables, **III**, 3 (1928).
(14) Johnstone, H. F., Pigford, R. L., and Chapin, J. H., *Trans. Am. Inst. Chem. Engrs.*, **37**, 95 (1941).
(15) Keenan, J. H., and Kay, J., "Thermodynamic Properties of Air," New York, John Wiley & Sons, 1936.
(16) Keenan, J. H., and Keyes, F. G., "Thermodynamic Properties of Steam," New York, John Wiley & Sons, 1936.
(17) Kirkwood, J. G., and Crawford, B., Jr., *J. Phys. Chem.*, 56, 1048 (1952).
(18) Langmuir, I., *Phys. Rev.*, **12**, 368 (1918).
(19) Lewis, G. N., *J. Am. Chem. Soc.*, **30**, 668 (1908).
(20) Linton, W. H., Jr., and Sherwood, T. K., *Chem. Eng. Progr.* **46**, 258 (1950).
(21) McAdams, W. H., "Heat Transmission," New York, McGraw-Hill Book Co., 1942.
(22) Maisel, B. S., and Sherwood, T. K., *Chem. Eng. Progr.*, 46, 131 (1950).
(23) Millikan, R. A., *Phil. Mag.*, [6] **19**, 209 (1910).
(24) Milne, W. H., "Numerical Calculus," Princeton, Princeton University Press, 1949.
(25) Opfell, J. B., and Sage, B. H., "Some Relations in Materia Transport," *Chem. Revs.*, to be published.
(26) Page, F., Jr., Corcoran, W. H., Schlinger, W. G., and Sagel B. H., IND. ENG. CHEM., **44**, 419 (1952).
(27) Powell, R. W., *Trans. Inst. Chem. Engrs.* (*London*), **18**, 36 (1940).
(28) Ranz, W. E., and Marshall, W. R., Jr., *Chem. Eng. Progr.* **48**, 141, 173 (1952).
(29) Reamer, H H., and Sage, B. H., *Rev. Sci. Instr.*, **24**, 362 (1953).
(30) Rossini, F. D., "Selected Values of Properties of Hydrocarbons," Natl. Bur. of Standards, Washington, D. C., November, 1947.
(31) Rubesin, M W., presented at the annual meeting, Am. Soc. Mech. Engrs., New York, *Paper* **48-A-43** (1948).
(32) Sato, K., Hsu, N. T., Reamer, H. H., and Sage, B. H., Am. Doc Inst., Washington 25, D. C., *Doc.* 4220 (1954).
(33) Schlinger, W. G., and Sage, B. H , Am. Doc. Inst., Washington 25, D. C., *Doc.* **4221** (1954).
(34) Seban, R. A , and Shimazaki, T. T., *Trans. Am. Soc. Mech. Engrs.*, **73**, 803 (1951).
(35) Sherwood, T. K., and Pigford, R. L., "Absorption and Extraction," New York, McGraw-Hill Book Co., 1952.
(36) Soret, C., *Arch. sci. phys. et nat.*, **2**, 48 (1879).
(37) *Ibid.*, **4**, 209 (1880).
(38) Stearns, J. C., *Phys. Rev.*, **27**, 116 (1926).
(39) Takahashi, I., *J. Met. Soc.* (*Japan*), **13**, 302 (1935).
(40) Whitman, W. J., *et al.* IND. ENG. CHEM., **18**, 363 (1926).

RECEIVED for review September 21, 1953. ACCEPTED January 18, 1954. Material supplementary to this article has been deposited as Document No. 4219, 4220, and 4221 with the ADI Auxiliary Publications Project, Photoduplication Service, Library of Congress, Washington 25, D. C. A copy may be secured by citing the document number and by remitting $3.75, $2.50, and $3.75, respectively, for photoprints or $2.00, $1.75, and $2.00, respectively, for 35-mm. microfilm. Advance payment is required. Make checks or money orders payable to Chief, Photoduplication Service, Library of Congress.

PART II.

THERMAL AND MATERIAL TRANSPORT FROM SPHERES INTO A TURBULENTLY FLOWING AIR STREAM

INTRODUCTION

Information, concerning evaporation rates from spherical surfaces and associated phenomena, is of importance in chemical engineering operations. Knowledge of the factors affecting the rate of heat and mass transfer from spherical surfaces will aid materially in the design of chemical engineering equipment. The operations of spray drying, spray absorption, and combustion of liquid droplets are merely a few examples in which information concerning factors of heat and mass transfer can be fruitfully employed.

Thermal transfer from heated spheres has been studied in detail and empirical and analytical expressions which describe the experimental data adequately are presented by McAdams (15) and Jakob (11). However detailed information relating the effect of turbulence level in the fluid stream to the convective heat transfer from heated spheres is meager. In order to investigate more fully the effect of turbulence on the heat transfer from heated spheres, the experimental studies described in this thesis were made.

The experimental data on the evaporation from spherical surfaces are few in comparison to the available heat transfer data. Investigations by Morse (17) on the sublimation of iodine beads led Langmuir (14) to develop the following expression describing the evaporation of small drops into

stagnant air:*

$$\dot{\underline{m}}_k = 2\pi d_s \frac{D_{v,k} M_k}{RT} \left(p_{k,ss} - p_{k,a}\right)$$

$$= 4\pi r_s D_{v,k} \left(\sigma_{k,g,ss} - \sigma_{k,g,a}\right) \qquad (1)$$

This relation is applicable only to situations in which the concentration of the diffusing component is exceedingly low. Experimental data obtained by Bradley et al. (3) on the evaporation of droplets of low volatility confirmed the validity of the Langmuir equation for the evaporation rate when material transfer is the predominant factor.

The evaporation of drops in a flowing stream was treated theoretically and experimentally by Frössling (8). From laminar boundary layer theory, Frossling established that the weight rate of evaporation from a spherical drop is related to the flow conditions in the following way:

$$\dot{\underline{m}}_k = 4\pi r_s D_{v,k} \left(\sigma_{k,g,ss} - \sigma_{k,g,a}\right)\left(1 + K Sc^{1/3} Re^{1/2}\right) \qquad (2)$$

where

$$\text{Schmidt number} = Sc = \frac{\nu}{D_{F,k}} \approx \frac{\nu}{D_{v,k}} = \frac{\nu P}{D_{m,k}} \qquad (3)$$

$$\text{Reynolds number} = Re = \frac{d_s U_a}{\nu} \qquad (4)$$

---

* The table of nomenclature on page 44 defines the symbols employed herein.

Ingebo (10) studied the rate of evaporation of liquids from saturated cork surfaces under flow conditions at low levels of turbulence. The evaporation of water and benzene drops into an air stream with a low level of turbulence has been measured by Ranz and Marshall (19). The experimental data obtained were expressed in terms of dimensionless parameters for thermal and material transfer by the following expressions:

$$\text{Nusselt number} = Nu = \frac{\mathring{Q}\, d_s}{k_j\,(t_a - t_{ss})} = 2\left(1 + 0.30\, Re^{\frac{1}{2}} Sc^{\frac{1}{3}}\right) \quad (5)$$

$$\text{Sherwood number} = Sh = \frac{\mathring{m}_k\, d_s\, M_j\, p_j}{M_k\, D_{v,k}\, \sigma_j\,(p_{k,ss} - p_{k,a})} = 2\left(1 + 0.30 Re^{\frac{1}{2}} Sc^{\frac{1}{3}}\right) \quad (6)$$

Equations 5 and 6 were based on the analysis for the evaporation rate from spherical surfaces through a laminar boundary layer.

The present investigation was conducted with the primary emphasis on correlating the effect of turbulence level on the over-all rates of material transfer and the associated phenomena.

All of the earlier work on the evaporation of drops appears to neglect the effect of the concentration of the diffusing component in the gas phase and to consider the gas phase as a perfect gas. In order to take into account the deviation of the gas phase from the perfect gas law, the utilization of the fugacity gradient as the driving force for

diffusion has been considered. A detailed analysis of the evaporation of drops which considers the gas phase to be an ideal solution is available (24). It appears worth while to present a brief derivation of the equation relating the rate of evaporation from a spherical surface employing the concepts of the fugacity gradient and ideal solutions.

Utilizing fugacity as a potential, the Maxwell hypothesis (16) can be expressed in the following manner:

$$\frac{\partial f_k}{\partial r} + C_k \sigma_{\circ j} \sigma_{\circ k} u_k = 0 \qquad (7)$$

$$\frac{\partial f_j}{\partial r} - C_j \sigma_{\circ j} \sigma_{\circ k} u_k = 0 \qquad (8)$$

The molal concentration of the components may be expressed as

$$\sigma_{\circ k} = \eta_{\circ k} \frac{P}{\mathcal{Z} R T} = (1 - \eta_{\circ j}) \frac{P}{\mathcal{Z} R T} \qquad (9)$$

$$\sigma_{\circ j} = \eta_{\circ j} \frac{P}{\mathcal{Z} R T} = (1 - \eta_{\circ k}) \frac{P}{\mathcal{Z} R T} \qquad (10)$$

Assuming that the gas phase surrounding the spherical surface is an ideal solution, Equation 7 can be restated as

$$f_k^{\circ} \left(\frac{\partial \eta_k}{\partial r}\right)_T + C_k \sigma_{\circ j} \sigma_{\circ k} u_k = 0 \qquad (11)$$

The molal rate of transfer per unit area can be expressed in terms of Equation 11 as follows:

$$\mathring{m}_{\circ k} = \sigma_{\circ k} u_k = - \frac{f_k^{\circ} \left(\frac{\partial \eta_{\circ k}}{\partial r} \right)_T}{C_k \sigma_{\circ j}} \tag{12}$$

Differentiating Equation 9 with respect to the radial distance,

$$\left(\frac{\partial \sigma_{\circ k}}{\partial r} \right)_T = \left(\frac{\partial \eta_{\circ k}}{\partial r} \right)_T \frac{P}{\mathcal{Z} R T} \tag{13}$$

A combination of Equations 10, 12, and 13 results in the relation,

$$\mathring{m}_{\circ k} = - \left(\frac{f_k^{\circ}}{P} \right) \left(\frac{\partial \sigma_{\circ k}}{\partial r} \right)_T \frac{\mathcal{Z}^2 R^2 T^2}{P C_k (1 - \eta_{\circ k})} \tag{14}$$

It may be combined with the Maxwell diffusion coefficient

$$D_{M,k} = \frac{R^2 T^2}{C_k} \tag{15}$$

to yield the following expression:

$$\mathring{m}_{\circ k} = - \left(\frac{f_k^{\circ}}{P} \right) \left(\frac{\partial \sigma_k}{\partial r} \right)_T \frac{\mathcal{Z}^2 D_{M,k}}{P (1 - \eta_{\circ k})} \tag{16}$$

From Equations 9 and 10, the following relations

$$\left(\frac{\partial \sigma_k}{\partial r}\right)_T = -\left(\frac{\partial \eta_j}{\partial r}\right)_T \frac{P}{\mathcal{Z} RT} \tag{17}$$

$$\left(1 - \eta_k\right) = \eta_j \tag{18}$$

are combined with Equation 16 to give

$$\begin{aligned} \dot{m}_k &= \left(\frac{f_k^\circ}{P}\right)\left(\frac{\partial \eta_j}{\partial r}\right)_T \frac{\mathcal{Z} D_{m,k}}{RT \eta_j} \\ &= \left(\frac{f_k^\circ}{P}\right) \frac{\mathcal{Z} D_{m,k}}{RT}\left(\frac{\partial \ln \eta_j}{\partial r}\right)_T \end{aligned} \tag{19}$$

Equation 19 may now be expressed in terms of the weight rate of transport in the following way:

$$\dot{m}_k = \dot{m}_k M_k = \left(\frac{f_k^\circ}{P}\right) \frac{\mathcal{Z} D_{m,k}}{b_k T}\left(\frac{\partial \ln \eta_j}{\partial r}\right)_T \tag{20}$$

Equation 20 describes the weight rate of transport per unit area for the components of an ideal solution in accordance with the Maxwell hypothesis, with fugacity as the driving potential. The total weight rate of transfer from a sphere

can be obtained from Equation 20 in the following way:

$$\underline{\dot{m}}_K = \dot{m}_K A_s = \dot{m}_K 4\pi r_s^2 = 4\pi r_s^2 \frac{\Sigma D_{M,K}}{b_K T}\left(\frac{f_K^\circ}{P}\right)\left(\frac{\partial \ln \eta_{\circ j}}{\partial r}\right)_T \qquad (21)$$

Integration of Equation 21 between the surface of the sphere and a point at an infinite distance from it yields the following expression:

$$\underline{\dot{m}}_k = -4\pi r_s \frac{\Sigma D_{M,K}}{b_K T} \frac{f_K^\circ}{P} \ln\left(\frac{\eta_{\circ j,ss}}{\eta_{\circ j,a}}\right) \qquad (22)$$

By considering the gaseous phase to be a perfect gas and the concentration of the diffusing component to be low, Equation 22 can be simplified to yield

$$\underline{\dot{m}}_K = \frac{4\pi r_s D_{M,K}}{b_K T}\left(\eta_{\circ K,ss} - \eta_{\circ K,a}\right) \qquad (23)$$

If the diffusion coefficient employed by Sherwood (25) is substituted for the Maxwell diffusion coefficient, the following form is obtained:

$$\underline{\dot{m}}_K = \frac{4\pi r_s D_{v,K}}{b_K T}\left(p_{K,ss} - p_{K,a}\right) \qquad (24)$$

Equation 24 is the form most commonly used in describing the behavior of evaporating spheres in a stagnant atmosphere, but it is valid only when the fugacity of the diffusing component is negligible compared to the fugacity of the stagnant component.

These equations, relating to the weight rate of material transfer from spheres, may be used in correlating the experimental data obtained in this investigation.

Utilizing the conventions described by Sherwood (25) and Equation 22, which is based on the assumption that the driving force for diffusion is the fugacity gradient and that the gas phase is an ideal solution, the dimensionless parameter for material transfer designated here as the Sherwood number may be expressed in the following manner:

$$Sh = \frac{m' l_o}{D_{V,K}} = - \frac{\dot{\underline{m}}_K \, b_K \, T}{\pi \, d_S \, \Sigma \, D_{M,K} \, \frac{f_K^\circ}{P} \, ln\left(\frac{n_{j,ss}}{n_{j,a}}\right)} \qquad (25)$$

The Sherwood number reduces to a constant value of 2 at the limiting case of a sphere evaporating into a stagnant gas. This follows directly from substitution of Equation 22, which gives the total weight rate of evaporation from a sphere into a stagnant atmosphere, in Equation 25.

$$Sh = - \frac{-4\pi r_s \, \frac{\Sigma D_{M,K}}{b_K T} \, \frac{f_K^\circ}{P} \, ln\left(\frac{n_{j,ss}}{n_{j,a}}\right) \, b_K T}{\pi \, d_S \, \Sigma \, D_{M,K} \, \frac{f_K^\circ}{P} \, ln\left(\frac{n_{j,ss}}{n_{j,a}}\right)} = 2 \qquad (26)$$

If the concentration of the diffusing component is low, Equation 25 reduces to the following form:

$$Sh = \frac{\underline{\dot{m}}_k \, b_k \, T}{\pi \, d_s \, D_{v,k} \, (p_{k,ss} - p_{k,a})} \qquad (27)$$

The evaporation of a liquid involves the transfer of thermal energy as well as transfer of material from the surface of evaporation. This interrelation permits evaluation of data on heat transfer from experimental measurements on evaporation rates. A brief derivation is presented of the equation relating the material and thermal transport at steady state.

The first law of thermodynamics for a system of variable weight can be expressed as

$$d\underline{E} = d(mE) = m\,dE + \Sigma_n \bar{E}\, dm \qquad (28)$$

Since the sum of the heat and work of a process must be equal to the change in internal energy of the system:

$$d\underline{E} = m(q - \omega) + \Sigma_n \bar{E}\, dm \qquad (29)$$

$$d\underline{E} = \underline{q} - \underline{\omega} + \Sigma_n \bar{E}\, dm \qquad (30)$$

The boundary of the system under consideration will be con-

sidered fixed:

$$d\underline{V} = 0 \tag{31}$$

The expression of the work becomes

$$\underline{\omega} = - P \bar{V} \, dm \tag{32}$$

Now consider the flow of material into the system as a liquid. The work term for material added becomes

$$\underline{\omega}_\ell = - P_\ell \bar{V}_\ell \, dm_\ell \tag{33}$$

For the material evaporating at the surface, the work is

$$\underline{\omega}_g = - P_g \bar{V}_g \, dm_g \tag{34}$$

Expanding the terms in Equation 30 and differentiating the variables with respect to time we obtain

$$\frac{d\underline{E}}{d\theta} = \frac{\Sigma \underline{q}}{d\theta} - \left(- P_\ell \bar{V}_\ell \frac{dm_\ell}{d\theta} - P_g \bar{V}_g \frac{dm_g}{d\theta} \right) + \bar{E}_\ell \frac{dm_\ell}{d\theta} + \bar{E}_g \frac{dm_g}{d\theta} \tag{35}$$

Under steady conditions, the following relations are necessary:

$$\frac{d\underline{E}}{d\theta} = 0 \tag{36}$$

$$\dot{m}_g + \dot{m}_\ell = 0 \tag{37}$$

Equation 35 reduces to the following forms:

$$\Sigma \dot{\underline{q}} + P_\ell \bar{V}_\ell \dot{m}_\ell - P_g \bar{V}_g \dot{m}_\ell + \bar{E}_\ell \dot{m}_\ell - \bar{E}_g \dot{m}_\ell = 0 \tag{38}$$

$$\Sigma \dot{\underline{q}} + \dot{m}_\ell \left(\bar{E}_\ell + P_\ell \bar{V}_\ell - \bar{E}_g - P_g \bar{V}_g \right) = 0 \tag{39}$$

The partial specific enthalpy is defined as

$$\bar{H} = \bar{E} + P\bar{V} \tag{40}$$

Equation 39 simplifies to

$$\Sigma \dot{\underline{q}} + \dot{m}_\ell \left(\bar{H}_\ell - \bar{H}_g \right) = 0 \tag{41}$$

$$\dot{m}_\ell = \frac{\Sigma \dot{\underline{q}}}{\bar{H}_g - \bar{H}_\ell} \tag{42}$$

If the liquid phase and the gas phase surrounding the evaporating surface behave as an ideal solution Equation 42 becomes

$$\dot{m}_\ell = \frac{\Sigma \dot{\underline{q}}}{H_g^\circ - H_\ell^\circ} \tag{43}$$

Under steady conditions, the evaporating rate per unit area of a pure substance is related to the total thermal flux

per unit area by the following equation:

$$\delta \underline{\dot{m}}_k = \frac{\sum \underline{\dot{q}}}{\left(H^{\circ}_{k,g} - H^{\circ}_{k,\ell}\right)} \tag{44}$$

The quantity $\sum \underline{\dot{q}}$ represents the sum of all forms of thermal transport to the surface including convection, conduction, and radiation. By summation of Equation 44 over the surface of the evaporating sphere, the following equation relating the macroscopic amounts of thermal and material transfer is obtained:

$$\underline{\dot{Q}}_r + \underline{\dot{Q}}_c = \underline{\dot{m}}_k \left(H^{\circ *}_{k,g} - H^{\circ}_{k,\ell,t}\right) \tag{45}$$

Since the thermal flux due to radiation was negligible for all conditions encountered in this investigation, the thermal flux due to convection obtained from Equation 45 may be correlated to the dimensionless Nusselt number for evaporating spheres by the following equation:

$$\text{Modified Nusselt number} = Nu' = \frac{\underline{\dot{Q}}_c \, d_s}{k_j \left(t_a - t_{ss}\right)} \tag{46}$$

The foregoing discussion described the dimensionless parameters used in correlating the experimental data on thermal and material transport obtained in this investigation.

APPARATUS

Air Supply

The thermal and material transfer measurements were made in a flowing air stream at atmospheric pressure. The details of the apparatus used in conditioning the air stream for the present investigation are essentially the same as those employed in earlier studies on the effect of shape on the evaporation of n-heptane drops (9). The major modification involved the addition of a punched plate at the exit of the air jet to produce a high level of turbulence. The arrangement of the air supply is shown schematically in Figure 1. Air obtained outside the building was used in order to eliminate any possible contamination from laboratory activities. A centrifugal blower powered by a Sterling Speedtrol unit made possible continuous variation of air velocities employed in the present series of measurements. The pressure difference of a venturi meter was used to establish the weight rate of air flow through the system. In order to provide a uniform temperature field at the cross-section of the jet, independently controlled heaters were installed at A and B of Figure 1. A series of low-thermal-

capacity electrical heaters were installed at C to allow energy to be added to different parts of the air stream independently to provide a more uniform temperature distribution at the air jet throat D. The air temperature was maintained at near constant values by the electric heater F controlled through an electronic modulating circuit (5). Copper-constantan thermocouples, 0.003 inch in diameter, were installed at points G and G' to follow the local variations in temperature of the flowing air stream. The gross air temperature was determined from the reading of the platinum resistance thermometer located at E.

The transverse velocity distributions were determined with a hot wire anemometer constructed of platinum wire, 0.0005 inch in diameter, and are shown in Figure 2. Employing the hot wire as a resistance thermometer, the transverse temperature distribution at the jet was obtained as shown in Figure 3. From the velocity and temperature distributions shown in these figures, it can be seen that the variation in the local velocity and temperature near the center of the jet where the test spheres were located was quite small.

The arrangement of the punched plate at the throat of the air jet is shown in Figure 4. Because the turbulence level of the flowing stream in the wake of the punched plate decreases with axial distance, studies at different levels of turbulence could be obtained by inserting the test spheres at the appropriate distance from the punched plate. This was

accomplished by changing the extension placed over the punched plate as shown in Figure 4. Figure 5 presents a photographic view of the apparatus with the shortest extension, 3 inches long, installed over the punched plate. The extensions shown in Figure 6 are provided with electrical heaters to keep the internal surfaces at the air stream temperature. Copper-constantan thermocouples located on the internal surfaces of the extnesions were employed to indicate the energy requirements of the jacket heaters necessary to maintain them within 0.1° F. of the air stream value.

Traverses were made with the hot wire anemometer in the wake of the punched plate. Apparently due to the higher level of turbulence, a more uniform temperature field was obtained in the wake of the punched plate. In the central portion of the flowing stream where the test spheres were located, the temperature variation never exceeded 0.2° F. The velocity distributions obtained with the hot wire anemometer for bulk air flow of 16 feet per second as a function of turbulence level are presented in Figure 7. At the highest turbulence level used in the present investigation, corresponding to an axial distance of 4.0 inches from the punched plate, the velocity profile appears to be a function of the location of the holes on the punched plate. The maximum variation in local velocity in the central 50 per cent of the jet was observed to be 12 per cent of the gross velocity. The maximum variation in local velocity in the region where

the test spheres were located was 8 per cent from the gross velocity. The error introduced by the velocity variations in the value of turbulence level, at X = 4.0 inches, was about three times that introduced by the linearized hot wire equations employed in evaluating turbulence level (6). At X = 7.0 inches, the velocity-profile variations were sufficiently small so that maximum error in turbulence level was of the same order as that introduced by the linearized hot wire equations. The velocity profiles obtained at X = 4.0 inches for bulk air speeds of 4, 8, 16, and 32 feet per second are presented in Figure 8. In all cases at X = 4.0 inches, the maximum variation in local velocity at the location of the test spheres was of the order of 8 per cent of the gross velocity.

These velocity profiles were calculated by the conventional hot wire equation introduced by King (12):

$$i^2 R_{HW} = \left(a + b\sqrt{u}\right)\left(R_{HW} - R_a\right) \qquad (47)$$

This equation is based on the assumption that the heat transfer coefficient from a wire is a single-valued function of air speed. This assumption is valid if the level of turbulence in the air stream is low and remains essentially constant at different air speeds. If the turbulence level is high and is not constant for different air speeds, then the assumption that the heat transfer coefficient is a unique

function of air speed is questionable. It appears that the apparent variation observed in the local velocity in the wake of a punched plate may be due to changes in the level of turbulence as well as changes in local air speed.

Heated Sphere

The heated sphere used in the present investigation was essentially the same as that employed by Baer et al. (1) for measurement of temperature profiles in the wake of a heated sphere. The addition of compensating heaters around the tube support was made in an effort to minimize conduction effects which appeared to be appreciable in the previous investigations (1). The details of construction of the sphere are presented in sectional form in Figure 9. A chromel wire heater was placed in the spiral groove of the inner copper sphere E and the leads were brought out through the supporting steel tube B. Four copper-constantan thermocouples to indicate surface temperatures were located at points F, G, H, and J on the internal surface of the silver shell D. Rotation of the sphere about the axis A-A permitted the determination of surface temperatures over four circular paths on the sphere normal to the axis of rotation. The compensating heaters I were of glass-insulated constantan wire coiled around the steel tube B within 0.125 inch of the solder joint C. Alternating current was employed in the compensating heaters in order to minimize any stray electrical effects on the surface thermocouple readings. The power input to each

heater was independently controlled by means of Variac auto-transformers. Lead storage batteries were used to supply electrical energy to the sphere heater. The energy input was determined by measuring the voltage applied to the sphere heater and the voltage drop across a standard resistor connected in series with the heater leads by use of precision potentiometers. A schematic diagram of the heater circuit is presented in Figure 10.

Porous Sphere

The sphere was shaped from a piece of processed diatomaceous earth known as Allen filter material. Owing to the softness of this material, extreme care was exercised in lapping the sphere into shape. The details of the porous sphere, 0.500 inch in diameter, employed in the studies of evaporation rates are presented schematically in Figure 11. The porous sphere A was suspended from a glass tube B, 0.030 inch in diameter, which extended to the center of the sphere. The space between the glass tube and the hole in the sphere was sealed off by a sodium silicate solution. A set of copper-constantan thermocouples was placed inside the glass tube B as shown in Figure 11. This permitted measurement of the fluid temperature in the tube at D which is away from the surface of the sphere and at C which is at the center of the sphere. A differential manometer E with one leg open to the atmosphere was connected directly to the tube to serve as an indication of the degree of surface saturation.

Fluid Injector

The controllable fluid injector used to establish the evaporation rate is depicted schematically in Figure 12. The evaporation rate was established by determining the value of liquid flow necessary to maintain steady conditions at the surface of the sphere. The details of the variable speed motor and the associated electronic system have been described (20). By means of the gear box and the range of motor speeds, a 6000-fold variation in the fluid rate could be achieved with a probable error of less than 0.1 per cent. Variation in the temperature of the agitated oil bath surrounding the injector and displacement piston is responsible for the greatest uncertainty in the actual displacement of fluid. Because the room temperature affects the temperature of the fluid in the lines connecting the injector to the sphere, oil from the injector bath was circulated in a jacket surrounding the feed line as shown in Figure 12. These precautions minimized temperature variations of the fluid in the feed lines, so that the instantaneous fluid rate was known with a probable error of not more than 0.1 per cent.

Traversing Thermocouple

A suitable system of gibs and ways was employed to permit accurate movement of the thermocouple junction in the vicinity of the test sphere. Precision dial gauges with a total travel of one inch and with 0.001 inch divisions were

used to locate the vertical X component and horizontal Z component of the thermocouple according to the system of coordinates shown in Figure 13. The thermocouple used in the transport studies in the free air jet is shown schematically in Figure 14. Adjustment of the spacing of the supporting needles was necessary to produce a slight tension in the thermocouple wire to prevent vibration in the flowing air stream. The platinum wires, 0.001 inch in diameter, were soldered to platinum leads, 0.010 inch in diameter, which terminated at the tips of the steel support needles. The measuring junction is located at point A while the reference junction is located at point B. A differential thermocouple was used to prevent small low frequency changes in air stream temperatures from being superimposed on the desired temperature profiles.

For measurements involving transport studies in the wake of the punched plate installed at the jet opening, the thermocouple support was modified as shown in Figure 15. The platinum-constantan thermocouple, 0.001 inch in diameter, was replaced by a platinum-platinum 10 per cent rhodium thermocouple, 0.0003 inch in diameter. The change was made to decrease the magnitude of the corrections on the readings obtained with the thermocouple because of thermal conduction along the wire. The reference junction was situated one inch away from the measuring junction as shown in Figure 15. Figure 16 shows the platinum-platinum 10 per cent rhodium thermocouple in relation to the porous sphere.

Electric Analog Computor

To facilitate the solution of the differential equation relating the steady state thermal conduction along the thermocouple wire, a simple network of adjustable electrical resistors was employed. Precision potentiometers with resistances of 100, 1,000, and 10,000 ohms and with a rated linearity of 0.1 per cent were oriented on the instrument panel as shown in Figure 17. Two plug receptacles were provided at each lead to provide for measurement of voltages at points connected by jumpers. The 100 ohm potentiometers were employed as the voltage dividers for the boundary conditions. Lead storage batteries provided the computer voltages through a simple network of resistors shown in Figure 18. Occasional adjustment of the 100-200 ohm series resistor kept the voltage supply within 0.02 per cent of the desired value. Figure 19 shows a photographic view of the analog panel with connecting jumpers in place for the solution of a typical problem.

MATERIALS

n-Hexane

The n-hexane used in these studies was obtained from the Phillips Petroleum Company and it was reported to contain less than 0.01 mole fraction of material other than n-hexane. Further purification was obtained by subjecting the material to fractionation in a 16-plate glass column at a pressure of 7 lb./sq.in. abs. The fractionation was carried out at a

reflux ratio of approximately 40 to 1. The initial and final 10% portions of the distillate were discarded. The partially purified material was passed through a column of activated alumina 7 ft. in length under ambient pressure and temperature. The purified n-hexane had a specific weight of 40.878 lb./cu.ft. at 77° F. and index of refraction relative to the D-lines of sodium of 1.3749 at 68° F. These values can be compared with 40.878 lb./cu.ft. and 1.37486 reported by Rossini (21) for n-hexane at the same states.

n-Heptane

The n-heptane also was obtained from the Phillips Petroleum Company and was reported to contain less than 0.01 mole fraction of impurities other than n-heptane. The material was subjected to the same sequence of purification steps as was the sample of n-hexane. The purified n-heptane had a specific weight of 42.429 lb/cu.ft. at 77° F. and an index of refraction relative to the D-lines of sodium of 1.3877 at 68° F. These values compare with 42.417 lb./cu.ft. and 1.3864 reported by Rossini (21) for n-heptane at the same states.

EXPERIMENTAL PROCEDURE

The experimental investigation presented here can be separated into two parts. These are:

(i) Measurement of the thermal transport from a heated sphere to a turbulent air stream at

different levels of turbulence.

(ii) Measurement of the evaporation rate of hydrocarbons from a moist porous sphere to a turbulent air stream at different levels of turbulence.

The air stream was maintained within 0.1° F. of the desired temperature by appropriate adjustment of the electrical heaters arranged along the air duct as shown in Figure 1. The weight rate of air flow was measured in terms of the venturi meter differential pressures and was kept within 0.2 per cent of the desired value.

In part i, the electrical energy input to the sphere was adjusted so as to bring the surface temperature to a value deemed satisfactory for the test being conducted. Occasional adjustment of the series resistor kept the energy input constant within 0.1 per cent for the duration of the test being conducted. The energy input was determined from voltage readings taken across the heater and a standard resistance as shown in Figure 10. The energy input to the sphere was determined with a probable error of 0.1 per cent for all conditions encountered. The compensating heaters situated on the sphere supports were adjusted to minimize the conduction losses. Here the sphere was rotated to a position where the surface thermocouples F, G, H, and J shown in Figure 9, were situated in a plane normal to the direction of air flow. At this position each of the surface thermocouples was in an equivalent position with respect to the

boundary-layer formation from the forward stagnation point of the sphere. Due to symmetry, the thermocouples of a heated sphere without thermal conduction through the supports would indicate identical readings at this position. In order to minimize the conduction losses from the heated sphere, the energy input to each compensating heater was adjusted until the thermocouples indicated the same temperature. The sphere was then rotated to different positions to determine the surface-temperature distribution as exhibited by the thermocouple readings.

In part ii the evaporating fluid was introduced at the center of the sphere by the supporting glass tube and it flowed radially through the porous material to the surface. The fluid was injected at a controlled rate from the precision injector previously described. The rate of addition of liquid was adjusted until it balanced the rate of evaporation of the liquid from the spherical surface. The porous nature of the material used in fabricating the sphere provided a convenient method for determining reproducible surface conditions. The pores on the surface of the material behaved in the same manner as capillary tubes containing a liquid which wets the surface. If the spherical surface were flooded with an excess of liquid, the rate of delivery exceeding the evaporation rate, the liquid pressure in the feed tube became slightly positive with respect to the atmosphere owing to the pressure drop experienced by the fluid flowing through

the porous material from the center of the sphere to the surface. This positive pressure difference caused the meniscus of the liquid in the manometer E of Figure 11 to rise. If the spherical surface were allowed to partially dry by decreasing the rate of delivery to the porous sphere, the liquid surface withdrew into the pores of the material. The capillary tension due to the liquid in the pores of the sphere caused the meniscus level in the manometer to change rapidly. Using this sensitive change as an indicator, the rate of liquid addition was controlled by maintaining a constant height of liquid in the manometer E. The changes in manometer level were sensitive enough to permit 0.2 per cent variations in the evaporation rates to be detected. The surface temperature of the porous sphere was determined from the indications of the traversing thermocouple when the measuring junction was in contact with the surface.

EXPERIMENTAL RESULTS

The experimental data obtained were separated into four parts. These were:

(i) Data on the thermal transport from a heated sphere to a turbulent air stream:

(a) Several surface temperatures were studied at the single low level of turbulence obtained with the unobstructed air jet. The data obtained are summarized in Table I.

(b) One nominal surface temperature was studied at several turbulence levels in the wake of a punched plate. The data obtained are summarized in Table II.

(ii) Data on the evaporation rates from a moist porous sphere:

(a) Evaporation rates of n-hexane and n-heptane were studied at a single low level of turbulence. The data obtained are summarized in Table III.

(b) Evaporation rates of n-heptane at several turbulence levels were studied. The data obtained are summarized in Table IV.

ANALYSIS OF RESULTS

The data obtained in part i-a from the studies of thermal transport from a heated sphere were analysed in terms of the conventional dimensionless quantities, Reynolds number and Nusselt number. These parameters have been previously defined by Equations 4 and 5 respectively. The average surface temperature of the sphere was established from the following integral:

$$t_{ss}^{*} = \frac{\oint_{o}^{A} t_{ss}\, dA}{A_s} = \frac{\oint_{o}^{A} t_{ss}\, dA}{\pi d_s^2} \qquad (48)$$

The variation in the local surface temperature obtained was never more than 3° F. for any conditions encountered. This can be compared to the temperature variation of 10° F. obtained with the same sphere in previous studies (1) when compensating heaters were not used on the sphere supports. The physical properties of air were taken from a critical review (18) and values are presented in Table V. The values of the dimensionless parameters were computed in three ways. The specific weight, viscosity, and thermal conductivity of air were based on the bulk air temperature of the flowing stream, the temperature of the sphere surface, and on the arithmetic average of the bulk air and sphere surface temperatures, the latter being usually designated as the film temperature. The calculated results are presented in Table VI and shown in Figure 20. The three sets of points form essentially a single curve with the parameters based on film temperatures yielding the best fit. These data yield lower values of Nusselt number based on physical properties at the film temperature than recommended by McAdams (15). The higher values of heat transfer coefficients obtained in previous studies (1) from the heated sphere without compensating heaters were probably due to thermal conduction along the sphere supports. Heat transfer measurements from spheres conducted under conditions near potential flow by Kramers (13) have been included in Figure 20 for comparison.

The measurements obtained in part i-b on thermal transfer

from a heated sphere in the wake of a punched plate have been analysed in terms of the same dimensionless quantities as in part i-a. The parameters were computed employing values of viscosity, specific weight, and thermal conductivity based on the bulk air temperature and on the film temperature.

The level of turbulence was obtained from the characteristics reported by Davis (16) for the punched plate used in this investigation. The turbulence measurements were made with a single wire normal to the mean flow of air. The hot wire was maintained at constant resistance by means of a self-balancing power supply. The hot wire current was set and the vacuum-thermocouple output was recorded continuously as the hot wire carriage was moved along the axis of the wind tunnel. The turbulence level was determined from the hot wire equation in the following manner.

$$\frac{i^2 R_{HW}}{R_{HW} - R_a} = a + b\sqrt{u} \qquad (49)$$

If R_{HW} is maintained at a constant value, then

$$i^2 = a' + b'\sqrt{u} \qquad (50)$$

Differentiation of Equation 50 gives

$$2\frac{di}{i} = \frac{\frac{1}{2} b'\sqrt{u}}{a' + b'\sqrt{u}} \frac{du}{u} \qquad (51)$$

Since in the region in which the hot wire was used

$$\frac{b' \sqrt{u}}{a' + b' \sqrt{u}} \sim 1 \qquad (52)$$

Equation 51 reduces to

$$\frac{di}{i} \sim \frac{1}{4} \frac{du}{u} \qquad (53)$$

The recorded current variation is converted into the desired speed variations by means of Equation 53. The axial distance X pertinent to the relation presented in Figure 21 was considered to be the distance between the forward stagnation point of the sphere and the trailing surface of the punched plate. The level of turbulence at the locality of the test sphere was obtained from the observed distance X and the relation presented in Figure 21. It is believed that the turbulence level is known within 2 per cent of the value indicated by a hot wire in the same position.

The calculated results obtained are summarized in Table VII and presented in Figure 22. The results obtained in part i-a and the curve recommended by McAdams (15) have been included for comparison. A cross-plot of Figure 22 which presents the effect of turbulence level on the Nusselt number is given by Figure 23. The results indicate that the heat transfer coefficient from spheres is not significantly increased by turbulence level at low air velocities, but the increase is

significant at the high air velocities.

The preliminary studies in part ii-a on the evaporation rate from spheres in the unobstructed jet were carried out with n-hexane. It soon became evident that n-hexane was too volatile for studies at the proposed higher air velocities, because the injection rates required to keep the sphere moist were near the upper limit even at air velocities low as 6 feet per second. When the change was made to n-heptane, the evaporation rate was found to be compatible with the range of air velocities to be studied. For comparison, the gross evaporation rates of n-hexane and n-heptane from a porous sphere, 0.500 inch in diameter, are presented in Figure 24 as a function of bulk air velocity into a stream maintained at a temperature of 100° F.

The data obtained in part ii-a from the studies of evaporation rates of n-heptane from a sphere in the free air jet were analysed in terms of the dimensionless quantities Schmidt number, Reynolds number, and Sherwood number. These parameters have been previously defined by Equations 3, 4, and 25 respectively. The properties of the free stream air were used in computing Reynolds number and Schmidt number because there is no satisfactory method of taking into account the variation in composition along the transfer path. The thermodynamic properties of n-heptane in the gas phase were obtained by application of the Benedict equation of state (12). The fugacity coefficients of n-heptane employed in calculating

Sherwood numbers were obtained from the Benedict equation of state. These coefficients are presented in Figure 25. It is believed that the probable errors in the fugacity and the concentration of n-heptane were less than 1 per cent for all conditions covered in this investigation. The vapor pressure and latent heat of vaporization of n-heptane were taken from a critical review by Rossini (21). The Maxwell diffusion coefficient of n-heptane was obtained from a recent study of diffusion coefficients of hydrocarbons in air at atmospheric pressure (23). The values of the vapor pressure, latent heat of vaporization, and diffusion coefficient of n-heptane are presented in Table V.

The temperature distribution on the surface of the porous sphere was established by applying the appropriate corrections to the experimental values as discussed in Appendix A. From the local surface temperatures around the sphere, the average surface temperature was established from Equation 48. Since surface traverses were obtained only once for each air velocity and turbulence level, a method was necessary to establish the average surface temperatures for the tests where traverses were not obtained. A limited correlation between the average surface temperature and the temperature of the liquid at the center of the sphere was established from the results presented in Table IV. The empirical correlation is presented in Figure 26. Though there is some scatter in the experimental points, the curve

will allow a reasonable estimate of the average surface temperature from the value of the liquid temperature at the center of the sphere. It is believed that the value of the surface temperature obtained from Figure 26 is within 0.5° F. of the actual value for all conditions covered in this investigation.

The data obtained in part ii-a are presented in terms of the dimensionless parameters Sherwood number and (Reynolds number)$^{1/2}$ (Schmidt number)$^{1/3}$. The calculated results are recorded in Table VIII and shown in Figure 27. The results obtained are compared with those by Frössling (8) and Ranz and Marshall (19) in Figure 27 and are found to be in good agreement. The data obtained in part ii-b on the evaporation of n-heptane from porous spheres in the wake of a punched plate were correlated employing the same dimensionless parameters as in part ii-a. The results are recorded in Table IX and shown in Figure 28. A cross-plot of Figure 28 which presents Sherwood number as a function of turbulence level shown in Figure 29 reveals behavior similar to that observed with Nusselt number for the heated sphere; namely, that the effect of turbulence is only significant at the higher air velocities.

After applying the appropriate corrections for thermal flux other than convective heat transfer as described in Appendix B, a modified Nusselt number may be evaluated for the evaporating porous sphere. The modified Nusselt number

has been defined previously by Equation 46 and was correlated in the conventional manner by the Reynolds number defined by Equation 4. The calculated results from part ii-a are recorded in Table X. The modified Nusselt number is compared with the Nusselt number obtained from the heated sphere in part i-a as shown in Figure 30. Both sets of points form a single curve with somewhat lower Nusselt numbers based on physical properties of the free stream than recommended by McAdams (15). The results obtained from part ii-b are presented in Table XI and are compared with the Nusselt number based on physical properties of the free stream from the heated sphere from part i-a as shown in Figure 31. A cross-plot of Figure 31 which presents modified Nusselt number as a function of turbulence level is shown in Figure 32.

CONCLUSIONS

Measurements have been made on thermal and material transfer from spheres in the range of Reynolds number, based on sphere diameter, from 500 to 8000.

The experimental data obtained have shown that the turbulence level in the flowing stream increased the magnitude of the thermal and material transfer coefficients appreciably only at Reynolds numbers in excess of 1800 which corresponded to air velocities in excess of 8 feet per second. In an air stream at Reynolds number of 3600 with a turbulence

level of 13 per cent, the Nusselt number increased by 11 per cent over the value obtained in the undisturbed air stream at the same Reynolds number. Under the same flow conditions, the Sherwood number was increased by 14 per cent. Further investigations with spheres of different diameters are needed to establish whether air velocity, diameter of the sphere, or magnitude of the Reynolds number is the critical factor which determines the region in which turbulence level exerts a marked influence on the magnitude of the transfer coefficients.

The present data indicate that the rate of material transfer from the evaporating surface has little effect on the heat transfer to the evaporating surface. The ratio of the weight of liquid evaporated per unit time per unit area of sphere surface to the weight rate of air flow per unit time per unit area of cross-section of the stream varied from 0.0006 to 0.0018 for the conditions encountered. The small value of this ratio probably accounts for the fact that the heat transfer was unaffected by the material transfer. It is believed that further investigation into the effect of material transfer on the heat transfer at higher evaporation rates would be useful in establishing this relationship.

NOMENCLATURE

a, a'	dimensional constants
A_s	surface area of sphere, sq. ft.
b, b'	dimensional constants
b	specific gas constant of component k, ft./$^{\circ}$ R.
C_k	Maxwell coefficient of component k, lb. sec. sq. ft./(mole)
C_p	isobaric heat capacity, Btu./lb.$^{\circ}$ F.
d	differential operator
d_s	diameter of sphere, ft.
$D_{F,k}$	Fick diffusion coefficient of component k, sq.ft./sec.
$D_{M,k}$	Maxwell diffusion coefficient of component k, lb./sec.
$D_{v,k}$	volumetric diffusion coefficient of component k, $D_{M,k}/P$; $D_{F,k}$ (η_k/n_k), sq. ft./sec.
e	Base of natural logarithms 2.71828
E	specific internal energy, Btu./lb.
$\underline{E}$	total internal energy, Btu.
$\overline{E}$	partial internal energy, Btu./lb.
f_k	fugacity of component k, lb./sq. in.
f_k°	fugacity of component k in the pure state, lb./sq. in.
h, h'	coefficient of heat transfer, Btu./sec.sq.ft.$^{\circ}$ F.
H_k°	specific enthalpy of component k in the pure state, Btu./lb.
$\overline{H}_k$	partial enthalpy of component k, Btu./lb.
i	current, amperes

k_j thermal conductivity of component j, Btu./sec.ft.$^{\circ}$ F.

K constant of proportionality

l_o characteristic length, ft.

ln natural logarithm

L_k latent heat of vaporization of component k, Btu./lb.

m weight, lb.

m' material transfer coefficient, ft./sec.

$\dot{m}_k$ transport rate of component k, lb./sq.ft.sec.

$\dot{\mathring{m}}_k$ molal transport rate of component k, lb. mole/sq. ft. sec.

$\dot{\underline{m}}_k$ total transport rate of component k, lb./sec.

$\delta \dot{\underline{m}}_k$ total transport rate of component k across a differential, interfacial area, an infinitesimal, lb./sec.

M_k molecular weight of component k, lb./mole

n_k weight fraction of component k

$\mathring{n}_k$ mole fraction of component k

Nu Nusselt number, $\frac{h d_s}{k_j}$

Nu' modified Nusselt number, $\frac{h' d_s}{k_j}$

p_k partial pressure of component k, lb./sq. in.

P pressure, lb./sq.in. abs.

q heat associated with an infinitesimal change in values of variables defining the state of a system, Btu./lb.

$\underline{q}$ total heat associated with an infinitesimal change in values of variables defining the state of a system, Btu.

$\dot{\underline{q}}$ total thermal transport to an infinitesimal area, Btu./sec.

$\dot{Q}$ thermal flux, Btu./sq.ft. sec.

$\dot{\underline{Q}}$ total thermal flux, Btu./sec.

r_s radius of sphere, ft.

R universal gas constant ft. lb./mole $^{\circ}$ R.

R_a resistance of hot wire corresponding to t , ohm.

R_{HW} fixed resistance of hot wire, ohm.

Re Reynolds number, $\frac{d_s U}{\nu}$

Sc Schmidt number, $\frac{\nu_s}{D_{F,k}} \approx \frac{P\nu_s}{D_{v,k}}$

Sh Sherwood number, $\frac{m' l_o P}{D_{M,k}}$

t temperature $^{\circ}$ F.

T thermodynamic temperature, $^{\circ}$ R.

t_{ss}^* average surface temperature of sphere, $^{\circ}$ F.

u local velocity, ft./sec.

U average velocity ft./sec.

$\underline{V}$ total volume, cu. ft.

$\overline{V}$ partial specific volume, cu. ft./lb.

w work associated with an infinitesimal change in values of variables defining the state of a system, Btu./lb.

$\underline{w}$ total work associated with an infinitesimal change in values of variables defining the state of a system, Btu.

X distance downstream from center of sphere, in.

y distance toward walls from center of sphere, in.

y_o $\frac{1}{2}$ distance between parallel walls, in.

Y horizontal distance from center of sphere to the walls, in.

Z horizontal distance from center of sphere normal to X-Y plane, in.

Z compressibility factor,

β dimensional quantity 1/ft.

Δ	difference operator
θ	time, seconds
π	mathematic symbol for 3.14159
σ_k	concentration of component k, lb./cu.ft.
$\sigma_{\circ k}$	molal concentration of component k, mole/cu. ft.
Σ_n	summation of n terms
∂	partial differential operator
$\oint$	surface integral

Superscript

*	average value of

Subscripts

a	free stream, at a distance from the sphere
B	air boundary layer
c	convection
Co	constantan
Cu	copper
f	film
g	gas phase
HW	hot wire
j	component in stream
k	diffusing component
l	liquid phase
n	node in analog circuit
Pt	platinum
r	radiation
sc	at center of sphere

ss	on surface of sphere
t	injection tube
w	wire
wr	water in air stream
x	along axis of injection tube

REFERENCES

1. Baer, D. H., Schlinger, W. G., Berry, V. J., and Sage, B. H., J. App. Mech., 20, 407 (1953).

2. Benedict, M., Webb, G. B., and Rubin, L. C., Chem. Eng. Progr., 47,419 (1951).

3. Bradley, R. S., Evans, M. G., and Whytlaw-Gray, R. W., Proc. Roy. Soc., (London), A186, 368 (1946).

4. Cole, J., and Roshko, A., Heat Transfer and Fluid Mech. Inst., 13-23, Univ. of Calif., Berkeley, June 30 - July 2, 1954.

5. Corcoran, W. H., Page, F., Jr., Schlinger, W. G., and Sage, B. H., Ind. Eng. Chem., 44, 410 (1952).

6. Davis, L., Jet Propulsion Laboratory, California Institute of Technology, Report No. 3-17, (1952).

7. Douglas, T. B., Furukawa, G. T., McCoskey, R. E., and Ball, A. F., J. Research, Nat'l. Bur. Standards, 53, 139 (1954).

8. Frössling, N., Gerlands Beitr. Geophys., 51, 167 (1937).

9. Hsu, N. T., Sato, K., and Sage, B. H., Ind. Eng. Chem., 46, 870 (1954).

10. Ingebo, R. D., Nat. Advisory Comm. Aeronaut., Tech. Note 2368 (1951).

11. Jakob, M., "Heat Transfer," vol. 1, New York, John Wiley and Sons, Inc., 1949.

12. King, L. V., Phil. Trans. Roy. Soc., A116, 170 (1927).

13. Kramers, H., Physica, 12, 61 (1946).

14. Langmuir, I., Phys. Rev., 12, 368 (1918).

15. McAdams, W. H., "Heat Transmission," New York, McGraw-Hill Book Co., 1942.

16. Maxwell, J. C., "Scientific Papers," 2, Cambridge University Press, 623 (1890).

17. Morse, H. W., Proc. Am. Acad. Sci., 45, 361 (1910).

18. Page, F., Jr., Corcoran, W. H., Schlinger, W. G., and Sage, B. H., Ind. Eng. Chem., 44, 419 (1952).

19. Ranz, W. E., and Marshall, W. R., Jr., Chem. Eng. Progr., 48, 141, 173 (1952).

20. Reamer, H. H., and Sage, B. H., Rev. Sci. Inst., 24, 362 (1953).

21. Rossini, F. D., Pitzer, K. S., Arnett, R. L., Braun, R. M., and Pimentel, G. C., "Selected Values of Physical and Thermodynamic Properties of Hydrocarbons and Related Compounds," Pittsburgh, Carnegie Press, 1953.

22. Schlichting, H., NACA TM No. 1217 (1949).

23. Schlinger, W. G., Reamer, H. H., Sage, B. H., and Lacey, W. N., Fundamental Research on Occurrence and Recovery of Petroleum (Biennial Volume 1952-53), pp. 70-106 API.

24. Schlinger, W. G., and Sage, B. H., Am. Doc. Inst., Washington 25, D. C., Doc. 4221 (1954).

25. Sherwood, T. K., and Pigford, R. L., "Absorption and Extraction," New York, McGraw-Hill Book Co., 1952.

26. Streeter, V. L., "Fluid Dynamics," McGraw-Hill Book Company, Inc., New York, 1948.

LIST OF FIGURES

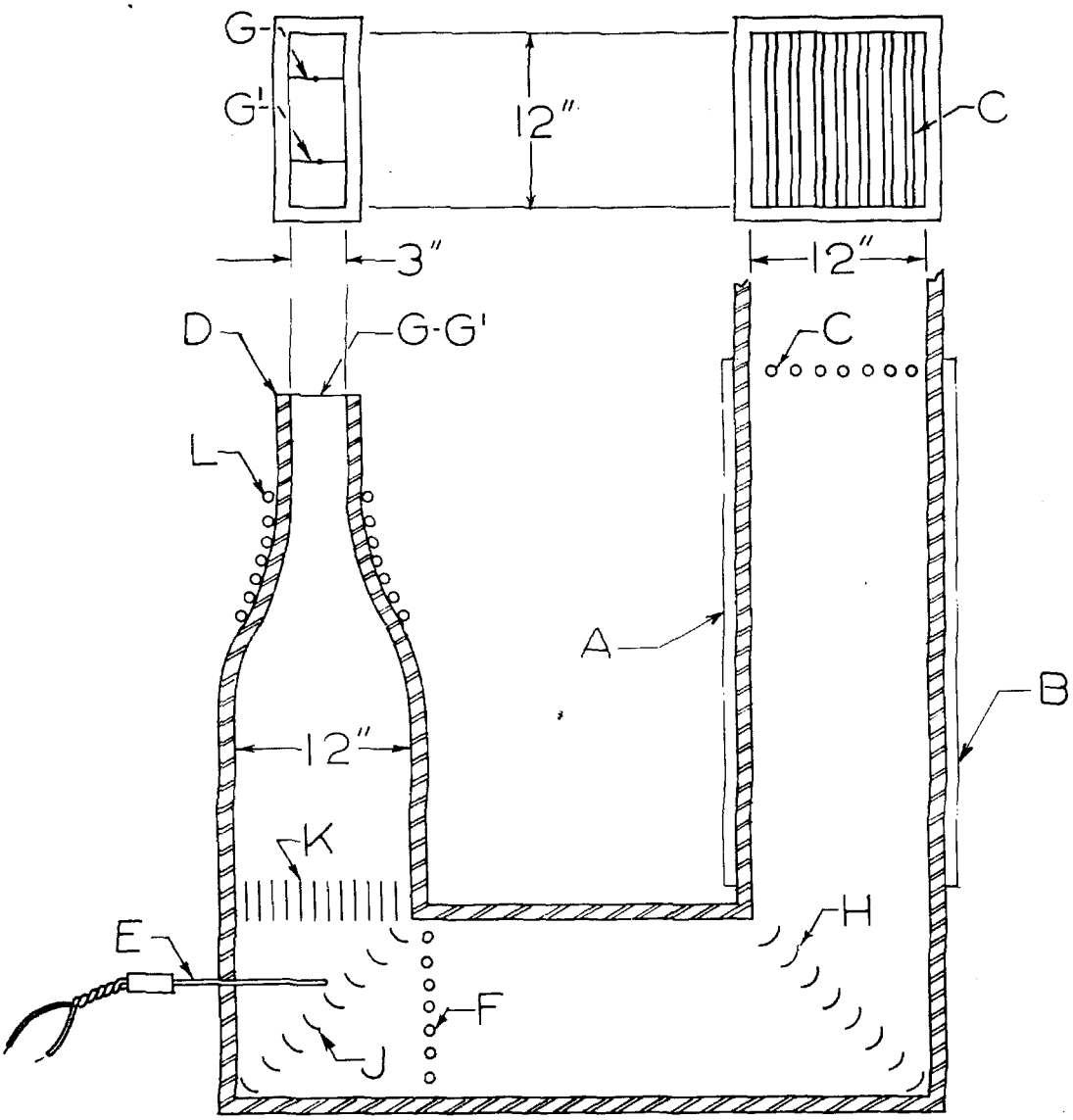

Figure 1. Arrangement of Air Supply

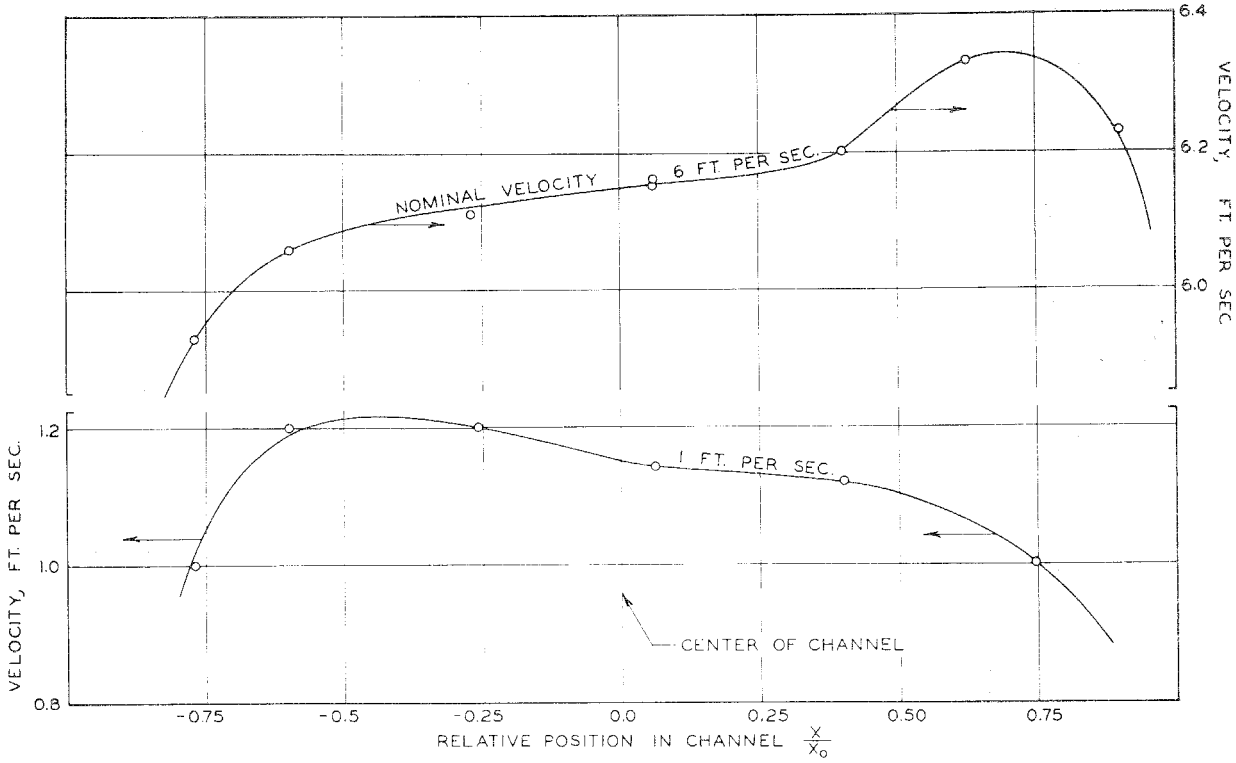

Figure 2. Velocity Distribution in Jet

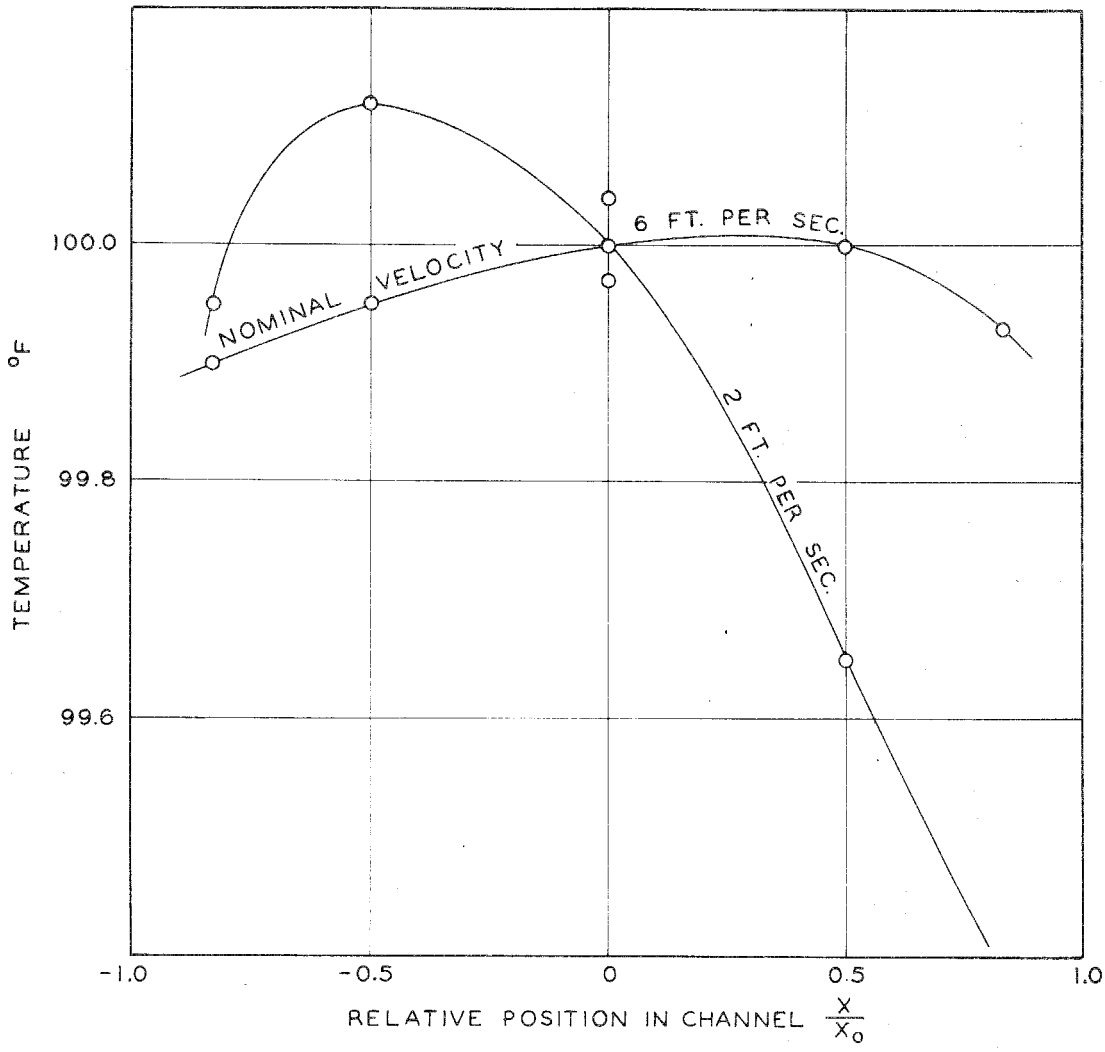

Figure 3. Time-Average Temperature Distribution in Jet

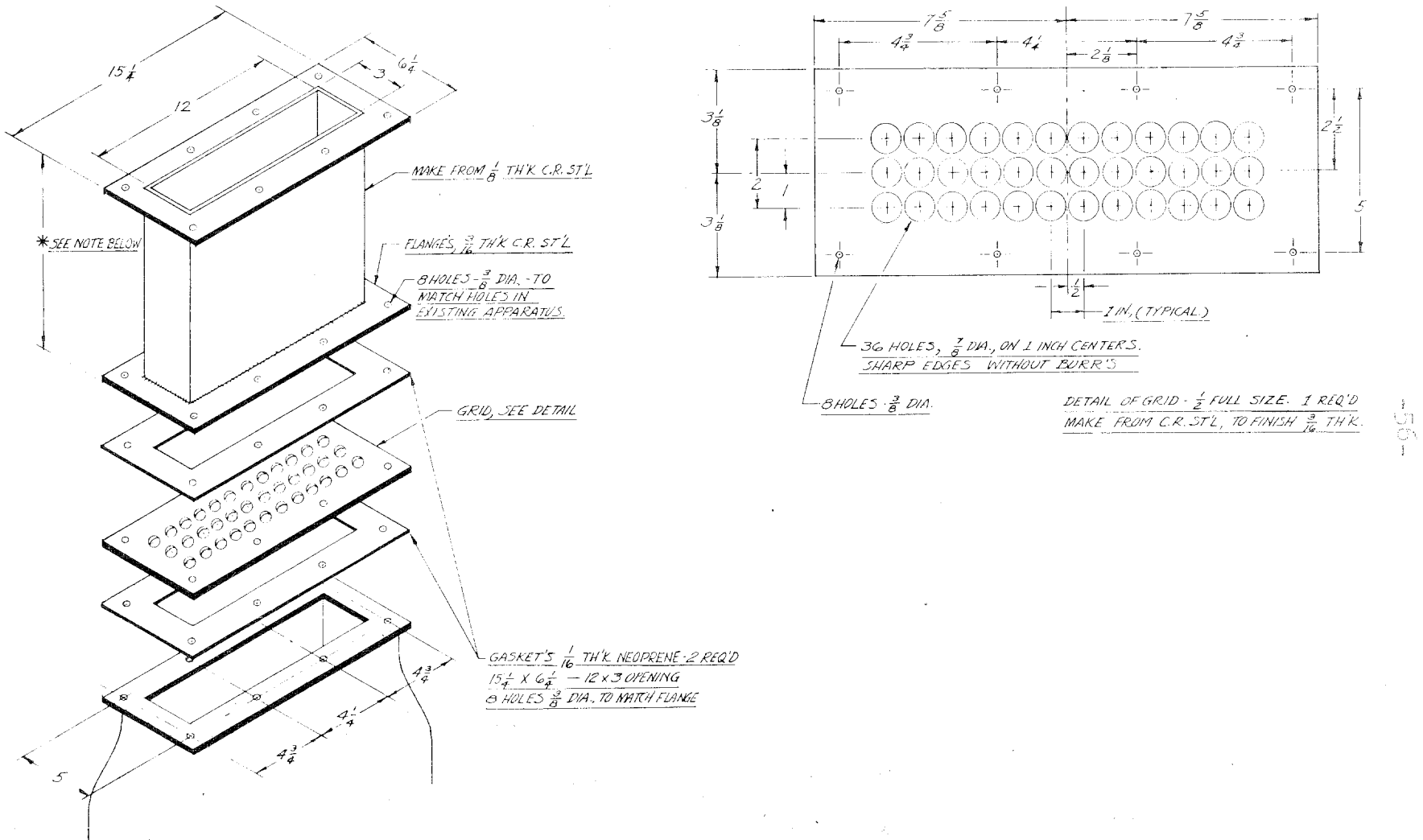

Figure 4. Details of Punched Plate and Extensions

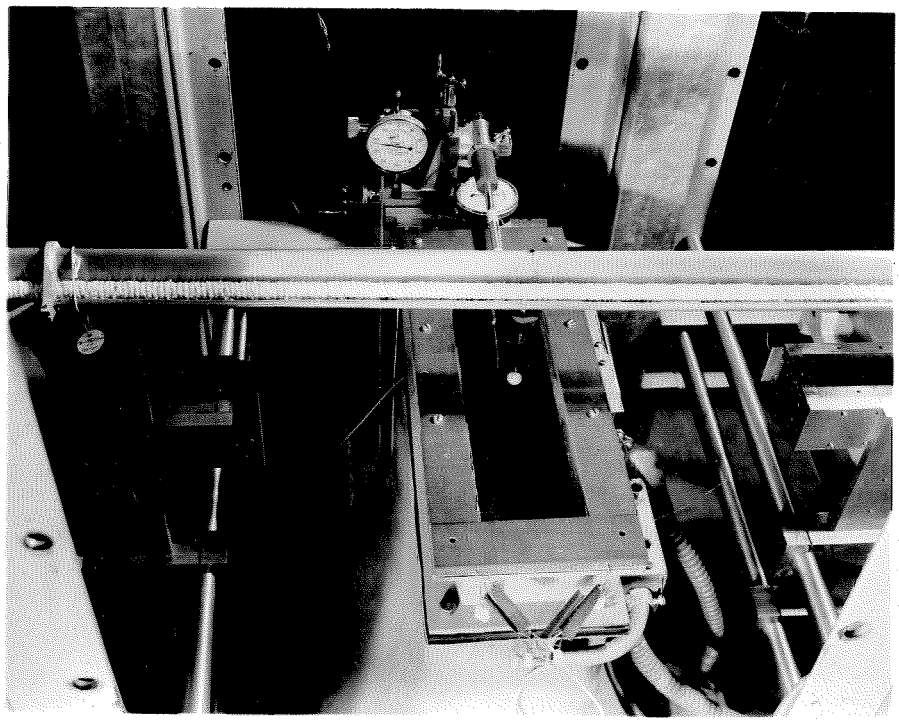

Figure 5. Punched Plate Assembly

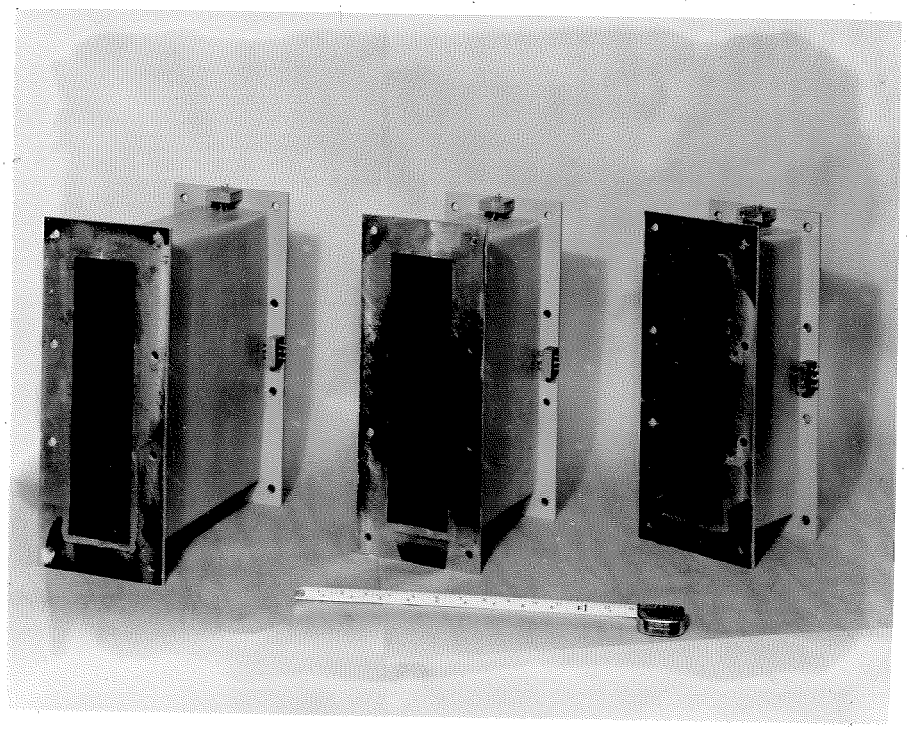

Figure 6. Extensions

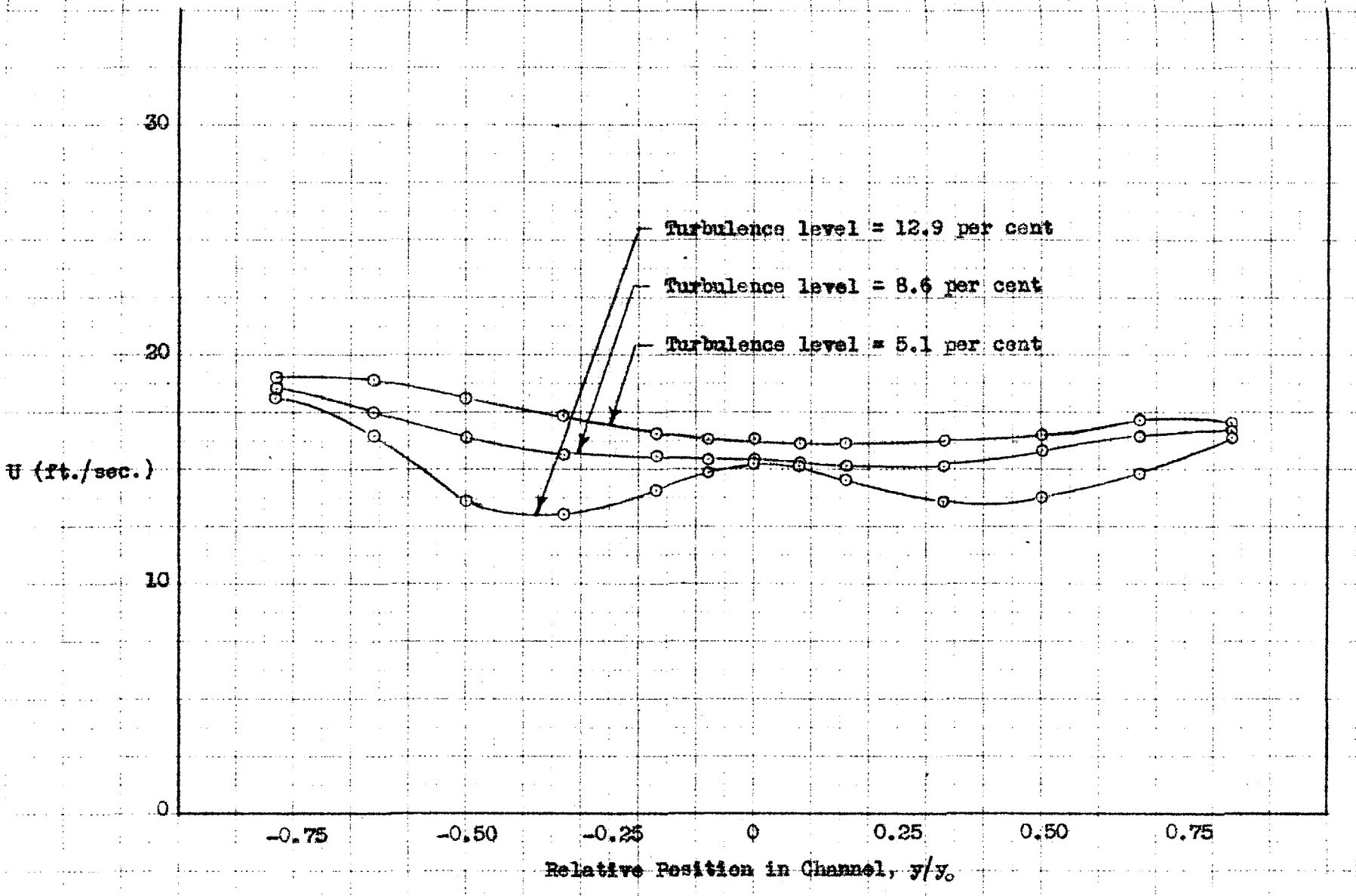

Figure 7. Velocity Distribution in Wake of Punched Plate for Gross Velocity of 16 feet per second

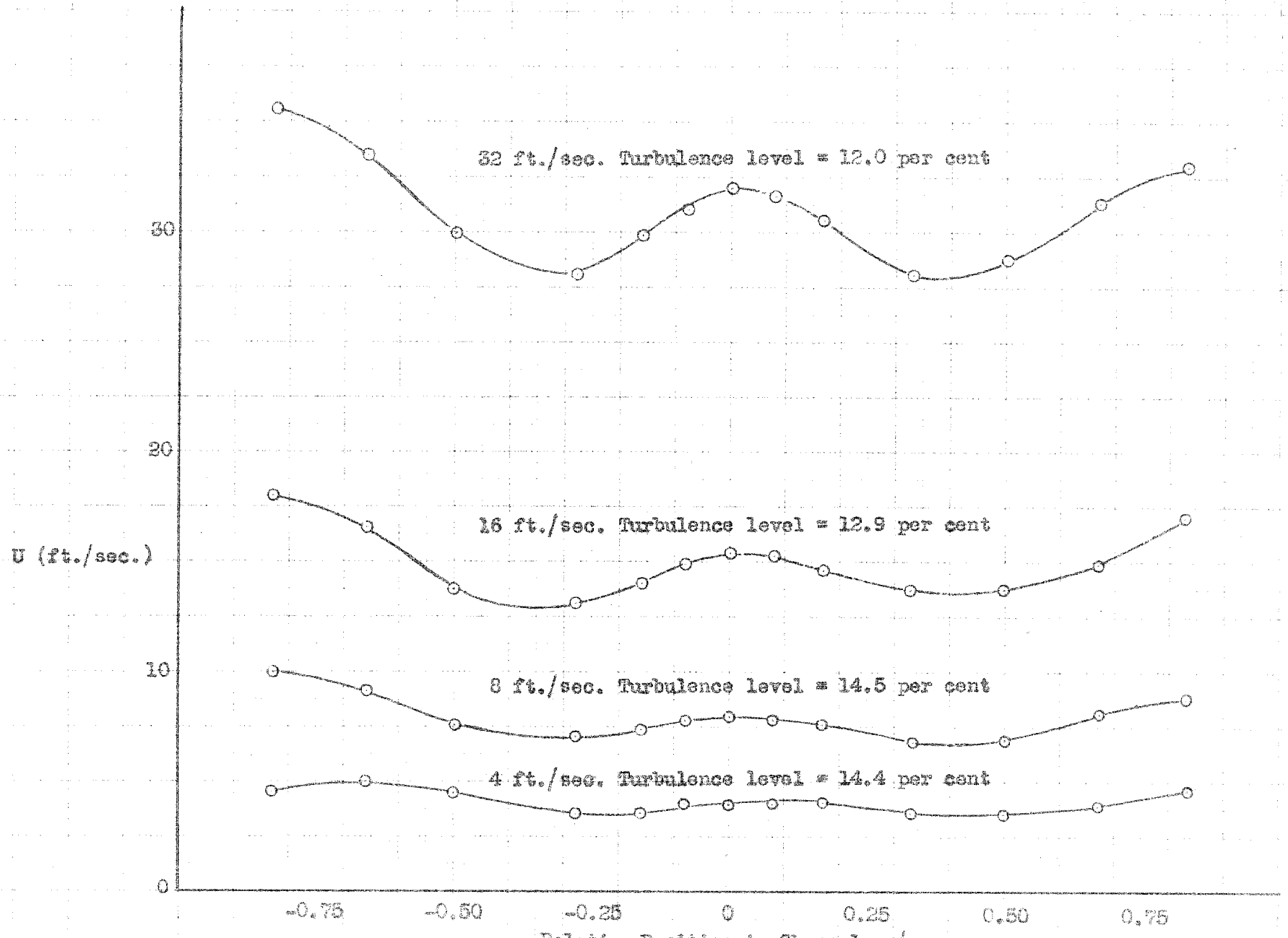

Figure 8. Velocity Distribution in Wake of Punched Plate for Gross Velocities of 4, 8, 16, and 32 feet per second

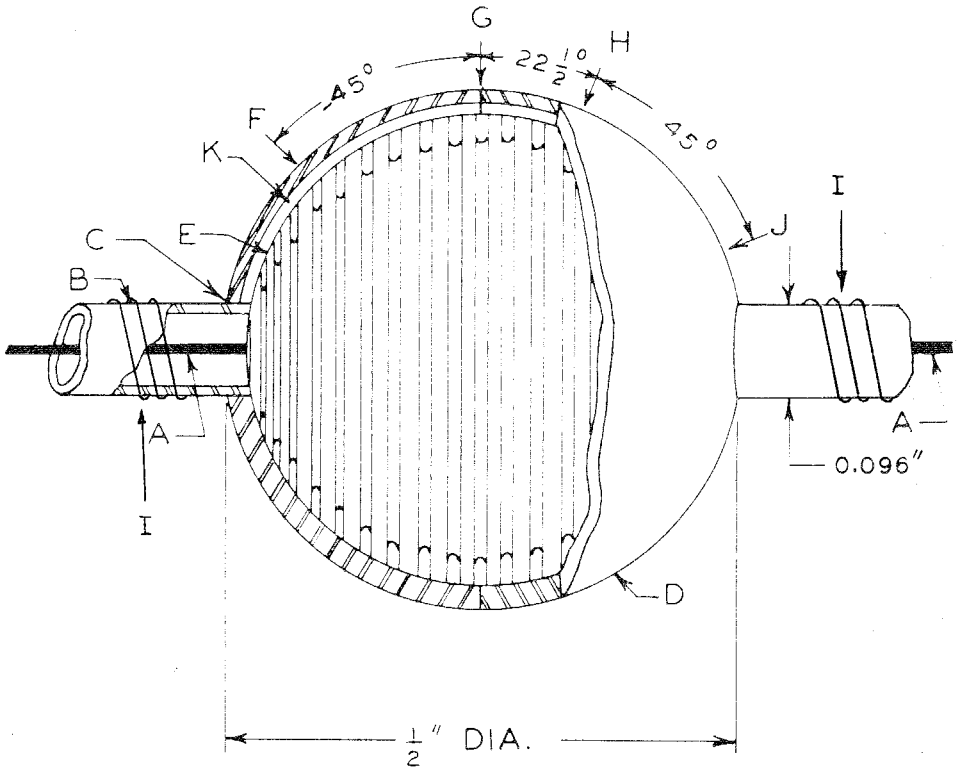

Figure 9
Sectional View of Heated Sphere

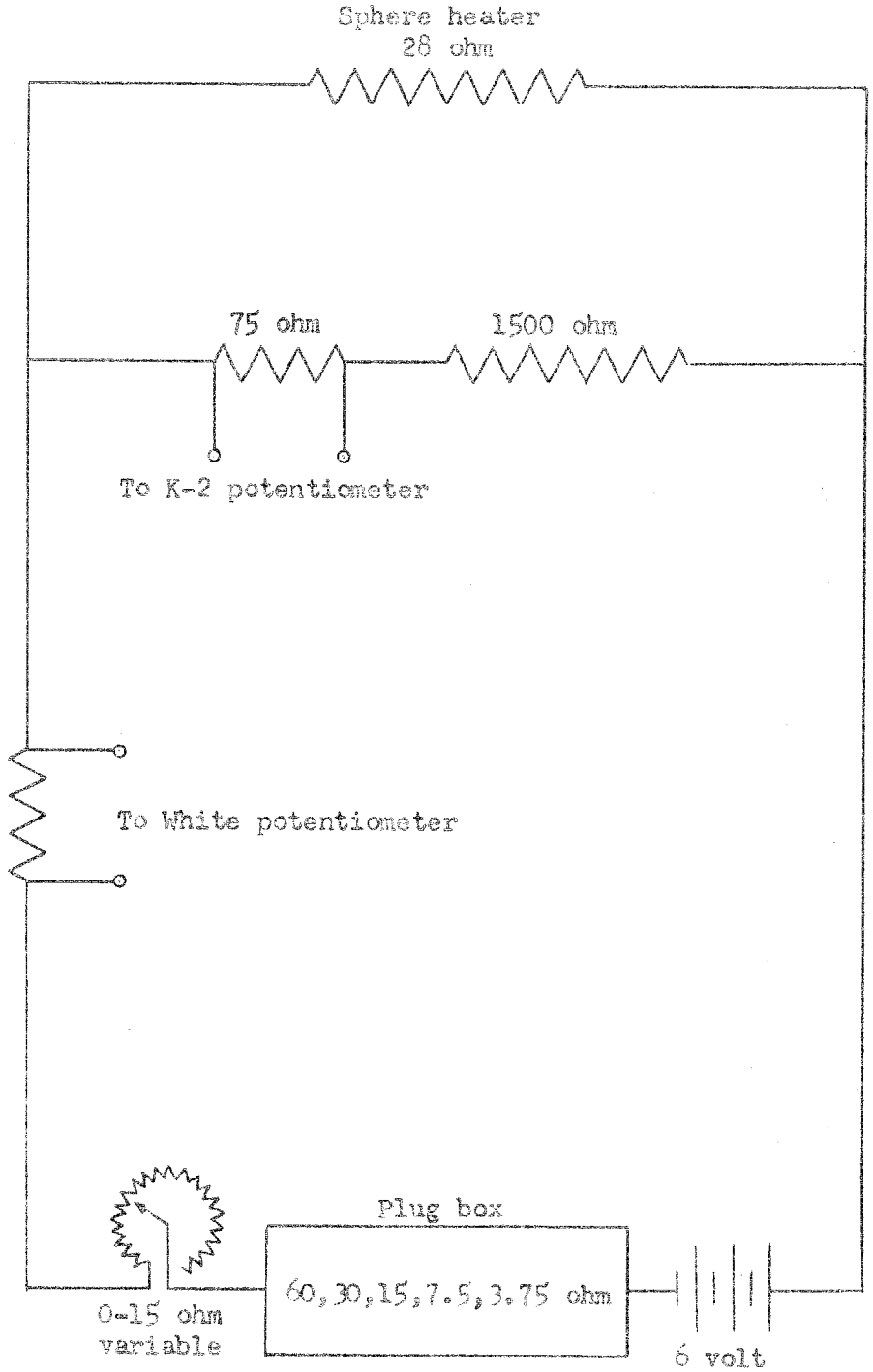

Figure 10. Heater Circuit for Sphere

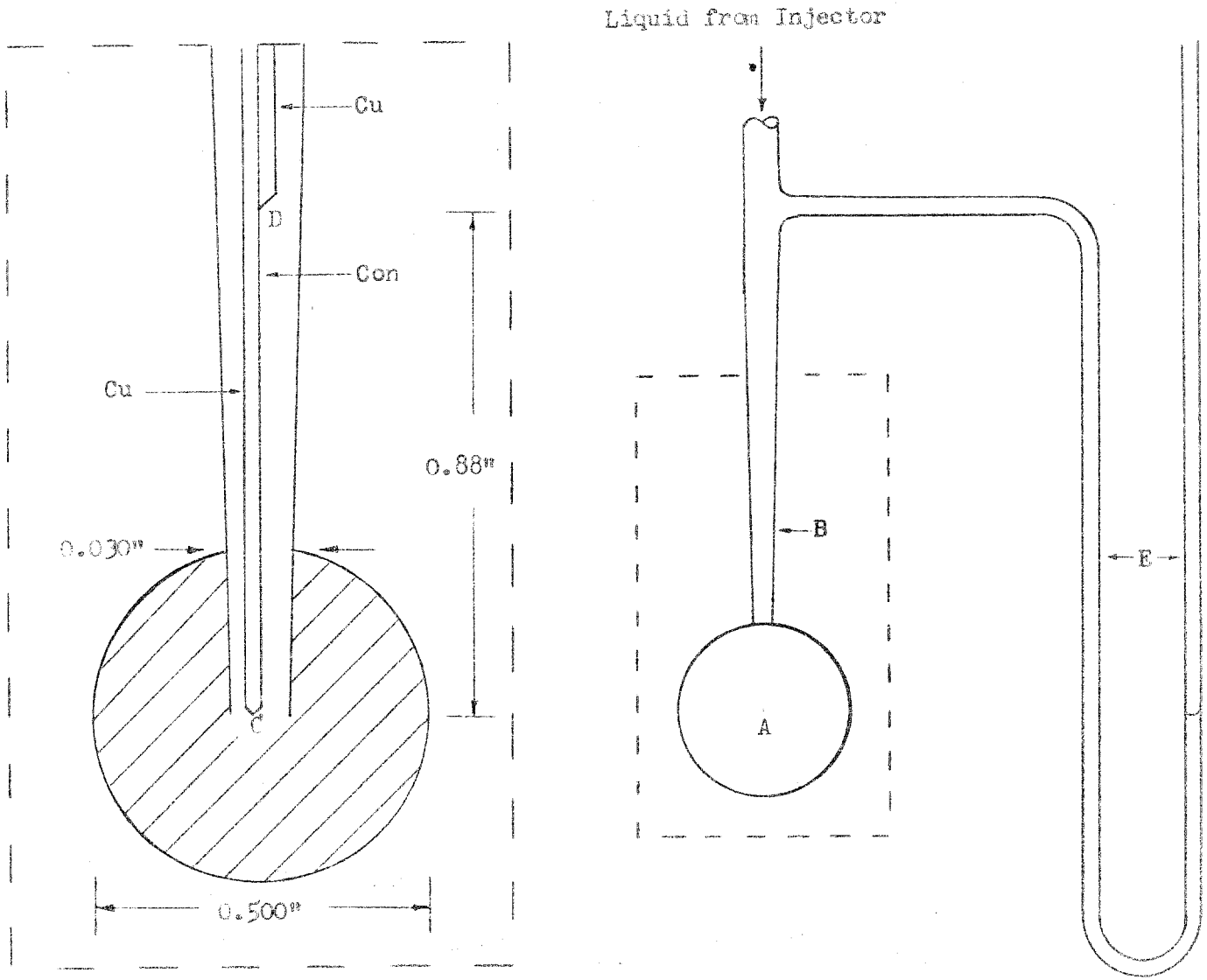

Figure 11. Details of Porous Sphere

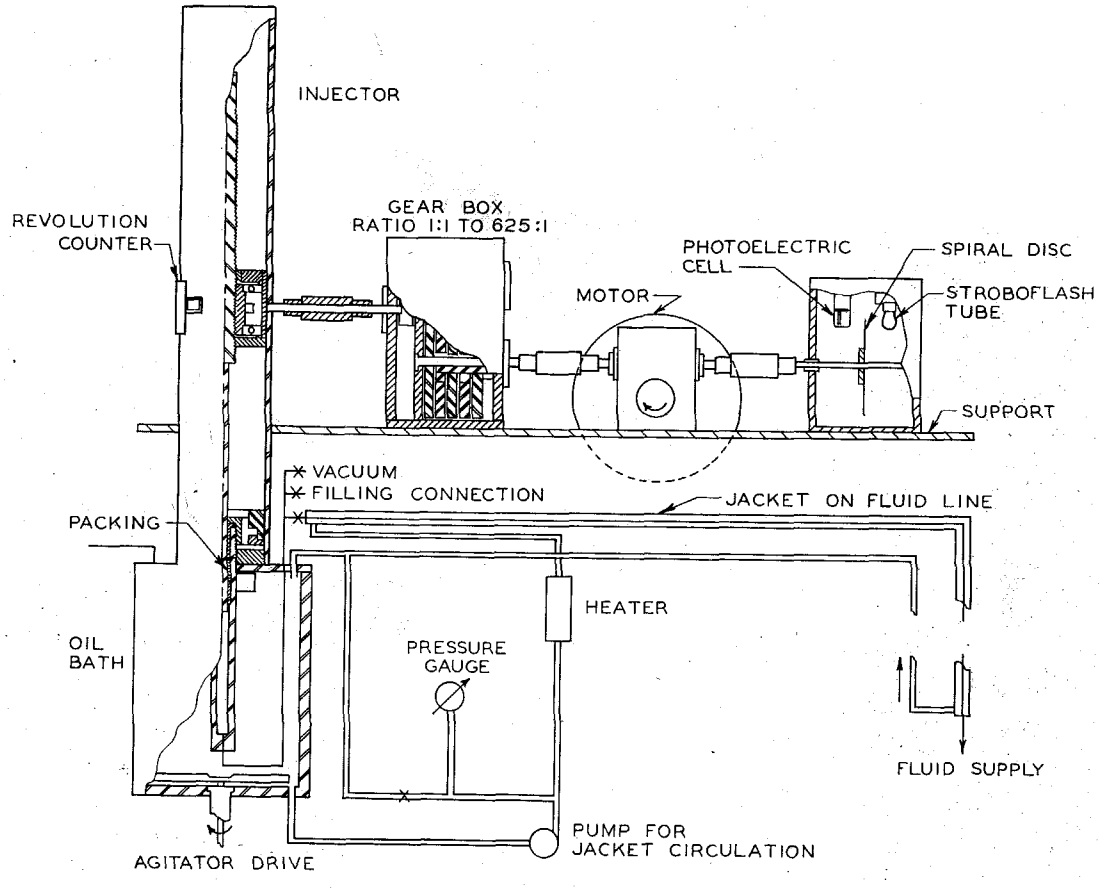

Figure 12. Fluid Injector System

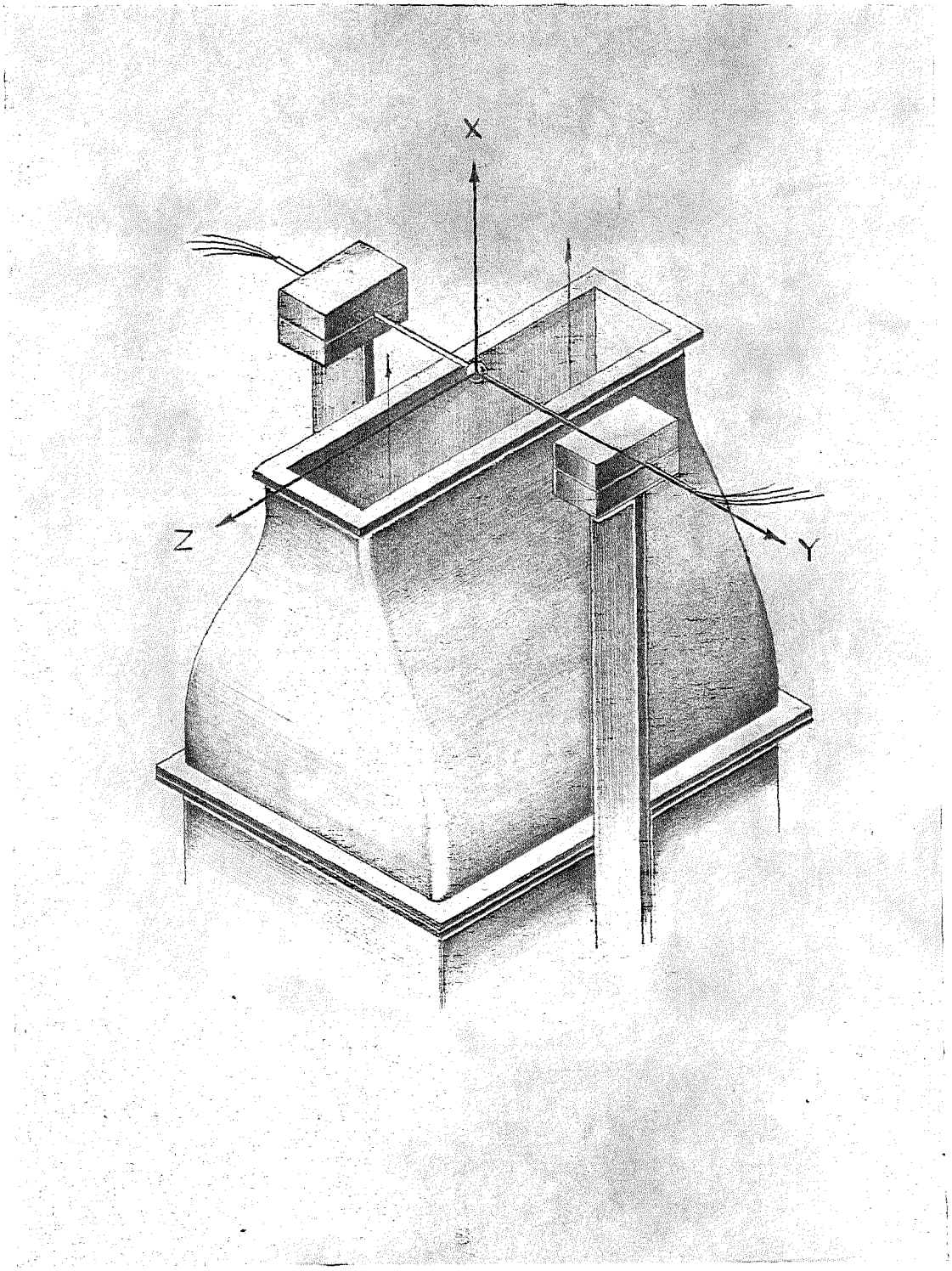

Figure 13. Sphere Coordinate System

The thermoelement is 0.001 in. diameter wire. The junctions are silver-soldered.

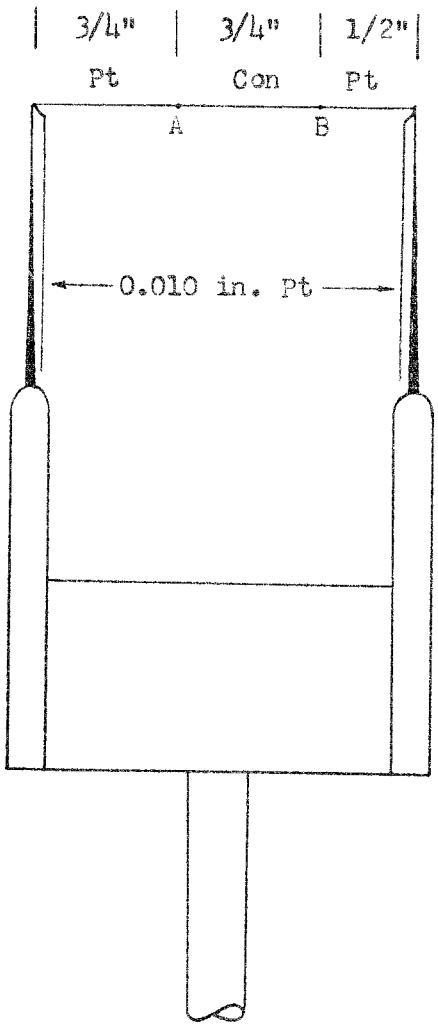

Figure 14. Details of Platinum-Constantan Thermocouple

Wires 0.0003 in. in diameter are flame-welded to form junction A. Wires 0.010 in. in diameter are silver-soldered to form junction B.

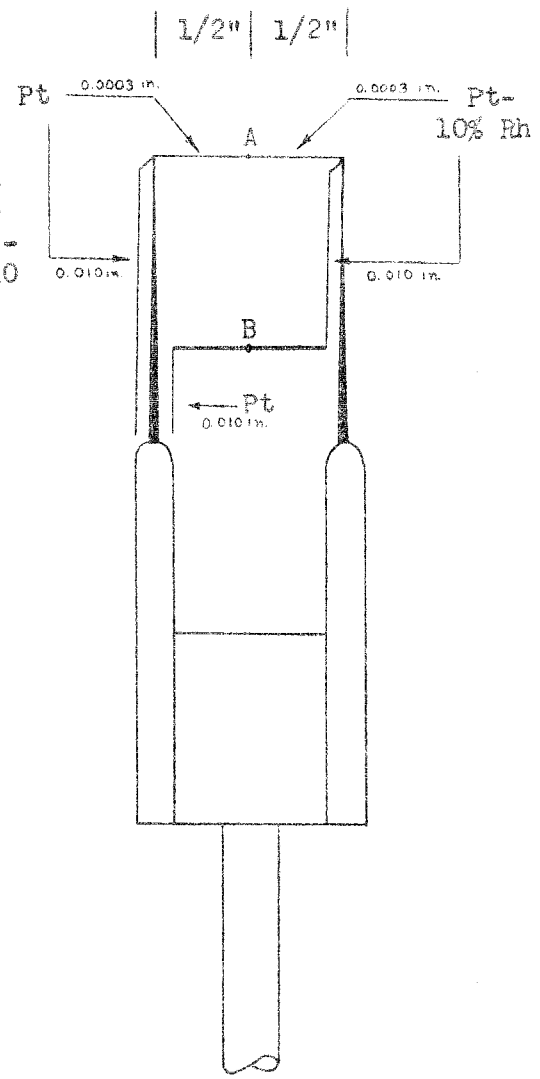

Figure 15. Details of
Platinum-Platinum 10% Rhodium Thermocouple

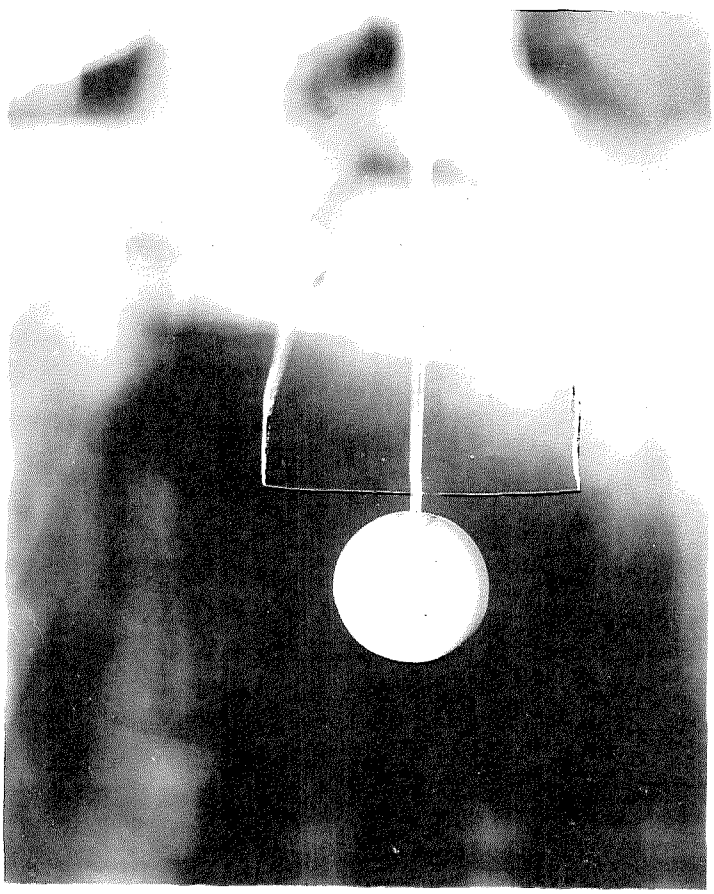

Figure 16. Porous Sphere and Thermocouple in Position

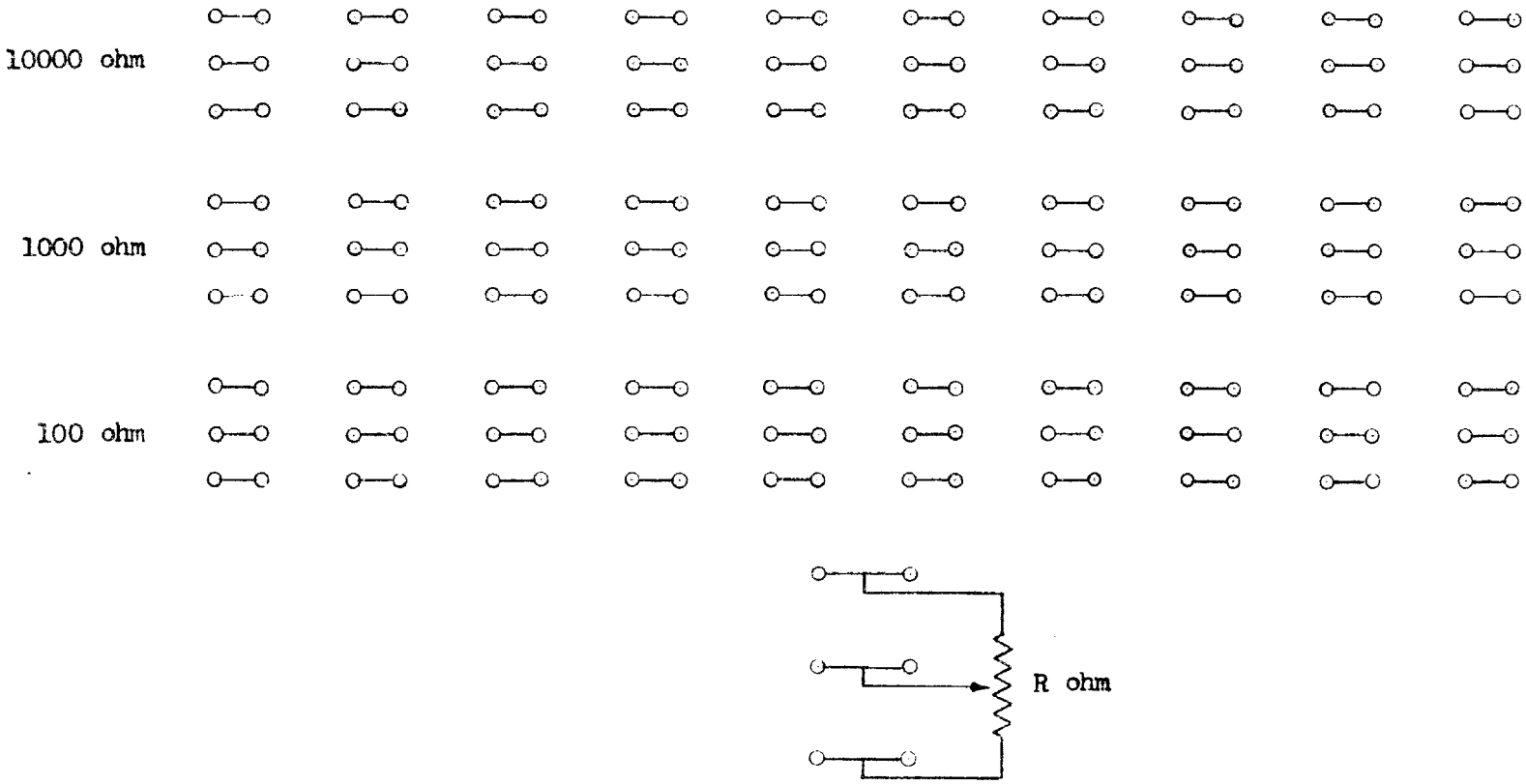

Figure 17. Analog Panel

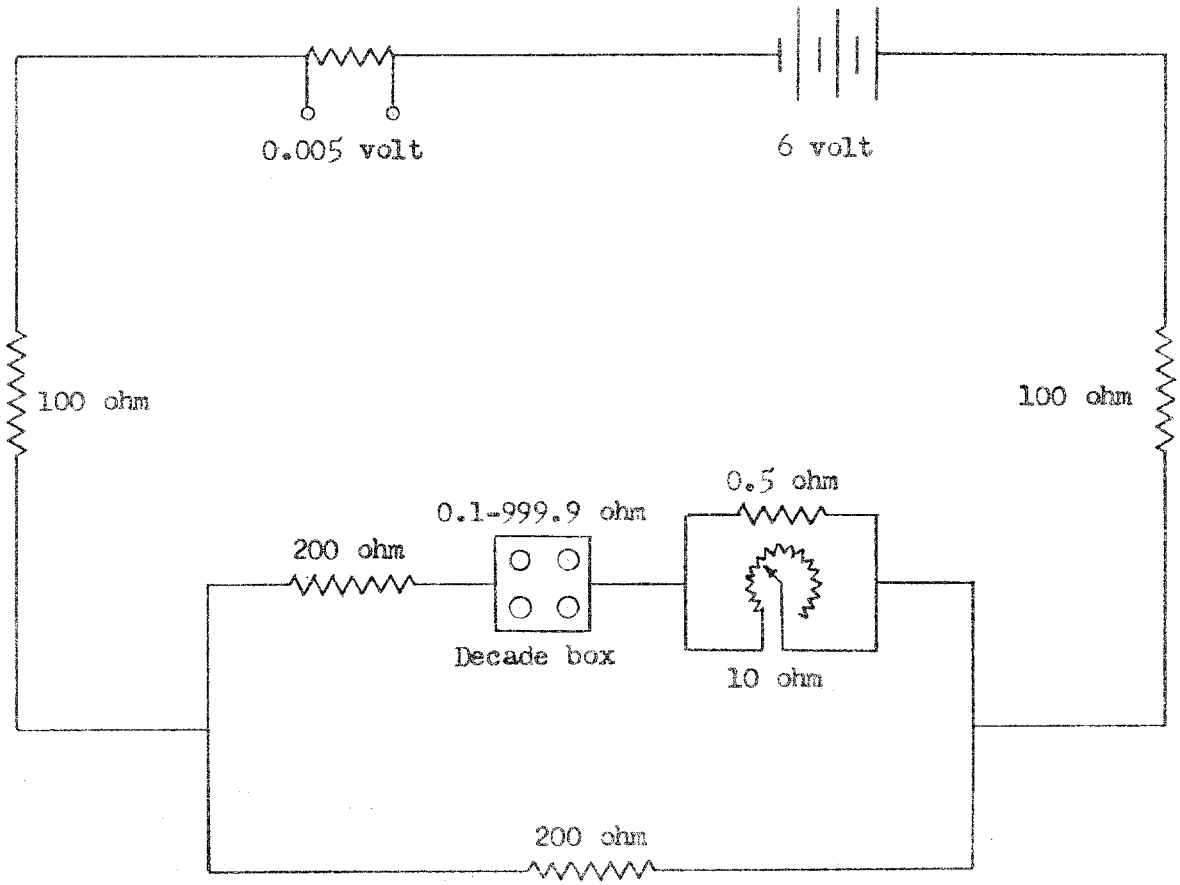

Figure 18. Analog Voltage Circuit

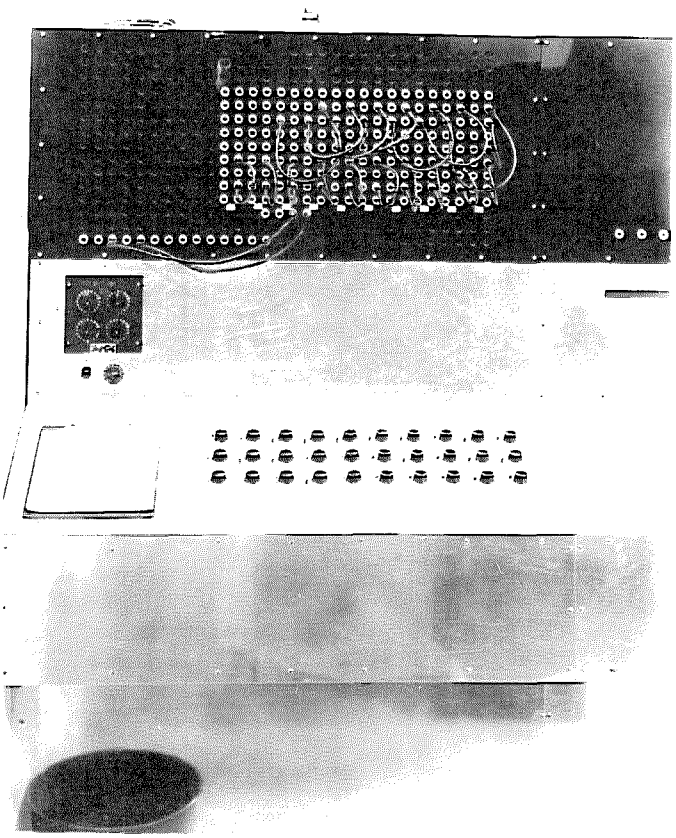

Figure 19. Analog Bench

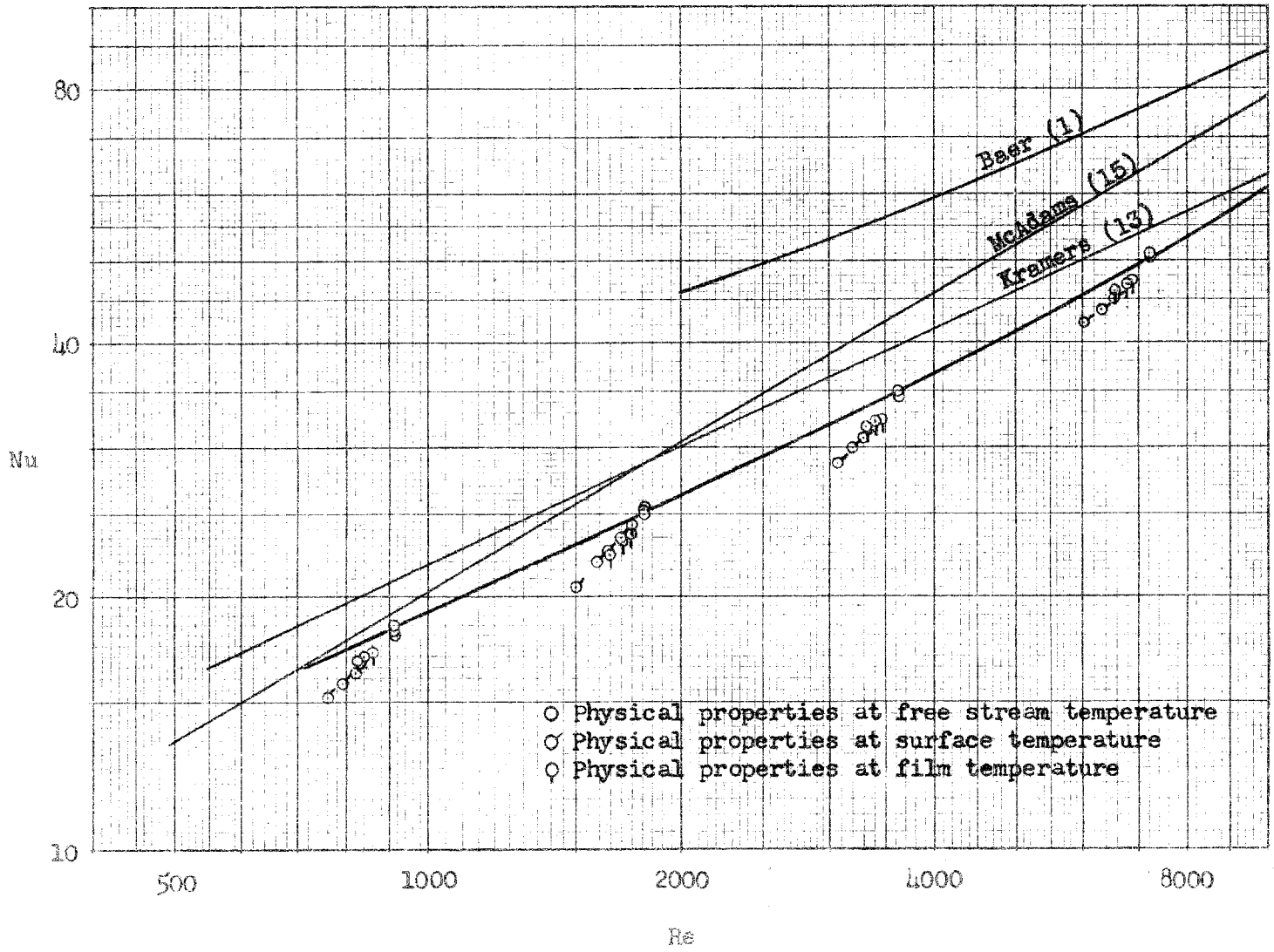

Figure 20. Nusselt number versus Reynolds number - Air Jet

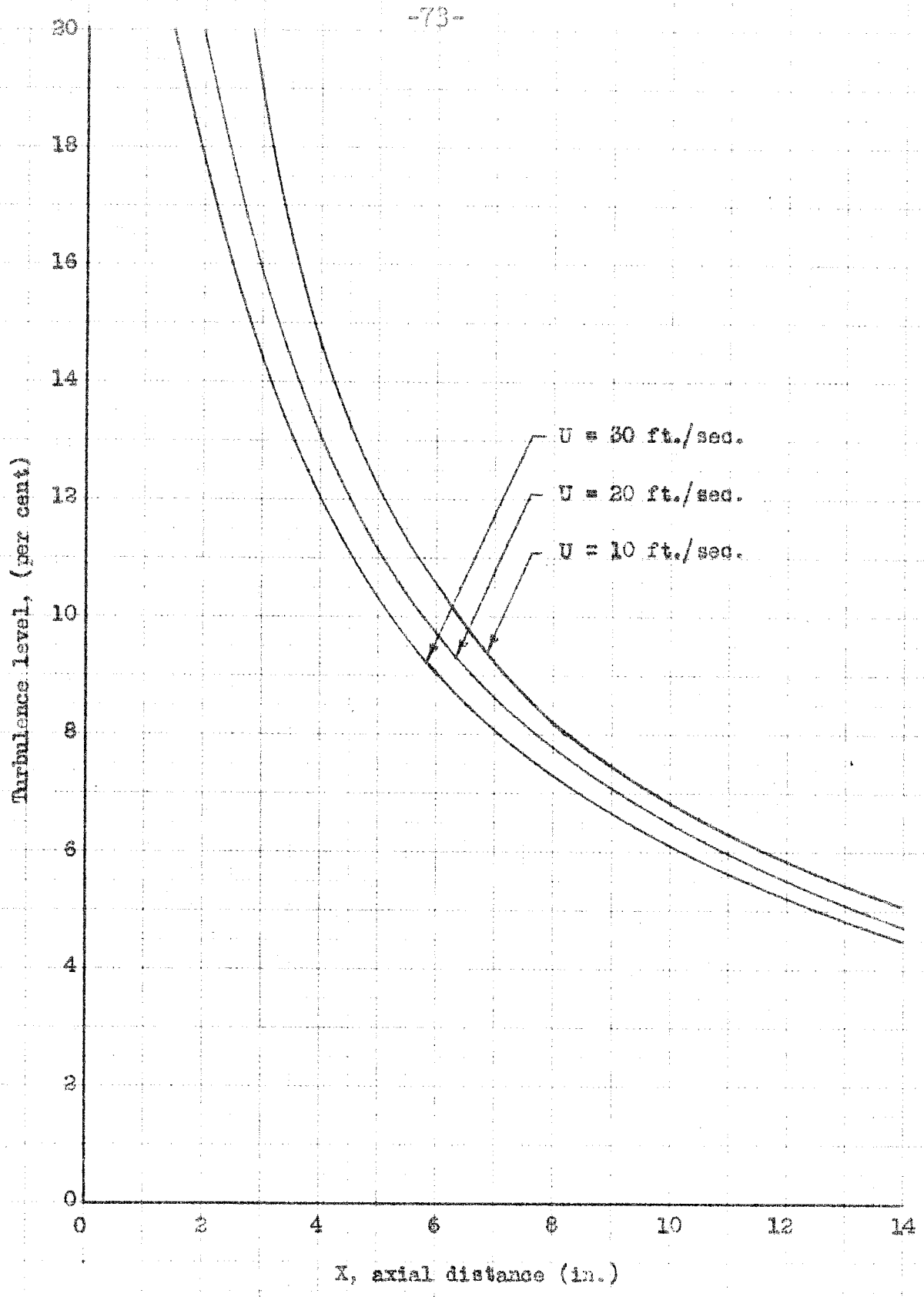

Figure 21. Turbulence Level versus Axial Distance

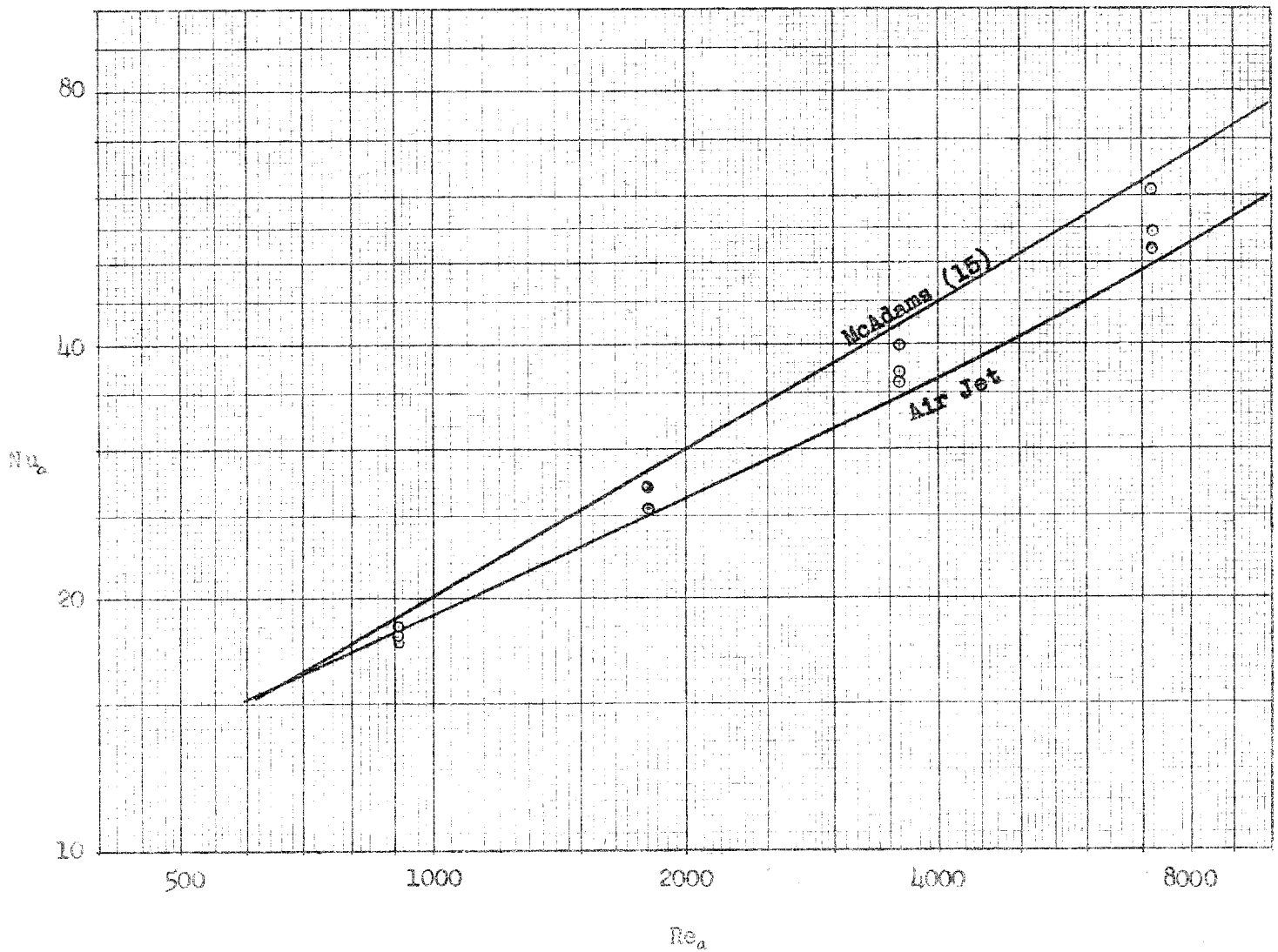

Figure 22. Nusselt number versus Reynolds number - Wake of Punched Plate

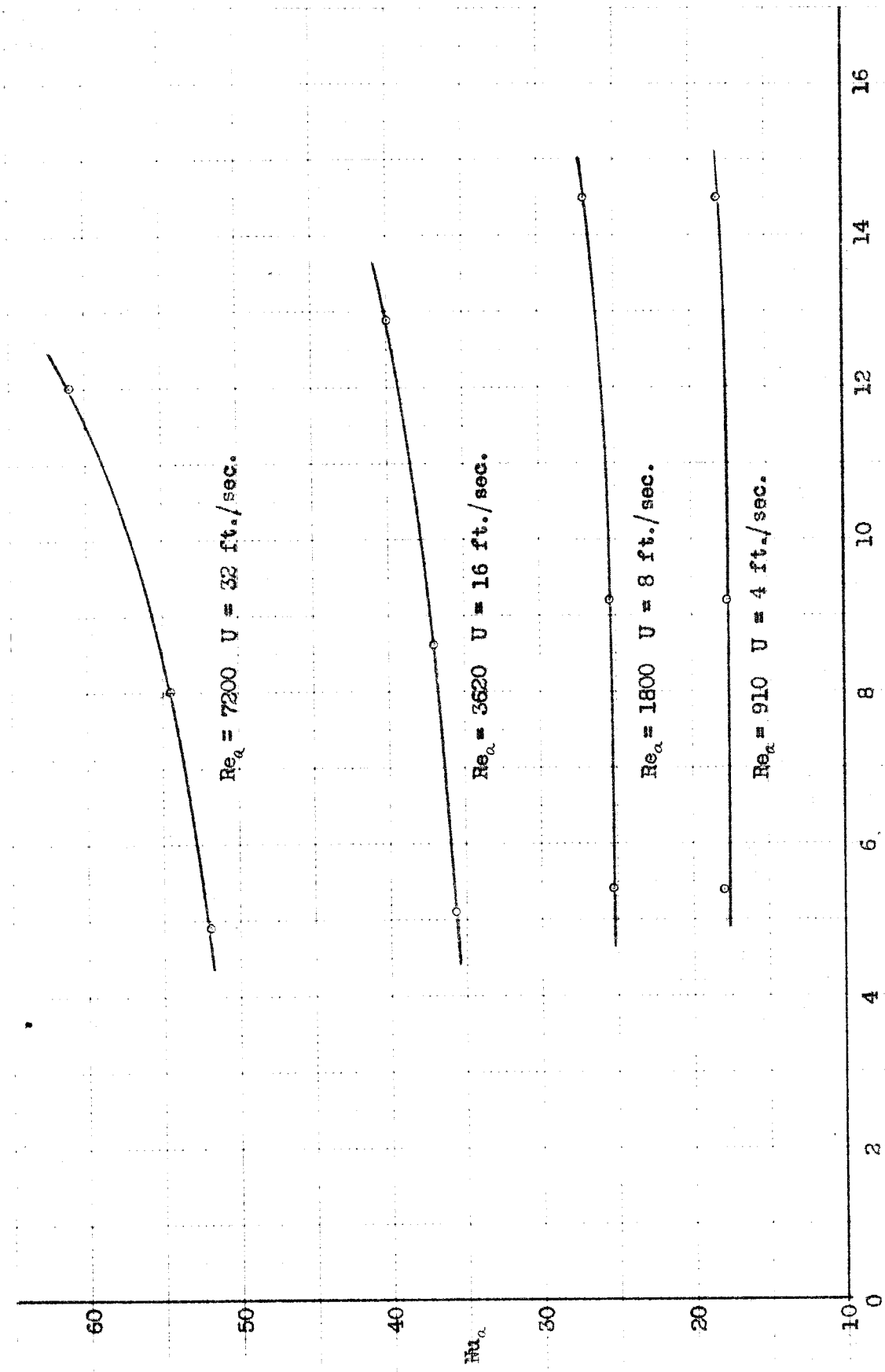

Figure 23. Nusselt number versus Turbulence Level - Wake of Punched Plate

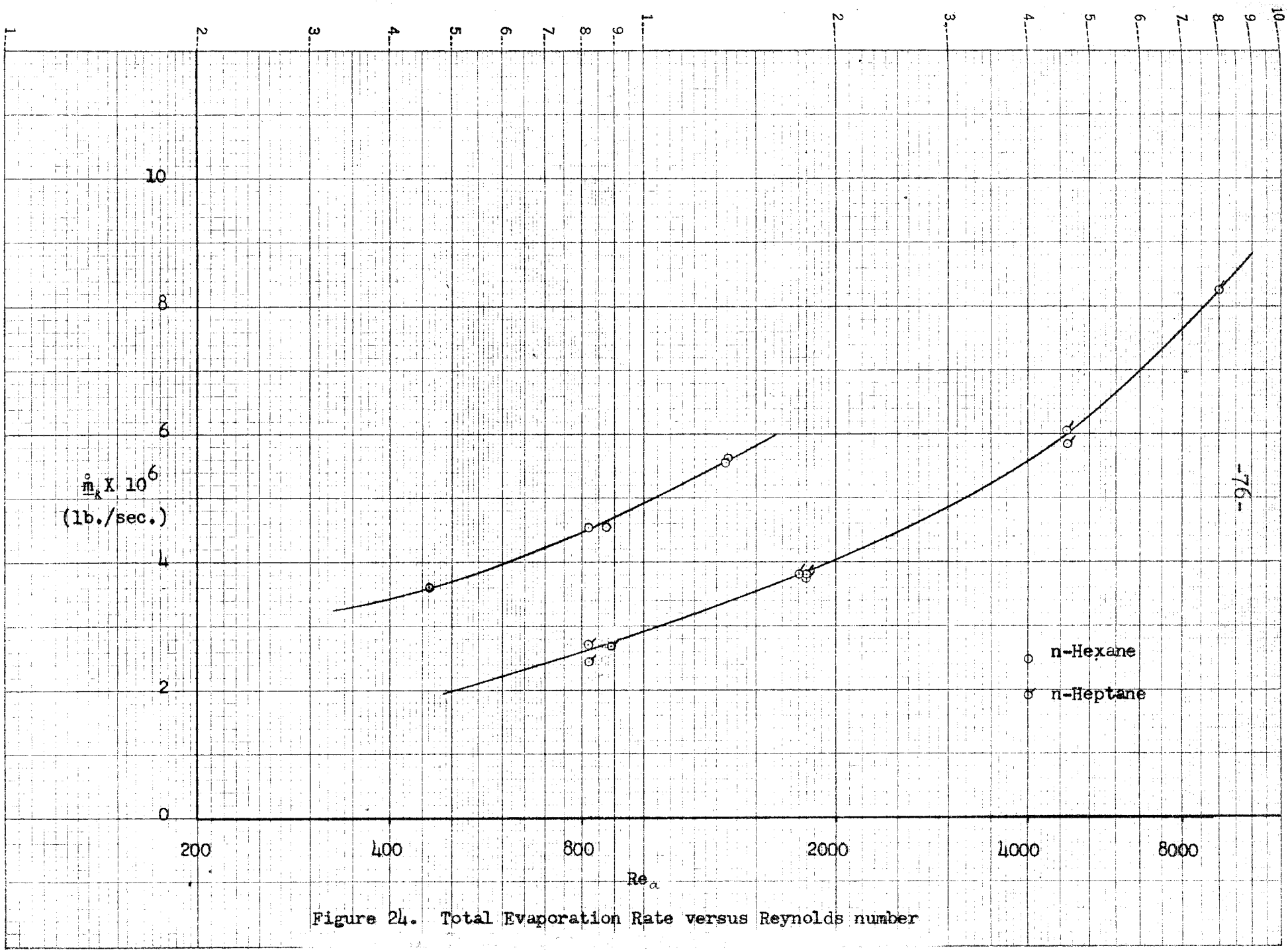

Figure 24. Total Evaporation Rate versus Reynolds number

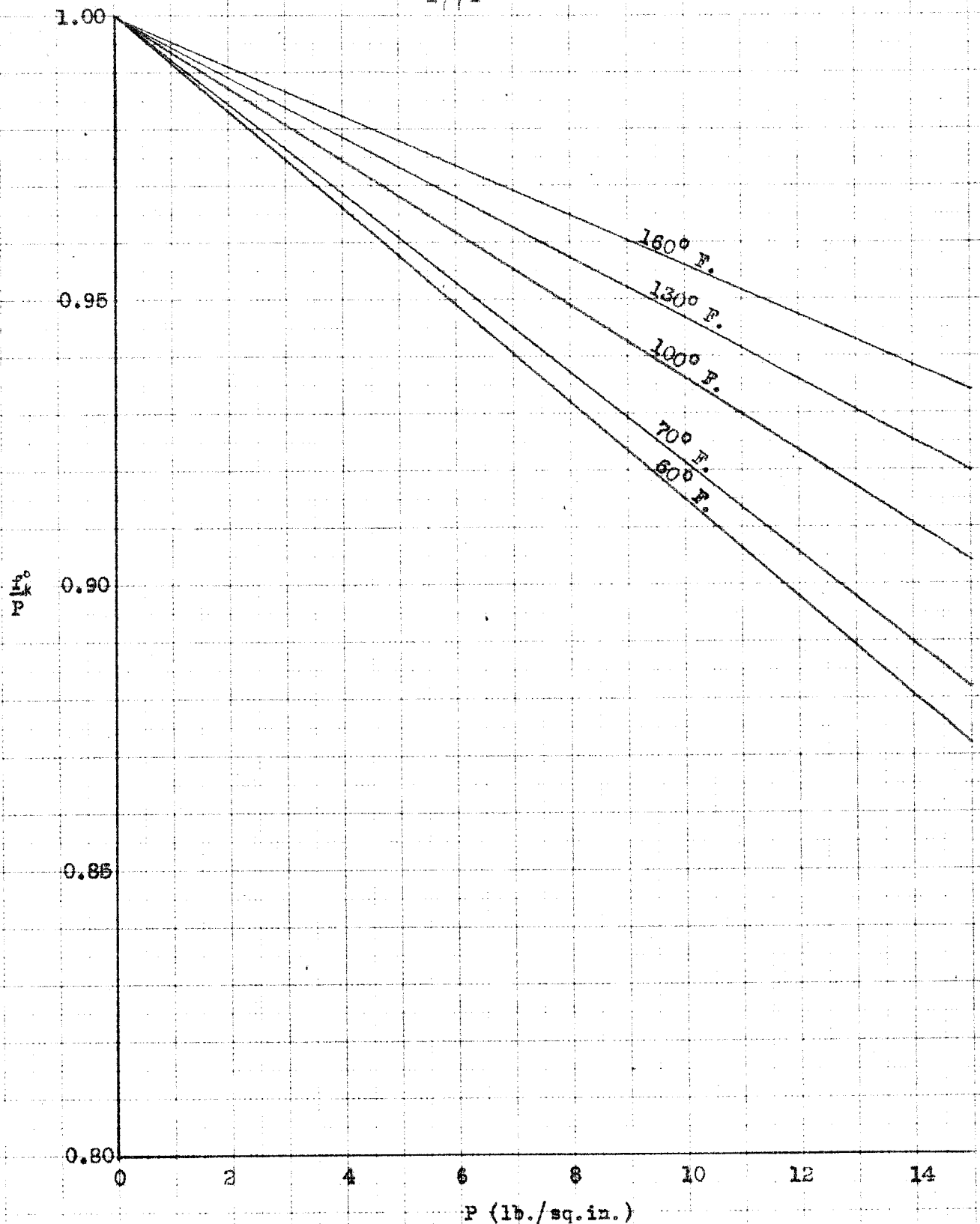

Figure 25. Fugacity of n-Heptane Vapor

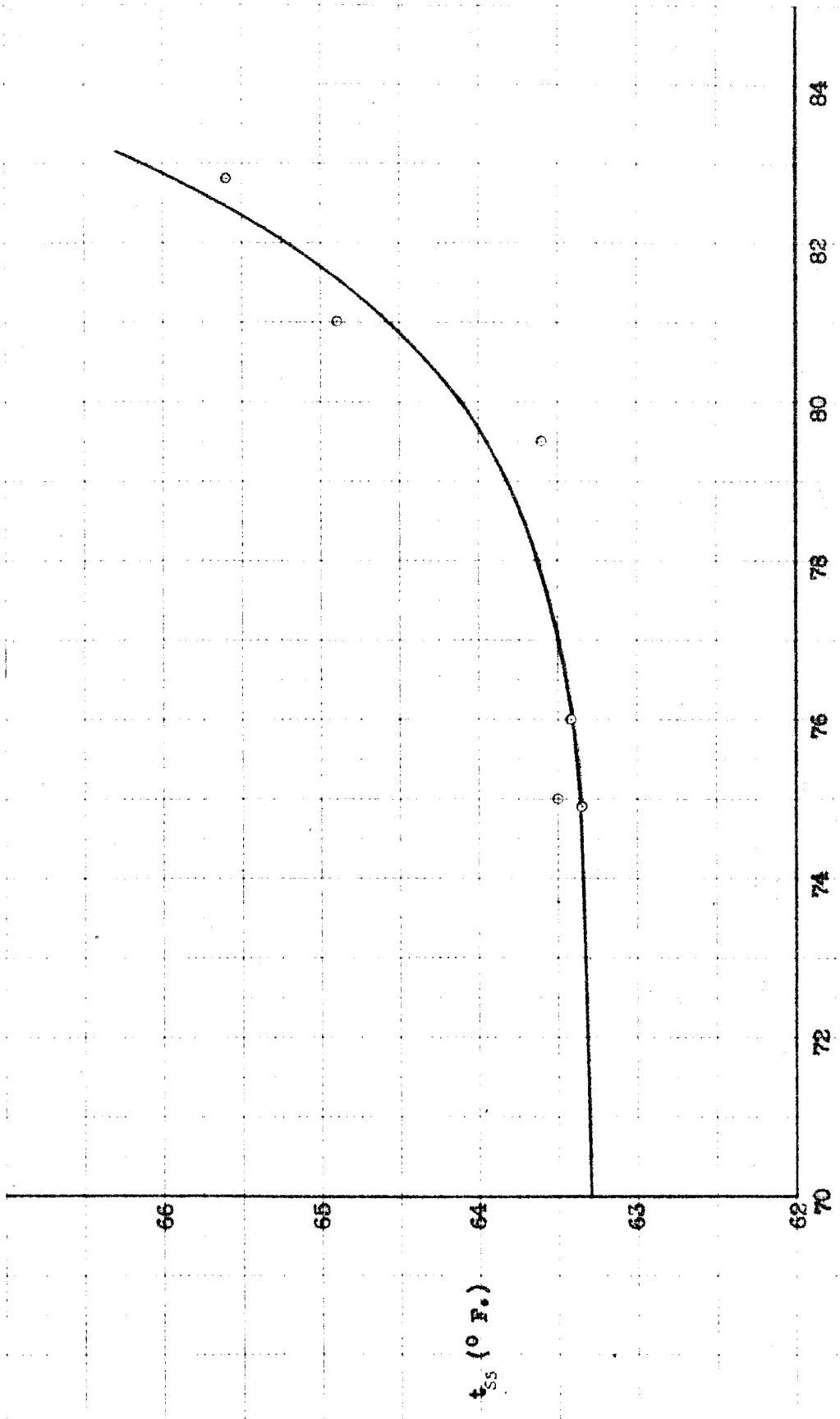

Figure 26. Average Surface Temperature versus Temperature at Center of Sphere

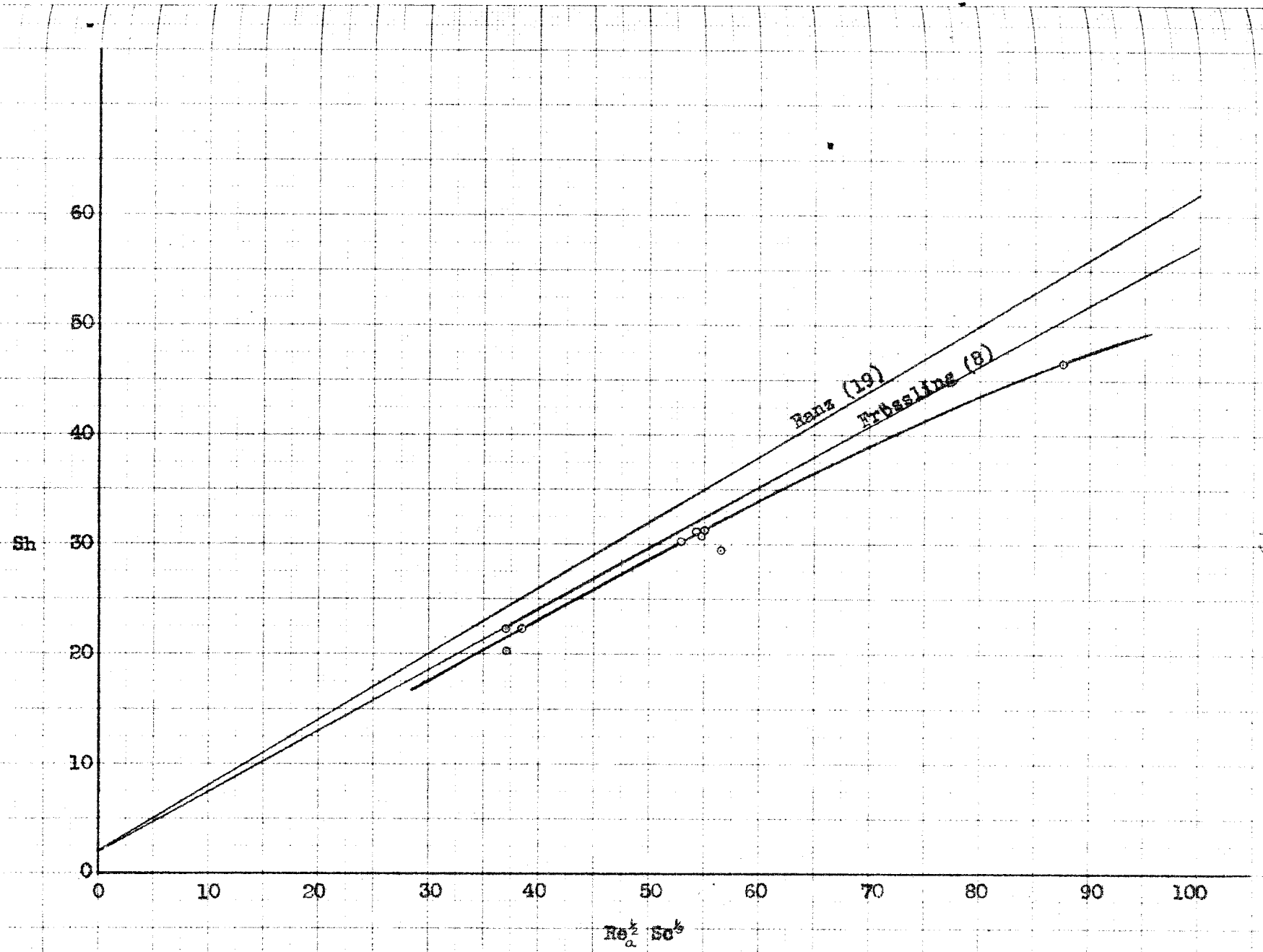

Figure 27. Sherwood number versus
(Reynolds number)$^{1/2}$ (Schmidt number)$^{1/3}$ - Air Jet

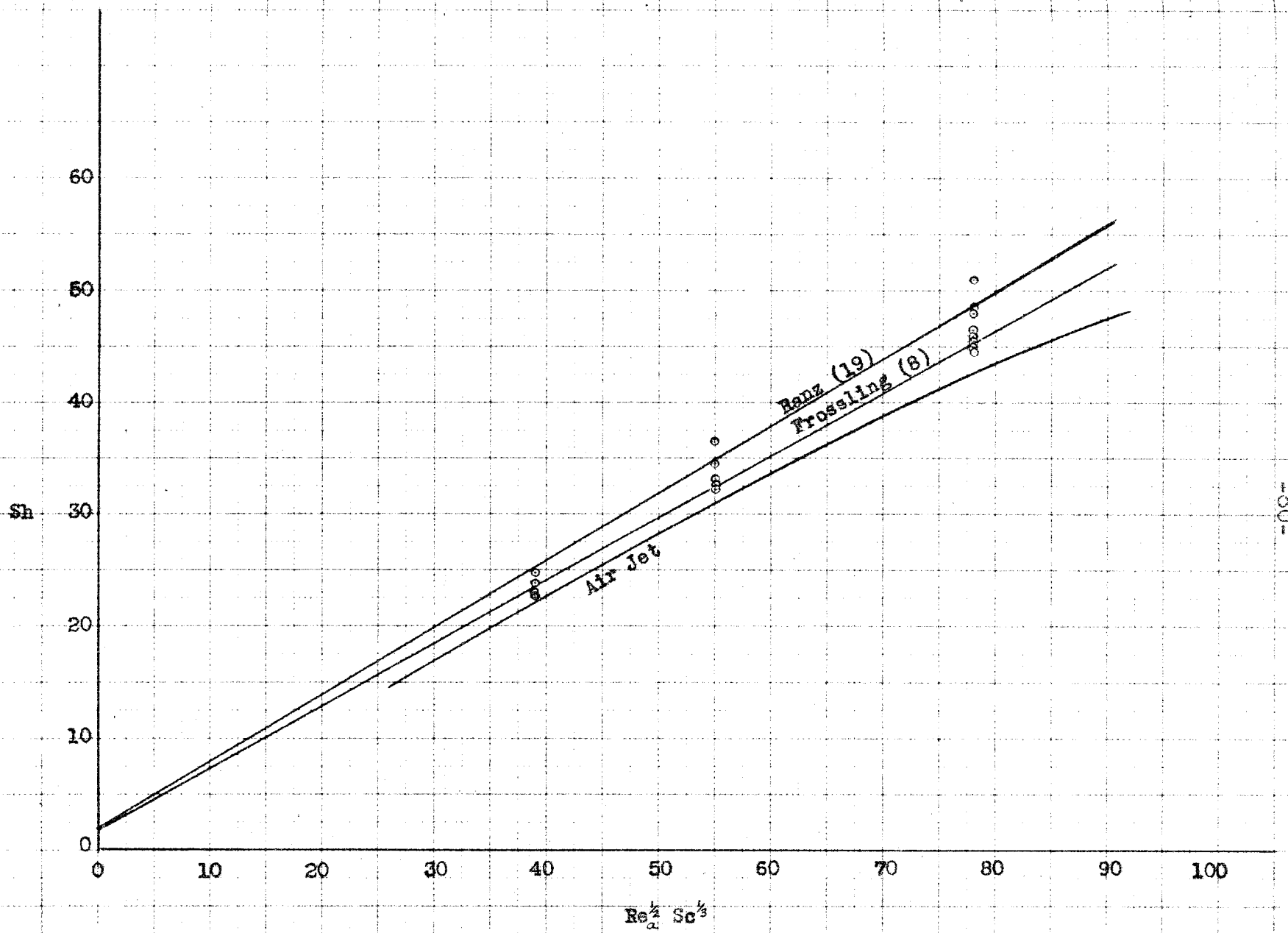

Figure 28. Sherwood number versus
(Reynolds number)$^{1/2}$ (Schmidt number)$^{1/3}$ - Wake of Punched Plate

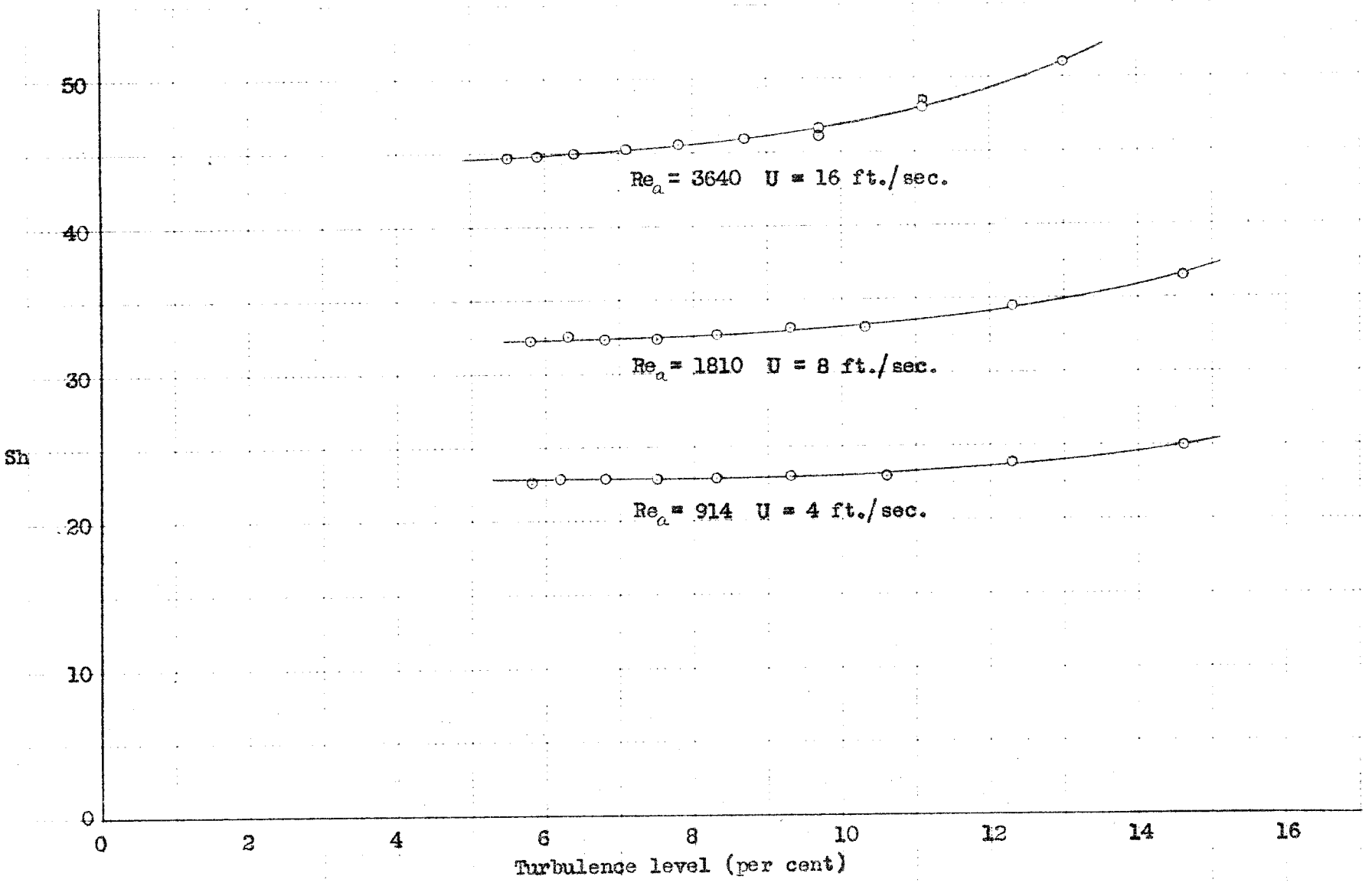

Figure 29. Sherwood number versus Turbulence Level - Wake of Punched Plate

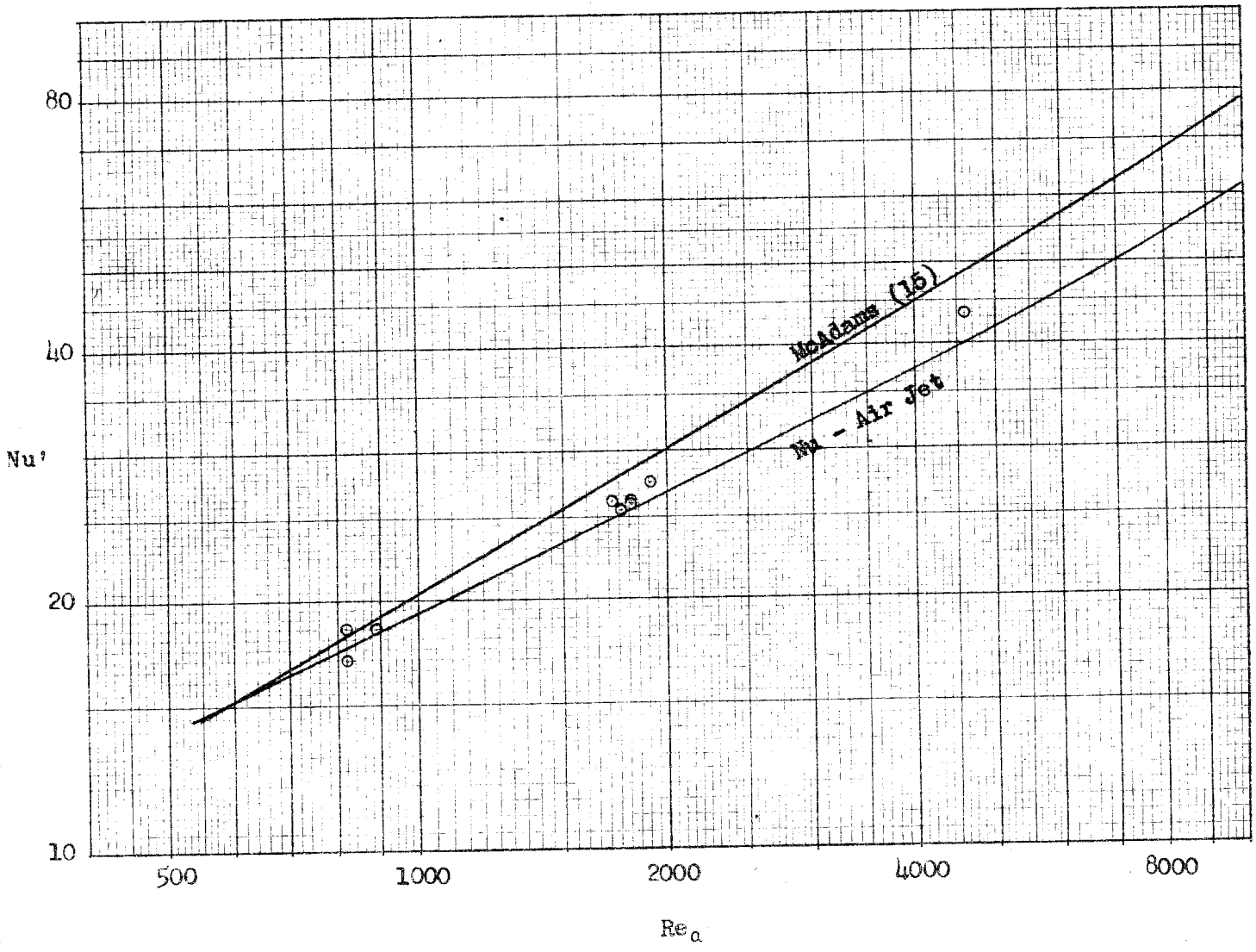

Figure 30. Modified Nusselt number versus Reynolds number - Air Jet

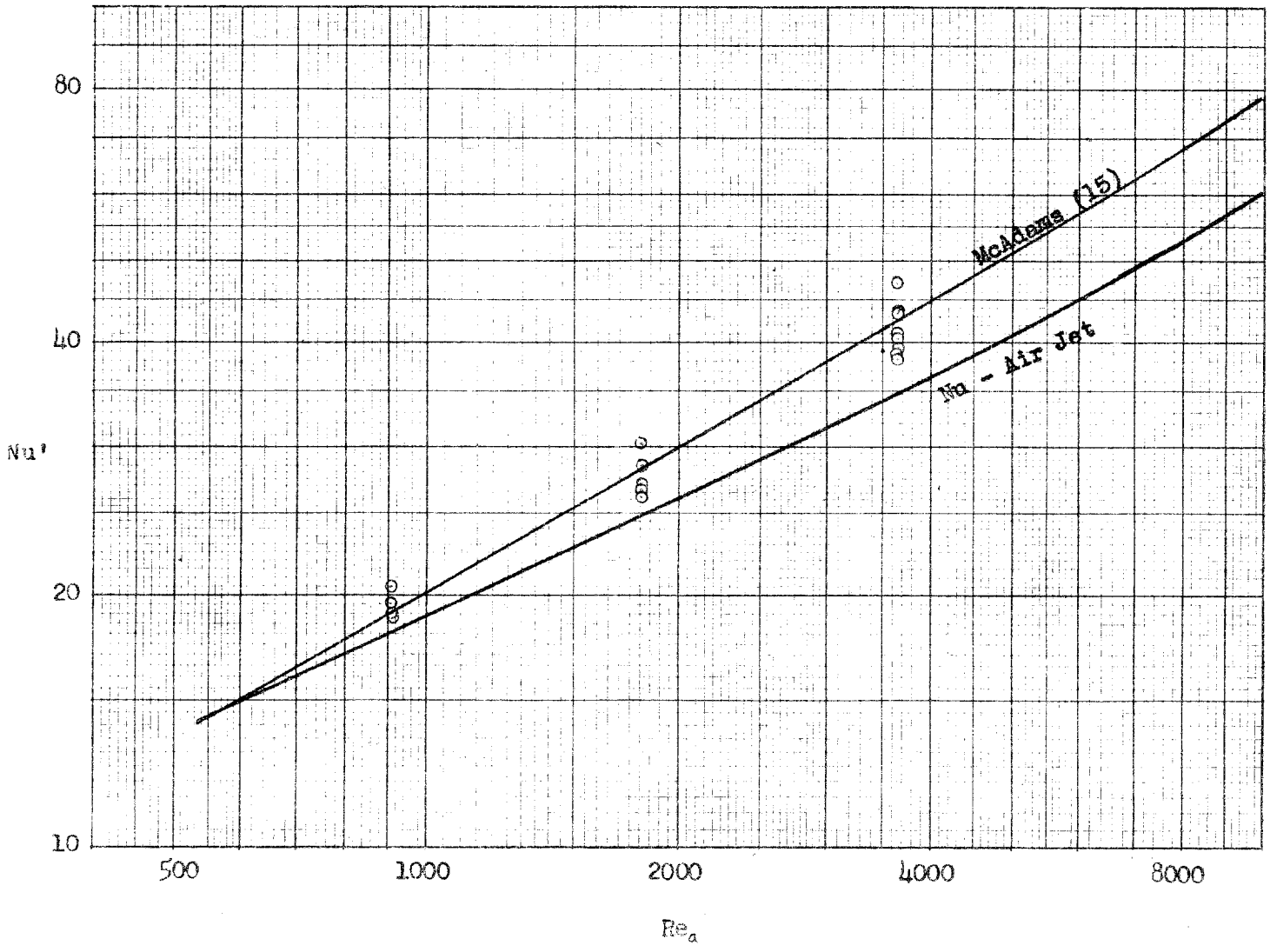

Figure 31. Modified Nusselt number versus Reynolds number - Wake of Punched Plate

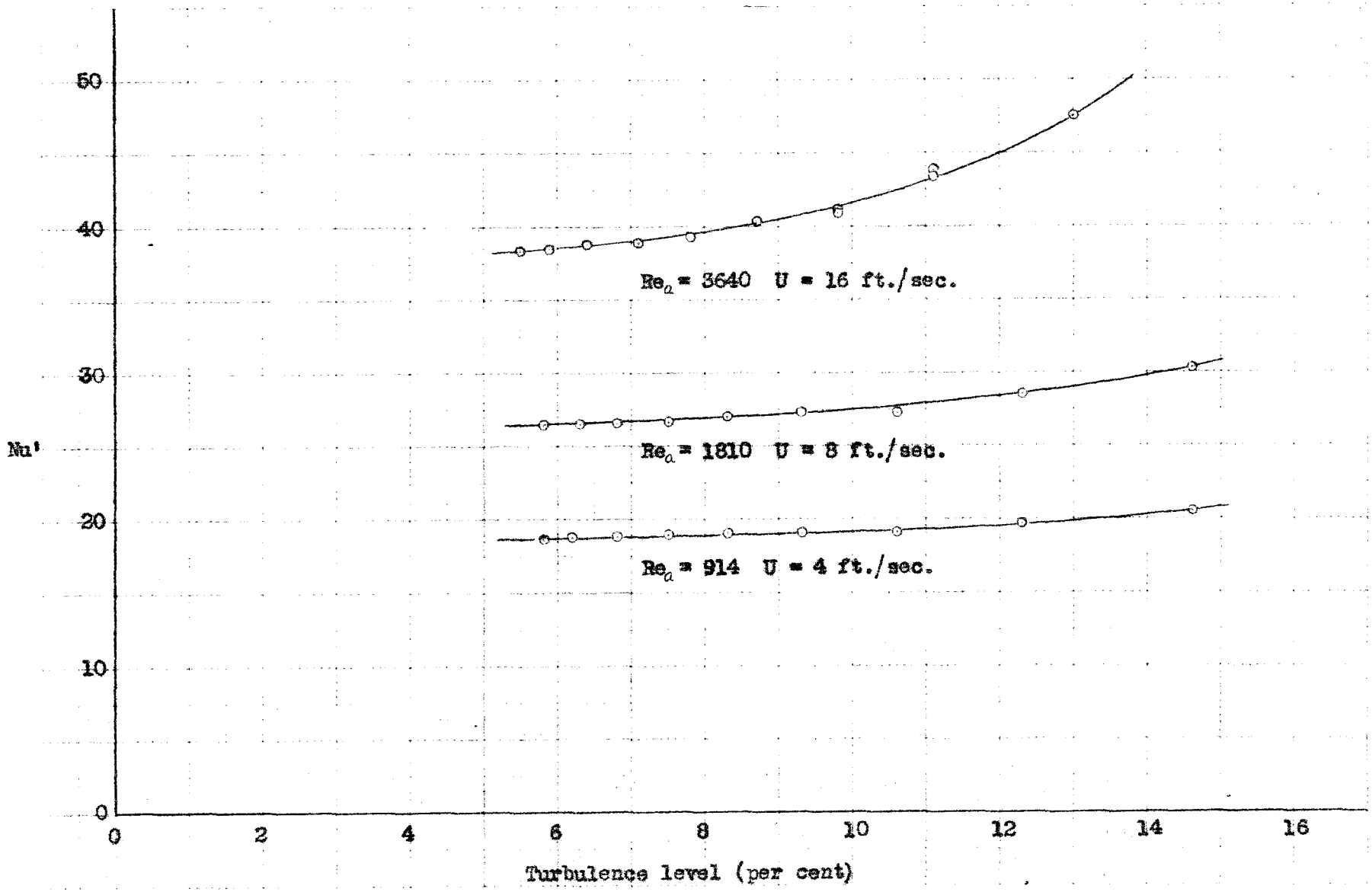

Figure 32. Modified Nusselt number versus Turbulence Level - Wake of Punched Plate

LIST OF TABLES

Table I.

Experimental Results of Heated Sphere in Air Jet

Test No.	Air Stream				Heated Sphere		
	P	t_a	n_{wr}	U	$\dot{Q} \times 10^3$	$\dot{Q}$	t_{ss}
	lb./sq.in.abs.	°F.	weight frac.	ft./sec.	Btu./sec.	Btu./sq.ft.sec.	°F.
60	14.339	100.2	0.0073	4.04	1.094	0.2006	205.1
64	14.340	100.1	0.0077	4.04	0.783	0.1436	175.9
68	14.308	100.2	0.0098	4.07	1.533	0.2810	245.1
61	14.360	99.8	0.0090	8.07	1.093	0.2005	176.6
66	14.362	100.0	0.0121	8.05	0.783	0.1436	154.4
69	14.372	100.1	0.0083	8.04	1.531	0.2807	205.9
80	14.287	100.1	0.0057	8.05	2.085	0.3823	245.9
70	14.332	100.0	0.0091	16.24	1.533	0.2810	178.2
71	14.370	100.1	0.0082	16.20	2.086	0.3824	205.5
73	14.195	100.1	0.0068	16.41	2.856	0.5236	243.8
74	14.426	100.0	0.0096	32.08	2.086	0.3825	173.1
75	14.384	100.1	0.0077	32.17	2.856	0.5235	199.5
79	14.323	100.0	0.0077	32.11	4.155	0.7617	243.0

Table II.

Experimental Results of Heated Sphere in Wake of Punched Plate

Test No.	Air Stream					Heated Sphere		
	P	t_a	n_{wr}	U	X	$\dot{Q} \times 10^3$	$\dot{Q}$	t_{ss}
	lb./sq.in.abs.	° F.	weight frac.	ft./sec.	in.	Btu./sec.	Btu./sq.ft.sec.	° F.
82	14.404	99.8	0.0048	4.03	4.13	0.784	0.1437	174.6
88	14.340	100.0	0.0100	4.06	7.12	0.783	0.1436	177.7
111	14.287	100.1	0.0064	4.07	13.04	0.783	0.1436	170.5
81	14.361	100.0	0.0054	8.01	4.07	1.094	0.2006	171.1
87	14.356	100.1	0.0088	8.05	7.12	1.094	0.2006	175.7
110	14.277	100.1	0.0042	8.06	13.03	1.094	0.2006	175.4
83	14.404	100.1	0.0057	16.13	4.13	1.533	0.2810	167.7
86	14.365	100.0	0.0093	16.22	7.12	1.533	0.2810	173.3
109	14.369	100.1	0.0030	16.13	13.04	1.533	0.2810	175.3
84	14.359	100.1	0.0059	32.05	4.13	2.087	0.3826	160.2
85	14.342	100.1	0.0093	32.19	7.12	2.087	0.3826	167.3
111	14.280	100.1	0.0043	32.22	13.04	2.085	0.3823	170.5

Table III.

Experimental Results of Porous Sphere in Air Jet

	Air Stream				Porous Sphere							
Test No.	P	t_a	n_{wr}	U	$\dot{m}_k \times 10^6$	$\dot{m}_k \times 10^4$	t_t	t_{sc}	t_{ss}	$f^\circ_{k,g}$	$f^\circ_{k,\ell}$	$n_{j_\circ}$
	lb./sq.in.abs.	°F.	weight frac.	ft./sec.	lb./sec.	lb./sq.ft.sec.	°F.	°F.	°F.	lb./sq.in.	lb./sq.in.	mole frac.
39	14.219	100.1	0.0046	6.01	5.518*			65.3				
40	14.286	100.1	0.0042	3.65	4.536*			61.0				
41	14.403	100.1	0.0057	2.05	3.633*			57.5				
42	14.361	100.0	0.0049	6.03	5.603*			65.6				
44	14.416	100.2	0.0043	3.88	4.550*			61.9				
45	14.226	99.9	0.0074	3.68	2.494	4.57		69.7	63.3**	12.548	0.594	0.9527
46	14.245	99.6	0.0069	8.06	3.777	6.92		73.0	63.3**	12.564	0.594	0.9527
47A	14.291	100.0	0.0069	35.55	8.218	15.07		93.5				
47B	14.300	100.1	0.0067	20.50	5.850	10.73		80.4	64.3**	12.613	0.612	0.9515
48	14.348	100.1	0.0060	3.65	2.721	4.99						
49	14.339	100.2	0.0071	7.82	3.795	6.96						
50	14.270	100.2	0.0057	3.97	2.720	4.99						
51	14.368	100.1	0.0056	20.39	6.049	11.09	97.7	82.2	65.4**	12.672	0.632	0.9501
52	14.322	100.1	0.0074	8.04	3.807	6.98	96.0	74.9	63.3	12.632	0.594	0.9530
53	14.265	115.0	0.0087	8.04	4.721	8.66	110.2	88.4	71.6	12.667	0.756	0.9403
54	14.263	85.1	0.0080	8.14	3.023	5.54	82.3	63.6	56.9	12.466	0.491	0.9606

* Evaporating liquid is n-hexane. n-Heptane employed in all other tests.

** Surface temperatures were determined from Figure 26.

Table IV.

Experimental Results of Porous Sphere in Wake of Punched Plate

Test No.	Air Stream P	t_a	n_{wr}	U	X	Porous Sphere $\dot{m}_K \times 10^6$	$\dot{m}_K \times 10^4$	t_t	t_{sc}	t_{ss}	$f^\circ_{K,g}$	$f^\circ_{K,\ell}$	n_j
	lb./sq.in.abs.	°F.	weight frac.	ft./sec.	in.	lb./sec.	lb./sq.ft.sec.	°F.	°F.	°F.	lb./sq.in.	lb./sq.in.	mole frac.
103	14.286	100.1	0.0058	16.25	6.06	5.875	10.77	98.3	81.2	64.7*	12.614	0.619	0.9509
					5.06	6.171	11.31	98.4	81.9	65.1		0.627	0.9503
104A	14.395	100.1	0.0063	16.15	12.04	5.564	10.20	98.0	79.9	64.1	12.682	0.611	0.9521
					11.04	5.604	10.27	98.2	80.1	64.2		0.613	0.9519
					10.04	5.624	10.31	98.3	80.2	64.2		0.613	0.9519
104B	14.372	100.1	0.0068	4.06	12.04	2.761	5.06	95.5	72.6	63.3	12.648	0.594	0.9530
					11.04	2.781	5.10	95.8	72.9	63.3		0.594	0.9530
					10.04	2.789	5.11	95.9	73.1	63.3		0.594	0.9530
104C	14.382	100.1	0.0058	8.03	12.03	3.911	7.17	97.0	75.6	63.3	12.657	0.594	0.9531
					11.03	3.937	7.22	97.1	75.8	63.3		0.594	0.9531
					10.03	3.942	7.23	97.3	76.0	63.4		0.596	0.9529
105A	14.326	100.1	0.0060	8.05	6.06	4.056	7.44	97.6	76.0	63.4	12.635	0.596	0.9528
					5.06	4.232	7.76	97.8	76.6	63.4		0.596	0.9528
					4.06	4.483	8.22	98.3	77.5	63.5		0.597	0.9528
105B	14.312	100.1	0.0065	4.07	6.06	2.828	5.18	96.3	72.9	63.3	12.623	0.594	0.9530
					5.06	2.914	5.34	96.7	73.3	63.3		0.594	0.9530
					4.06	3.051	5.59	97.6	74.0	63.3		0.594	0.9530

Table IV. (continued)

Test No.	Air Stream P	t_a	n_{wr}	U	X	Porous Sphere $\mathring{m}_K \times 10^6$	$\mathring{m}_K \times 10^4$	t_t	t_{sc}	t_{ss}	$f^\circ_{K,g}$	$f^\circ_{K,\ell}$	n°_j
	lb./sq.in.abs.	°F	weight frac.	ft./sec.	in.	lb./sec.	lb./sq.ft.sec.	°F.	°F.	°F.	lb./sq.in.	lb./sq.in.	mole frac.
105C	14.314	100.1	0.0058	16.22	6.06	5.890	10.80	98.5	80.7	64.4	12.639	0.614	0.9514
					5.06	6.179	11.33	98.5	81.2	64.7		0.619	0.9510
					4.06	6.631	12.16	98.8	82.3	65.5		0.634	0.9498
106A	14.301	100.1	0.0060	16.21	9.01	5.654	10.37	98.1	80.0	64.1	12.613	0.608	0.9518
					8.01	5.719	10.49	98.1	80.1	64.1		0.608	0.9518
					7.01	5.796	10.63	98.4	80.5	64.4		0.614	0.9513
106B	14.349	100.1	0.0055	8.03	9.01	3.951	7.24	97.3	75.8	63.4	12.655	0.596	0.9529
					8.01	4.001	7.34	97.5	76.2	63.4		0.596	0.9529
					7.01	4.035	7.40	97.9	76.5	63.4		0.596	0.9529
106C	14.323	100.1	0.0063	4.05	9.01	2.785	5.11	95.8	72.8	63.3	12.633	0.594	0.9530
					8.01	2.802	5.14	96.1	73.0	63.3		0.594	0.9530
					7.01	2.823	5.18	96.3	73.2	63.3		0.594	0.9530
98	14.307	100.1	0.0107	8.08	7.07			97.0	76.0	63.4			
99	14.305	100.1	0.0057	16.22	7.07			98.3	81.0	64.9			
100	14.417	100.1	0.0052	16.22	4.09			98.8	82.8	65.6			
101	14.346	100.1	0.0060	8.03	4.09			97.8	77.2	63.5			
107	14.349	100.1	0.0065	8.04	13.04			96.9	75.0	63.5			
108	14.308	100.1	0.0061	16.23	13.03			97.9	79.5	63.6			

*Surface temperatures were determined from Figure 26 for Tests 103-106 inclusive.

Table V.

Physical Properties of Air and n-Heptane

Property	Units				Reference
Air*					
		70° F.	100° F.	130° F.	
Viscosity x 10^7	lb.sec./sq.ft.	3.82	3.98	4.14	(18)
Thermal conductivity x 10^6	Btu./ft.sec.°F.	4.14	4.34	4.54	(18)
Specific volume	cu.ft./lb.	13.348	14.105	14.862	(18)
Compressibility factor			0.9998		(18)
n-Heptane					
		t,° F.			
Vapor pressure	lb./sq.in.	50	0.398		(21)
		55	0.465		
		60	0.541		
		65	0.628		
		70	0.726		
		75	0.836		
Maxwell Diffusion Coefficient	lb./sec.	85	0.1689		(23)
		100	0.1773		
		115	0.1854		
Latent heat of vaporization	Btu./lb.	77	156.83		(21)
		209.2	135.99		
Isobaric heat capacity of liquid n-heptane	Btu./lb.°F.	80	0.536		(7)
Specific gas constant	ft./°F.		15.4228		(21)

* Properties of dry air at 14.696 lb./sq.in.abs.

Table VI.

Calculated Results of Heated Sphere in Air Jet

Test No.	Air Stream			Heated Sphere			
	Re_a	Re_{ss}	Re_f	$h \times 10^3$ Btu./sq.ft.sec.°F.	Nu_a	Nu_{ss}	Nu_f
60	904	791	843	1.912	18.35	15.80	16.99
64	904	821	860	1.896	18.20	16.29	17.20
68	908	760	826	1.938	18.61	15.20	16.72
61	1808	1639	1720	2.612	25.1	22.4	23.7
66	1799	1678	1738	2.640	25.3	23.4	24.3
69	1802	1578	1682	2.652	25.5	21.9	23.6
80	1797	1500	1635	2.621	25.2	20.5	22.6
70	3627	3288	3445	3.593	34.5	30.8	32.5
71	3629	3174	3390	3.626	34.8	29.9	32.2
73	3636	3046	3319	3.642	35.0	28.7	31.5
74	7208	6564	6863	5.232	50.2	45.1	47.5
75	7215	6367	6757	5.270	50.6	43.9	47.0
79	7171	6021	6546	5.327	51.1	42.0	46.0

Table VII.

Calculated Results of Heated Sphere in Wake of Punched Plate

Test No.	Air Stream			Heated Sphere		
	Re_a	Re_f	Turbulence Level per cent	$h \times 10^3$ Btu. / sq.ft.sec.°F.	Nu_a	Nu_f
82	907	864	14.4	1.922	18.45	17.50
88	907	862	9.2	1.849	17.75	16.79
111	910	868	5.4	1.883	18.08	17.15
81	1797	1715	14.5	2.821	27.1	25.7
87	1802	1717	9.2	2.653	25.5	24.2
110	1798	1711	5.4	2.661	25.5	24.2
83	3627	3470	12.9	4.159	39.9	37.9
86	3630	3456	8.6	3.838	36.9	34.9
109	3624	3450	5.1	3.787	35.9	34.0
84	7185	6907	12.0	6.358	61.0	58.4
85	7191	6880	8.0	5.692	54.6	52.0
111	7204	6875	4.9	5.431	52.1	49.5

Table VIII.

Calculated Results of Porous Sphere in Air Jet

	Air Stream			Porous Sphere
Test No.	Re_a	Sc	$Re_a^{1/2} Sc^{1/3}$	Sh
45	822	2.14	37.0	20.3
46	1802	2.14	54.7	30.8
48	822	2.15	37.0	22.3
49	1759	2.15	54.1	31.1
50	889	2.15	38.5	22.2
51	4590	2.16	87.6	46.6
52	1808	2.15	54.9	31.2
53	1717	2.15	53.0	30.4
54	1908	2.16	56.5	29.5
39	1342			
40	819			
41	463			
42	1360			
44	876			
47A	7978			
47B	4601			

Table IX.

Calculated Results of Porous Sphere in Wake of Punched Plate

Test No.	Air Stream				Porous Sphere
	Re_a	Sc	$Re_a^{1/2} Sc^{1/3}$	Turbulence Level per cent	Sh
103	3639	2.15	77.9	9.7	46.1
				11.1	47.9
104A	3647	2.16	78.1	5.5	44.7
				5.9	44.9
				6.4	45.1
104B	915	2.16	39.1	5.8	22.6
				6.2	22.8
				6.8	22.9
104C	1811	2.16	55.0	5.8	32.2
				6.3	32.4
				6.8	32.3
105A	1810	2.15	54.9	10.6	33.1
				12.3	34.5
				14.6	36.5
105B	914	2.15	39.0	10.6	23.0
				12.3	23.8
				14.6	24.9
105C	3644	2.15	77.9	9.7	46.6
				11.1	48.5
				13.0	51.0
106A	3639	2.15	77.9	7.1	45.2
				7.8	45.6
				8.7	45.9
106B	1808	2.15	54.9	7.5	32.2
				8.3	32.7
				9.3	33.0
106C	912	2.15	39.0	7.5	22.8
				8.3	22.9
				9.3	23.0

Table X.

Calculated Results of Heat Transfer to Porous Sphere in Air Jet

Test No.	Air Stream	Porous Sphere			
	Re_a	$\dot{Q} \times 10^4$ Btu./sec.	$\dot{Q} \times 10^2$ Btu./sq.ft.sec.	$h \times 10^3$ Btu./sq.ft.sec.°F.	Nu'
45	822	3.53*	6.47	1.767	16.96
46	1802	5.34*	9.80	2.699	25.9
48	822	3.85*	7.06	1.918	18.41
49	1759	5.37*	9.84	2.667	25.6
50	889	3.85*	7.05	1.911	18.35
51	4590	8.55	15.67	4.516	43.4
52	1808	5.39	9.87	2.683	25.8
53	1717	6.47	11.85	2.731	26.2
54	1908	4.42	8.11	2.874	27.6

* Correction term for thermal flux introduced by supporting tube was assumed to be 11 per cent for these tests, since t_t was not measured.

Table XI.

Calculated Results of Heat Transfer to Porous Sphere in Wake of Punched Plate

Test No.	Air Stream		Porous Sphere			
	Re_a	Turbulence Level per cent	$\dot{Q} \times 10^4$ Btu./sec.	$\dot{Q} \times 10^2$ Btu./sq.ft.sec.	$h \times 10^3$ Btu./sq.ft.sec.°F.	Nu'
103	3639	9.7	8.27	15.16	4.282	41.1
		11.1	8.69	15.94	4.553	43.7
104A	3647	5.5	7.83	14.35	3.985	38.3
		5.9	7.88	14.45	4.024	38.6
		6.4	7.90	14.49	4.036	38.8
104B	915	5.8	3.91	7.17	1.949	18.71
		6.2	3.94	7.22	1.961	18.83
		6.8	3.95	7.24	1.966	18.87
104C	1811	5.8	5.51	10.11	2.746	26.4
		6.3	5.55	10.17	2.763	26.5
		6.8	5.55	10.18	2.774	26.6
105A	1810	10.6	5.70	10.45	2.848	27.3
		12.3	5.95	10.90	2.971	28.5
		14.6	6.29	11.53	3.151	30.3
105B	914	10.6	3.99	7.31	1.987	19.08
		12.3	4.11	7.54	2.049	19.67
		14.6	4.29	7.87	2.137	20.5
105C	3644	9.7	8.28	15.17	4.249	40.8
		11.1	8.69	15.94	4.502	43.2
		13.0	9.33	17.11	4.945	47.5
106A	3639	7.1	7.95	14.58	4.049	38.9
		7.8	8.04	14.74	4.094	39.3
		8.7	8.15	14.94	4.184	40.2
106B	1808	7.5	5.56	10.20	2.778	26.7
		8.3	5.63	10.32	2.811	27.0
		9.3	5.67	10.39	2.832	27.2
106C	912	7.5	3.94	7.23	1.964	18.86
		8.3	3.96	7.26	1.973	18.94
		9.3	3.99	7.31	1.986	19.04

APPENDIX A

THERMOCOUPLE CORRECTION

The surface temperatures of the porous sphere were obtained by correcting the indicated temperatures of the reference junction in contact with the sphere at the traverse locations indicated in Figure 1-A. The apparent temperatures were corrected by the following differential equation for the steady state thermal conduction along the wire:

$$t_a = t_w - \left(\frac{d_w k}{4h}\right) \frac{d^2 t_w}{dy^2} = t_{w,n} - \left(\frac{d_w k}{4h}\right) \frac{t_{w,n-1} - 2t_{w,n} + t_{w,n+1}}{(\Delta y)^2} \quad (1)$$

The solution to this equation was obtained by means of the electrical analog previously described. In Figure 2-A, the electrical resistance R_B represents the local resistance to thermal transfer through the boundary layer surrounding the thermocouple wire. The electrical resistances R_{Pt} and R_{Co} represent the local resistance to thermal transfer along the platinum and constantan wires. From Equation (1) the following relation between R_B and R_{Pt} or R_{Co} must be satisfied:

$$\frac{R_B}{R_{Pt}} = \frac{d_w k_{Pt}}{4h(\Delta y)^2} \quad (2)$$

The remaining boundary conditions involving the local values of the heat transfer coefficient and temperature distribution along the wire were established in the following manner.

The value of the local heat transfer coefficient from the thermocouple wire was established as follows. The exact solution to the velocity distribution in a boundary layer surrounding a sphere was not available so the exact boundary layer solution for a circular cylinder derived by Schlichting (22) was combined with the potential solution of the flow around spheres (26) to permit estimation of the velocity distribution in the boundary layer surrounding the sphere. The heat transfer data obtained by Cole and Roshko (4) for small platinum wires were used to establish the relation between the local air velocity and the heat transfer coefficient of the thermocouple wire which is shown in Figure 3-A. From the velocity distribution around the sphere and the relation presented in Figure 3-A, the local heat transfer coefficient may be established for any point along the wire. The resistance ratio R_B/R_{Pt} may be established from Equation 2 at each node from the local heat transfer coefficient and the distance along the wire between each node. Since d_w and k_{Pt} are essentially constant under the conditions encountered, R_{Pt} will be the same at each node. The value of R_{Pt} is determined arbitrarily to keep the values of R_B within the limited range of resistances available from the potentiometers. The appropriate values of R_B can then be established from

Equation 2 for each node.

In order to establish the temperature gradient imposed on the wire in the vicinity of the spherical surface, the experimental temperatures obtained from the traverses were plotted in the Y-Z plane from the surface to a point in the air stream that was sufficiently remote to be unaffected by the presence of the sphere. From this plot, the temperature distribution along the wire could be established for each experimental point.

The voltage (0.005 volt) imposed on the network of resistors was sufficiently low as to eliminate any thermal effect on the resistances from current dissipation. Each 100 ohm potentiometer of the voltage divider in Figure 2-A was adjusted until the voltage corresponding to the wire temperature was attained at each wire node as established by the plot of experimental temperatures in the Y-Z plane. At the thermocouple junction node, the voltage corresponding to the corrected air temperature is obtained. The temperature correction corresponds to the voltage drop that occurs across R_s of the thermocouple junction node. The temperature corrections for Test 50 have been carried out to completion. The isotherms obtained around the surface of the sphere are presented in Figure 4-A. The magnitude of the corrections applied to the apparent temperatures is presented in Figure 5-A.

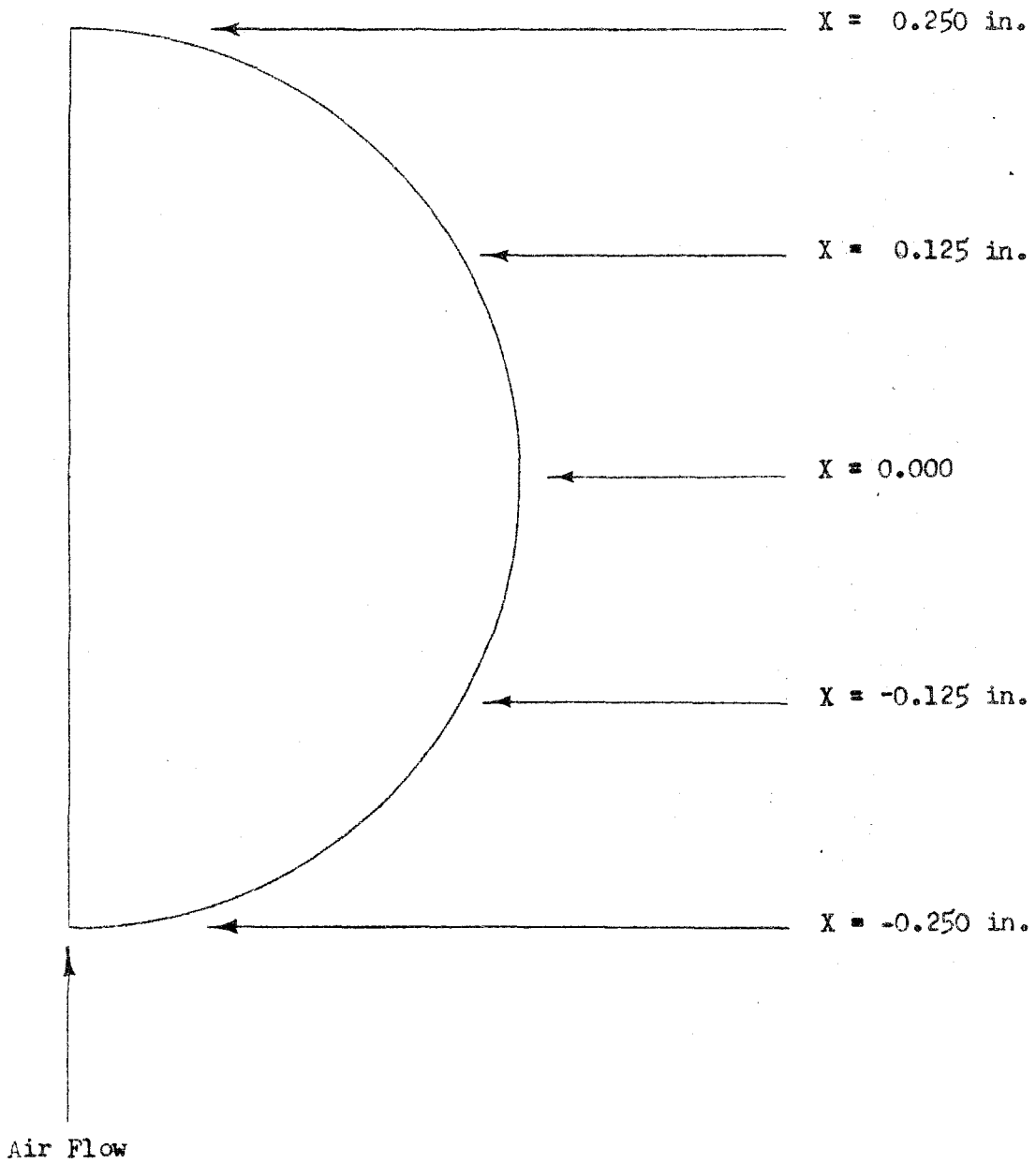

Figure 1-A. Traverse Locations

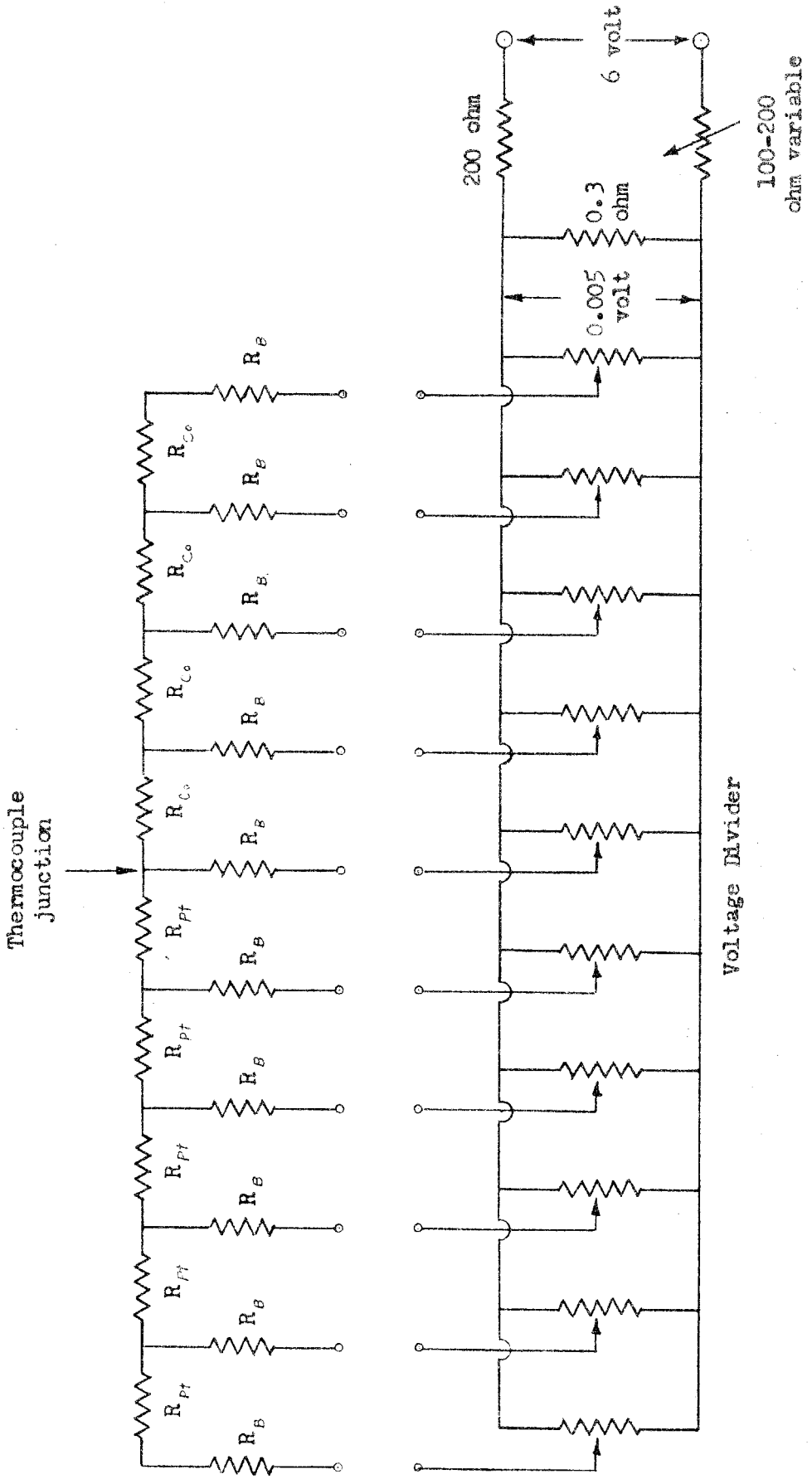

Figure 2-A. Typical Analog Arrangement

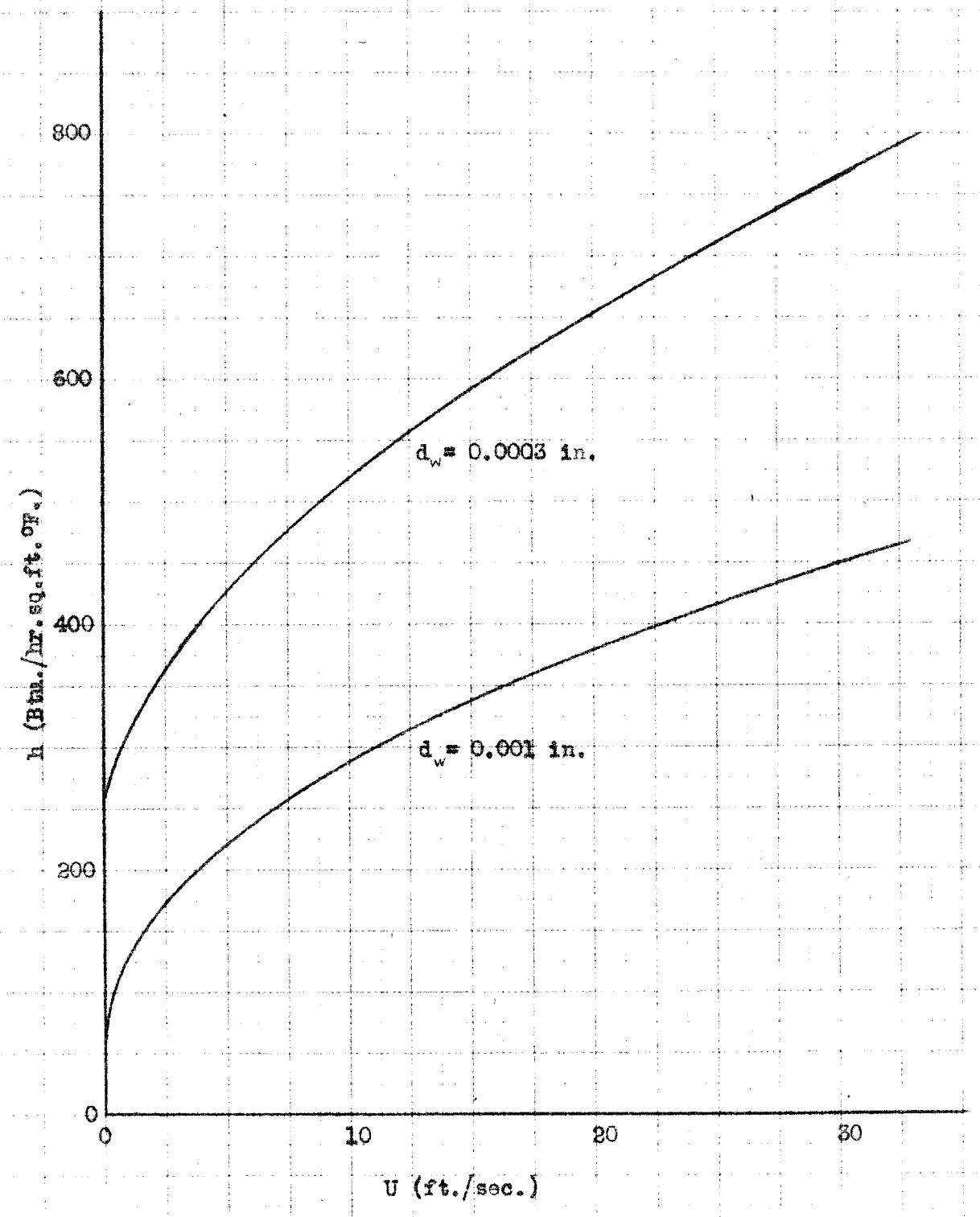

Figure 3-A. Heat Transfer Coefficient versus Air Velocity

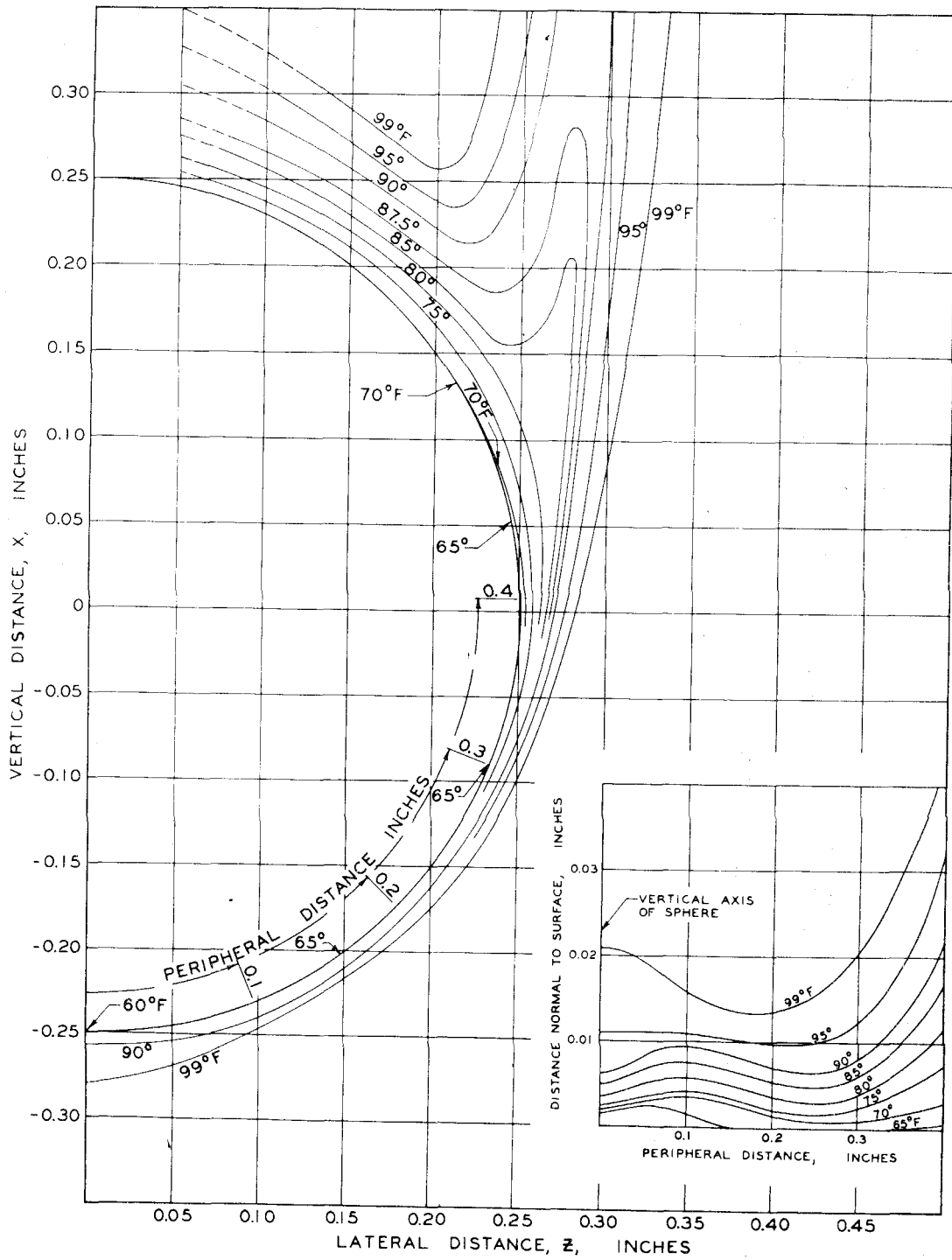

Figure 1-A

Temperature Distribution Around Porous Sphere

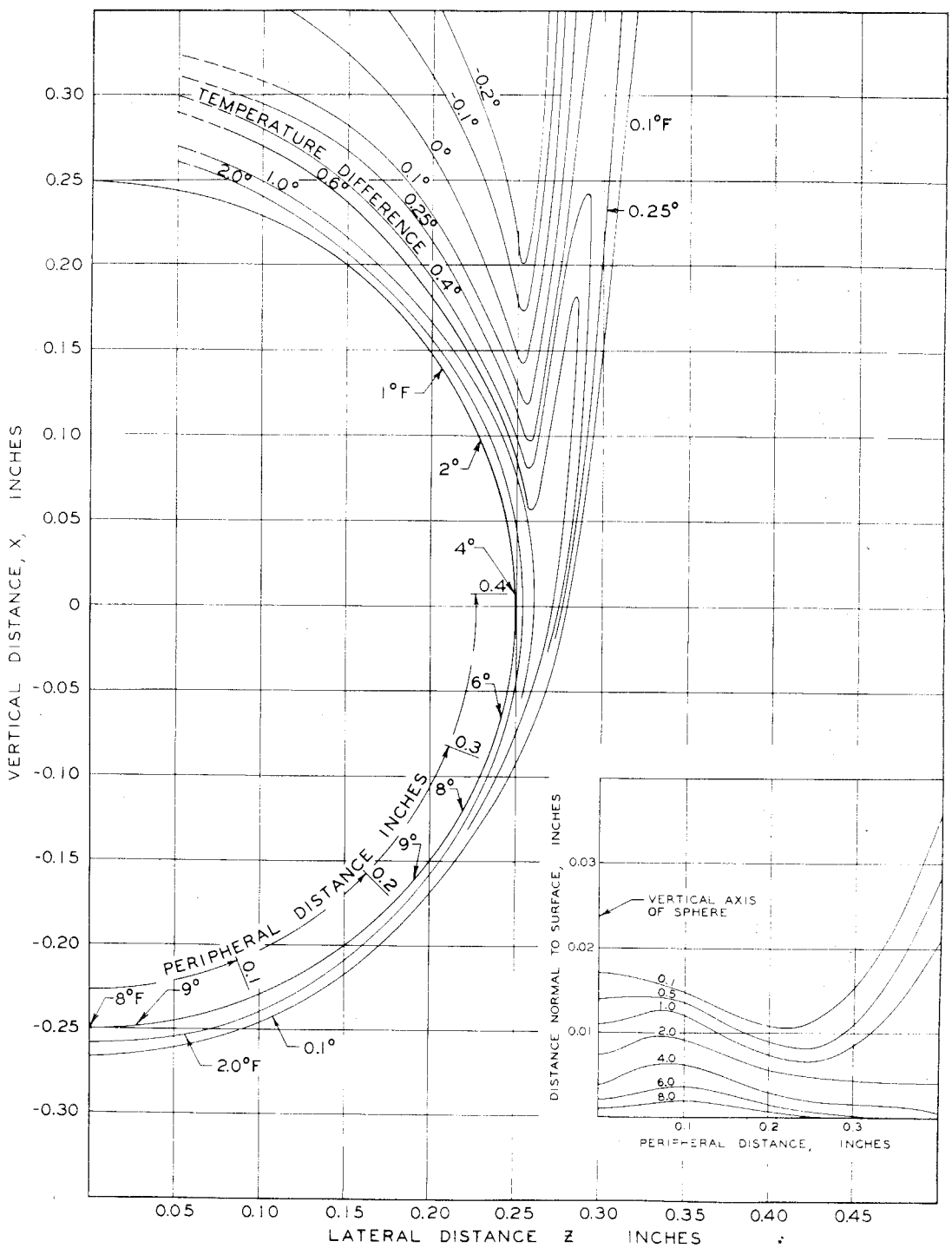

Figure 5-A

Corrections Applied to Platinum-Constantan Thermocouple, 0.001 inch in Diameter, Around Porous Sphere

APPENDIX B

THERMAL CONDUCTION CORRECTION

The general energy equation for steady conditions describing the thermal flux in the supporting tube may be expressed as

$$\left(A_t k_t + A_k k_k + A_{cu} k_{cu} + A_{co} k_{co}\right)\frac{d^2t}{dx^2} + \left(A_k C_{p,k,\ell}\sigma_{k,\ell} u_x\right)\frac{dt}{dx} + \pi d_t h\left(t_{ss} - t\right) = 0 \qquad (1)$$

The solution of the differential equation yields an expression of the form

$$t = t_{ss} - \left(t_a - t_{ss}\right) e^{-\beta x} \qquad (2)$$

where the coefficient β is given by

$$\beta = \frac{1}{2}\left[\frac{A_k C_{p,k,\ell}\sigma_{k,\ell} u_x}{A_t k_t + A_k k_k + A_{cu} k_{cu} + A_{co} k_{co}} + \sqrt{\left(\frac{A_k C_{p,k,\ell}\sigma_{k,\ell} u_x}{A_t k_t + A_k k_k + A_{cu} k_{cu} + A_{co} k_{co}}\right)^2 + \frac{4\pi d_t h}{A_t k_t + A_k k_k + A_{cu} k_{cu} + A_{co} k_{co}}}\right] \qquad (3)$$

Evaluation of β from Equation 3 indicates that most of the thermal flux through the supporting tube is due to the decrease in enthalpy of the flowing fluid. The expression for the decrease in enthalpy of the liquid introduced through the supporting tube is

$$\Delta \dot{\underline{H}} = \dot{\underline{m}}_k \, c_{p,k,l} \left(t_{t,k} - t_{ss} \right) \qquad (4)$$

Although the magnitude of the correction term is somewhat large, the evaluation of the term is relatively simple and precise. From the temperature indicated by the thermocouple at point D in Figure 11 and the average surface temperature of the sphere, and the specific heat of liquid n-heptane, the necessary correction term expressed by Equation 4 may be evaluated. The value of the specific heat of liquid n-heptane (7) for the conditions encountered is presented in Table V. The thermal flux through the supporting tube amounted to 11% of the total thermal transfer to the surface of the sphere for the majority of the conditions encountered.

PART III.

TEMPERATURE GRADIENTS IN TURBULENT GAS STREAMS

RECOVERY FACTORS IN STEADY, UNIFORM FLOW

TEMPERATURE GRADIENTS IN TURBULENT GAS STREAMS

Recovery Factors in Steady, Uniform Flow

J. B. Opfell, K. Sato, and B. H. Sage

California Institute of Technology
Pasadena, California

INTRODUCTION

The recovery factor has become an important quantity in the analysis of supersonic flow. Early work was directed to relating the indicated temperature of thermocouples or resistance thermometers to the temperature of rapidly moving streams in which they were immersed. Methods of measurement of the undefined concept temperature (4, 12) have been summarized and assembled in a systematic form (1). For this reason there is little need for reviewing the methods of measurement of temperature and its application in laminar and turbulent flow. McAdams (20) correlated the data relating to convective thermal transfer to small cylinders, and a recent experimental study has considered the effect of position in the flowing stream upon the thermal transport (26) to small cylinders located transverse to the direction of flow. In the measurement of the temperature of a moving stream by means of a stationary wire, it is necessary to take into account the rise in temperature of the fluid immediately surrounding the wire as a result of a substantially adiabatic change in state, and also the dissipation of kinetic energy as a result of viscous and turbulent shear in the vicinity of the wire. The

study of this quantity (3) has been particularly emphasized in the field of aerodynamics. Earlier studies (5,8,9,11, 13, 22) with air yielded values of the recovery factor from 0.62 to nearly unity.

Throughout the current discussion the recovery factor will be defined by the equation,

$$r' = \frac{T_o - T_b}{T_s - T_b} = \frac{T_o - T_b}{U^2/2g C_p} \qquad (1)$$

More recently, Hottel and Kalitinsky (15) measured the recovery factor for air on circular wires at velocities from 140 to 320 feet per second. A recovery factor of 0.66 was obtained for the lower velocity. This value is somewhat smaller than was obtained by Eckert (8,9) for small wires. Good agreement was obtained between the behavior for longitudinally mounted wires (8,21) and the values predicted by Emmons and Brainerd (10) for a flat plate located in an infinite stream. McAdams and coworkers (21) determined the recovery factor for air within lucite tubes and obtained values varying between 0.875 and 0.905, which were in reasonable agreement with the predictions of Emmons and Brainerd (10), Pohlhausen (23), and Eckert and Weiss (9). The last mentioned investigators predicted that the recovery factor for a flat plate in an infinite stream should be approximated by the square root of the Prandtl number. Such a relation-

ship is not strictly in accordance with Pohlhausen's calculations but represents a reasonable simplification.

More recently, active interest in recovery factors for supersonic flow has developed primarily as a result of the need for understanding aerodynamic heating. The studies of Eber (7), Tifford and Chu (28), and of Probstein and Lees (24) exemplify the interest in aerodynamic heating problems. Kaye and coworkers (16) carried out extensive studies of recovery factors for supersonic flow of air in tubes, and Levy and Seban (19) presented recovery factor values for wedge flows, utilizing the Hartree solution of the momentum equation (14). In addition, they predicted recovery factors for a fluid with a Prandtl number of 0.7 at separation of the boundary layer. Work relating to this problem was carried out by DeLauer and Nagamatsu (6) at rather high Mach numbers as a part of a general study of thermal transfer in hypersonic flow. These references indicate the widespread interest in recovery factors.

Wilson and Mitchell (29) recently made computations of the effect of viscous dissipation of kinetic energy on the pressure and viscosity for liquids in Couette flow. These authors assumed a uniform temperature distribution perpendicular to the direction of flow and no thermal flux parallel to the hydrodynamic velocity.

No analysis appears to have been made of the steady temperature profiles in streaming fluids involving both a pres-

sure gradient in the direction of flow and a finite hydraulic radius. Pohlhausen (23) predicted the recovery factor for a flat plate with incompressible flow and no pressure gradient, whereas Emmons and Brainerd (10) considered the analogous case for a compressible fluid. The predictions have often been used as the basis for the prediction of recovery factor values for wires, plates, and the walls of flowing streams which are parallel to the axis of flow.

DERIVATIONS

The following discussion relates to recovery factors associated with the unidirectional flow of an incompressible fluid between infinite parallel plates and in a channel of constant circular cross section. For present purposes, a uniform stream is considered as one in which the velocity at a given location in the cross section is invariant in the direction of flow, although other point properties of the fluid do vary in this direction. In the course of such a flow process for real fluids there exists a dissipation of kinetic energy because of the viscosity of the fluid. In order to estimate the recovery factor it is necessary to determine the form of the dissipation function and to establish from an energy balance the temperature distribution necessary to promote a condition of maximum entropy for the boundary conditions imposed. Figure 1 presents a force balance upon an element of volume in a two-dimensional uniform stream

having a unit depth in the other direction.

Because the total volume of the element shown in Figure 1 remains constant with respect to time, a force balance for this volume results for steady uniform flow in the following equation:

$$\frac{\partial \tau^{xx}}{\partial x} = -\frac{\partial \tau^{xy}}{\partial y} \qquad (2)$$

Under steady conditions, the dissipation of kinetic energy in the element through shear must equal the net rate at which energy transfer from the element is accomplished. The balance of these energy changes and the fluxes may be written as (17,18,25)

$$\sigma u_x \left\{ \frac{\partial E}{\partial x} - \frac{1}{\sigma} \frac{\partial \tau^{xx}}{\partial x} \right\} + \frac{\partial \mathring{Q}_x}{\partial x} = -\frac{\partial \mathring{Q}_y}{\partial y} + \frac{\partial u_x \tau^{yx}}{\partial y} \qquad (3)$$

The shear in steady uniform flow of a Newtonian fluid may be related to the pressure gradient by (2)

$$\frac{\partial \tau^{xy}}{\partial y} = \frac{\partial P}{\partial x} \qquad (4)$$

Equation 4 may be rewritten as

$$\tau^{xy} = \tau_o \ell / \ell_o \qquad (5)$$

From Equations 2 and 4, it follows that:

$$\tau^{xx} = -P \tag{6}$$

Combination with Equation 3 results in

$$\sigma u_x \left\{ \frac{\partial E}{\partial x} + \frac{1}{\sigma} \frac{\partial P}{\partial x} \right\} + \frac{\partial \mathring{Q}_x}{\partial x} = \sigma u_x \frac{\partial H}{\partial x} + \frac{\partial \mathring{Q}_x}{\partial x}$$
$$= \frac{1}{\ell_o} \frac{\partial \mathring{Q}_y}{\partial L} - \frac{\tau_o}{\ell_o} \frac{\partial u_x L}{\partial L} \tag{7}$$

The thermal transport transverse to the direction of flow may be expressed as

$$\mathring{Q}_y = \frac{\sigma C_p \underline{\epsilon}_c}{\ell_o} \frac{\partial T}{\partial L} \tag{8}$$

A combination of Equations 7 and 8 results in

$$\underline{\epsilon}_m \frac{\sigma C_p}{\ell_o^2} \frac{\partial T}{\partial L} = \underline{\mathcal{P}_r} \frac{\tau_o}{\ell_o} u_x L + \underline{\mathcal{P}_r} \frac{\partial}{\partial x} \int_o^L \sigma u_x H \, dL \tag{9}$$

Equation 9 represents the energy balance for the flowing system expressed in terms of the Prandtl number and an integral describing the energy transport in the direction of flow. Equation 9 can be developed from the theory of irreversible thermodynamic processes as described by Kirkwood and

Crawford (17) by making appropriate simplifications to conform with the present boundary conditions. It is emphasized that Equation 9 is limited to the steady uniform flow of an incompressible fluid; no effort was made to establish the thermal transport in the x direction because of a temperature gradient since the flow was considered uniform.

ADIABATIC FLOW

For uniform, steady flow under adiabatic conditions with an axis of symmetry it follows that:

$$\frac{\partial T}{\partial L} = 0 \qquad \text{at} \qquad \ell = 0$$
$$\frac{\partial T}{\partial L} = 0 \qquad \text{at} \qquad \ell = \ell_o \tag{10}$$

If these boundary conditions are applied to Equation 9, there is obtained

$$\frac{\partial}{\partial x} \int_0^L \sigma u_x H \, dL = 0 \tag{11}$$

This equation shows that there is no change in enthalpy in the direction of flow. Equation 9 may then be simplified to the form,

$$\frac{dT}{dL} = \underline{P_r} \, \frac{\ell_o \tau_o}{\sigma C_p} \, \frac{u_x L}{\underline{\epsilon}_m} \tag{12}$$

This differential expression describes the variation in temperature across the channel for adiabatic flow. It may be integrated for various boundary conditions.

If Equation 12 is applied to the laminar flow between parallel plates of infinite extent, there is obtained

$$\frac{dT}{dL} = \frac{P_R}{} \frac{24}{R_e} \frac{l_o}{\nu} \frac{3}{2} U(1-L^2)\left(\frac{U^2}{2gC_p}\right)L \qquad (13)$$

In deriving Equation 13 the Reynolds number was taken as

$$R_e = \frac{4 l_o U}{\nu} \qquad (14)$$

In laminar flow the total viscosity is equal to the kinematic viscosity, and Equation 13 may be integrated to yield

$$T - T_a = \frac{q}{2} \frac{P_R}{} \left(L^2 - \frac{L^4}{2}\right)\left(\frac{U^2}{2gC_p}\right) \qquad (15)$$

In obtaining Equation 15 the viscosity was assumed to be a constant.

It is often of interest to consider the temperature at the wall in reference to the bulk temperature of the stream. Under the foregoing circumstances the difference between the bulk and wall temperatures is

$$T_o - T_b = \frac{54}{35} \underline{P_r} \left(\frac{U^2}{2gC_p} \right) \tag{16}$$

From the definition of the recovery factor as given in Equation 1 it follows that:

$$r' = \frac{54}{35} \underline{P_r} \tag{17}$$

Equation 17 describes the recovery factor for the laminar flow of an incompressible fluid under steady uniform conditions when moving between adiabatic, infinite parallel plates. The temperature distribution in such a laminar stream may be generalized by rewriting Equation 15 in such a form that one side depends upon position in the stream alone.

$$\left(\frac{2}{9 \underline{P_r}} \right) \left(\frac{T - T_a}{U^2/2gC_p} \right) = L^2 - \frac{L^4}{2} \tag{18}$$

The left hand side of Equation 18 is plotted as a function of position in Figure 2. This diagram represents a generalized temperature distribution in a laminar flowing stream. In most conditions of laminar flow the temperature differences will be small. However, if the Prandtl number is large, as

is sometimes encountered with viscous oils, these effects become significant. It should be realized that there exists a uniform increase in temperature with the distribution indicated in Figure 2 as the fluid progresses in the direction of flow. The enthalpy is constant but the linear decrease in pressure results in a linear increase in internal energy as indicated by the following expression:

$$T_o - T_b = \frac{\partial P}{\partial x} = -\sigma C \frac{\partial T}{\partial x} \tag{19}$$

In turbulent streams the situation is somewhat more complicated. It is convenient to employ two parameters to describe the position and velocity pattern (2).

$$y^+ = \frac{y}{\nu}\sqrt{\frac{\tau_o g}{\sigma}} = \frac{y u_*}{\nu} \tag{20}$$

$$u^+ = \frac{u}{\sqrt{\frac{\tau_o g}{\sigma}}} = \frac{u}{u_*} \tag{21}$$

Following correlations which have been developed from experiment (26), these parameters were related in the following empirical fashion:

$$u^+ = 5.5 + 2.5 \ln (1-L) + 2.5 \ln \frac{Re}{4}\sqrt{\frac{f}{2}} \quad ; y^+ > 26.7 \qquad (22)$$

$$u^+ = \frac{1}{0.0695} \tanh (1-L)\left(0.0695 \frac{Re}{4}\sqrt{\frac{f}{2}}\right) \quad ; y^+ < 26.7 \qquad (23)$$

$$y^+ = (1-L)\frac{Re}{4}\sqrt{\frac{f}{2}} \qquad (24)$$

From these it has been established (27) that

$$\epsilon_m = -\frac{\tau^{xy} g/\sigma}{\partial u_x/\partial \ell} = -\frac{\tau_o \ell g/\sigma}{\partial u_x/\partial L} = -\frac{f}{2}\frac{\ell_o^2 U^2 L}{\nu}\frac{\left(\frac{Re}{4}\sqrt{\frac{f}{2}}\right)^{-1}}{\partial u^+/\partial L} \qquad (25)$$

$$\epsilon_m = -\nu\left(\frac{f}{2}\frac{U^2\ell_o^2}{\nu^2}\right)\left(\frac{Re}{4}\sqrt{\frac{f}{2}}\right)^{-1}\frac{L}{\partial u^+/\partial L} = -\left(\frac{Re}{4}\sqrt{\frac{f}{2}}\right)\frac{\nu L}{\partial u^+/\partial L} \qquad (26)$$

Substituting Equation 26 in Equation 12 and evaluating the shear at the wall in terms of the friction factor, there is obtained

$$\frac{dT}{dL} = -\underline{Pr}\ \frac{f}{2}\left(\frac{U^2}{2gC_p}\right)\frac{\partial(u^+)^2}{\partial L} \qquad (27)$$

The integration of Equation 27 results in

$$T - T_a = -\frac{f}{2}\left(\frac{U^2}{2gC_p}\right)\int_{L=0}^{L=1} \underline{Pr}\ d(u^+)^2 \qquad (28)$$

The temperature distribution in an air stream as a function of position is shown in Figure 3 for Reynolds numbers of 20,000 and 100,000 and the corresponding values of the bulk temperature and recovery factor are presented in Table I. The data of Figure 3 and Table I refer to air at a bulk temperature of 100° F. and at substantially atmospheric pressure. The physical properties of air which were employed in these calculations are recorded in the footnotes of Table I. In these calculations the variation in the molecular properties of the air with position in the flowing stream was assumed to be negligible.

It appears profitable to consider the corresponding expressions that are obtained for flow in a circular conduit. The same methods as have been outlined for the flow between

between parallel plates result in an expression of the following form which is the analog to Equation 12:

$$\frac{dT}{dR} = \underline{Pr}\ \frac{r_o T_o}{\sigma C_p}\ \frac{u_x R}{\epsilon_m} \tag{29}$$

In Equation 29 the radius at any point is related to the radius of the conduit by

$$r = r_o R \tag{30}$$

If desired, the temperature gradient of Equation 29 may be expressed in terms of the bulk velocity and the friction factor. Under these circumstances there is obtained

$$\frac{dT}{dR} = \underline{Pr}\ f r_o \left(\frac{U^2}{2gC_p}\right) \frac{u_x R}{\epsilon_m} \tag{31}$$

In laminar flow Equation 31 reduces to

$$\frac{dT}{dR} = \underline{Pr}\ \frac{16}{Re}\ \frac{r_o}{\nu}\ 2U(1-R^2)\left(\frac{U^2}{2gC_p}\right) R \tag{32}$$

Equation 32 may be integrated from the center of the conduit to yield the following expression for the temperature distri-

bution in the adiabatic laminar flow of an incompressible fluid in a circular conduit:

$$T - T_a = 8 \underline{P_r} \left(R^2 - \frac{R^4}{2} \right) \left(\frac{U^2}{2g C_p} \right) \tag{33}$$

Again it has been assumed that the physical properties of this stream do not change with radial position. The similarity between Equations 15 and 33 is evident. If it is desired to relate the temperature of the wall to the bulk temperature of the fluid, there is obtained,

$$T_o - T_b = 2 \underline{P_r} \left(\frac{U^2}{2g C_p} \right) \tag{34}$$

In the case of flow in circular conduits the recovery factor may be established from

$$r' = 2 \underline{P_r} \tag{35}$$

The values of the recovery factor obtained from Equation 35 are somewhat larger than those obtained for the flow between parallel plates as indicated in Equation 17. Those determined by Equations 17 and 35 are linear with respect to the Prandtl number in contradistinction to the results obtained by

Pohlhausen (23) for isobaric conditions of flow along a flat plate.

In the case of circular conduits the Reynolds number is

$$\mathcal{R}_e = \frac{2r_o U}{\nu} \tag{36}$$

For turbulent flow in circular conduits the analog to Equation 40 becomes

$$\frac{dT}{dR} = -\mathcal{P}_R \frac{f}{2}\left(\frac{U^2}{2gC_p}\right)\frac{\partial(u^+)^2}{\partial R} \tag{37}$$

It should be realized that the Reynolds number for a given characteristic dimension corresponds to a somewhat different bulk velocity in the case of flow in a circular conduit than in the flow between parallel plates. Table I records pertinent information concerning the recovery factor and the temperature distribution for turbulent flow in circular conduits.

ISOTHERMAL FLOW

In situations where the kinetic energy dissipated in the flowing stream is transferred through the boundaries as heat, a somewhat different condition is found. In steady uniform flow there is no change in temperature with distance along the stream for any particular position in the cross section.

The change in internal energy with distance along the stream and the thermal flux in the direction of flow are zero. Under such circumstances Equation 3 reduces to

$$\frac{\partial \mathring{Q}_y}{\partial y} = \tau^{xy} \frac{\partial u_x}{\partial y} = -\tau_o \frac{L}{l_o} \frac{du_x}{dL} = -\frac{1}{l_o^2} \frac{d}{dL} \left\{ \sigma C_p \underline{\epsilon}_c \frac{dT}{dL} \right\} \qquad (38)$$

From the relationship of shear at the wall to the friction factor it follows that:

$$\frac{d}{dL} \left(\underline{\epsilon}_c \frac{dT}{dL} \right) = f l_o L \left(\frac{U^2}{2g C_p} \right) \frac{du_x}{dL} \qquad (39)$$

The analogous expression for flow in a circular conduit is

$$\frac{1}{R} \frac{d}{dR} \left\{ R \underline{\epsilon}_c \frac{dT}{dR} \right\} = f r_o \left(\frac{U^2}{2g C_p} \right) \frac{dR u_x}{dR} \qquad (40)$$

A typical temperature profile for laminar flow between parallel plates is shown in Figure 4. The information of this figure was obtained from

$$T - T_a = -\frac{3}{2} \underline{Pr} \left(\frac{U^2}{2g C_p} \right) L^4 = -\frac{1}{3} \frac{\eta}{K} U_{max.}^2 L^4 \qquad (41)$$

After the bulk temperature of the stream is obtained, the isothermal recovery factor becomes

$$r' = -\frac{48}{35}\,\underline{Pr} \tag{42}$$

In turbulent flow the temperature distribution under isothermal conditions may be established as

$$T - T_a = -f\left(\frac{U^2}{2g\,C_p}\right)\int_{L=0}^{L=L} \underline{Pr}/L \int_{L=0}^{L=L} L\,du^+du^+ \tag{43}$$

The temperature distribution in turbulent flow at a Reynolds number of 20,000 is shown in Figure 4 and the corresponding recovery factors are recorded as a function of Reynolds number in Table I. These factors were obtained from

$$r' = -f\left\{\int_{L=0}^{L=l} \underline{Pr}/L \int_{L=0}^{L=L} L\,du^+du^+ - \frac{\int_0^l u^+ \int_{L=0}^{L=L} \underline{Pr}/L \int_{L=0}^{L=L} L\,du^+du^+\,dL}{\int_0^l u^+\,dL}\right\} \tag{44}$$

The temperature distribution for isothermal laminar flow in a circular conduit is given by

$$T - T_a = -2\,\underline{Pr}\left(\frac{U^2}{2g\,C_p}\right)R^4 \tag{45}$$

Again, after the bulk temperature is obtained, the recovery factor may be evaluated as

$$r' = -\frac{62}{35}\,\underline{Pr} \tag{46}$$

Equation 46 indicates a linear relationship of the recovery factor to the Prandtl number. Values of the recovery factor for air in isothermal flow are recorded in a part of Table I. In the case of turbulent flow under isothermal conditions in a circular conduit the temperature distribution may be established from

$$T - T_a = -f\left(\frac{U^2}{2g\,C_p}\right)\int_{R=0}^{R=R} \underline{Pr}/R^2 \int_{R=0}^{R=R} R^2\,du^+\,du^+ \tag{47}$$

The recovery factor is related to the conditions of flow in the following way:

$$r' = -f\left\{\int_{R=0}^{R=1} \underline{Pr}/R^2 \int_{R=0}^{R=R} R^2\,du^+\,du^+ - \frac{\int_0^{1} u^+ \int_{R=0}^{R=R} \underline{Pr}/R^2 \int_{R=0}^{R=R} R^2\,du^+\,du^+\,dR^2}{\int_0^{1} u^+\,dR^2}\right\} \tag{48}$$

Equations 47 and 48 for turbulent flow in circular channels under isothermal conditions are analogous to Equations 43 and 44 for similar flow between parallel plates.

The marked difference in the temperature distribution

in turbulent flow is clearly evident from comparison of Figures 3 and 4. In the case of adiabatic flow the maximum temperature occurs at the wall of the conduit and the energy transport is from the wall to the center of the stream. In the case of isothermal flow the maximum temperature is found at the center of the stream and the thermal flux is in the direction of the wall.

The primary difference between this evaluation of the temperature distribution in a steady, uniformly flowing stream with pressure gradients and finite hydraulic radius and that found by Pohlhausen (23) for isobaric flow along a flat plate lies in the linear relationship between the recovery factor and the Prandtl number in the former situation. In all cases evaluated here for laminar flow the recovery factor is a linear function of the Prandtl number. In the case of turbulent flow it is a function of Reynolds number as well. Figure 5 presents a comparison of the recovery factors for flat plates with infinite hydraulic radius based upon the data of Pohlhausen (23) for the Eckert approximation (8), and for the current information for uniform flow with finite hydraulic radius.

For all laminar flows involving finite hydraulic radius there exists a linear relationship between the Prandtl number and the recovery factor. Such is not the case for the flow around bodies under isobaric conditions. The approximations of Emmons (10) and Eckert (8) involving the square

root of the Prandtl number are in fair agreement with Pohlhausen (23). This approximation is satisfactory for many of the conditions of nonuniform flow encountered in practice.

The recovery factors reported by Emmons and Brainerd (10) for a compressible fluid increased with Mach number for subsonic flow and decreased with this parameter in the supersonic region. This effect may be explained in terms of the compressibility of the fluid since Pohlhausen (23) found the recovery factor to be essentially independent of velocity and Reynolds number for laminar, incompressible boundary layers on flat plates. McAdams (21) found that the recovery factor decreased with increasing Reynolds number in the subsonic turbulent flow of air through a circular conduit. The present calculations which apply to an incompressible fluid show that the recovery factor increases with an increase of Reynolds number, at the same Prandtl number, for turbulent flow of air through a circular conduit. The present calculations which apply to an incompressible fluid show that the recovery factor increases with an increase of Reynolds number, at the same Prandtl number, for turbulent flow in circular conduits. As the bulk velocity becomes increasingly large, the generalized velocity profile indicates that the primary viscous dissipation will be confined to thinner and thinner regions adjacent to the wall. Physical considerations indicate that the temperature attainable in this region approaches some finite limit with increasing velocity. The

stagnation temperature, on the other hand, is not so limited. Consequently, an ultimate decrease in the recovery factor with increasing Reynolds number is to be expected for both compressible and incompressible turbulent flow. Further experimental work will be required in order to determine the accuracy with which the several analyses describe the recovery factor for fluids with Prandtl numbers differing materially from unity.

NOMENCLATURE

C	heat capacity, (ft.)(lb.)/(lb.)($^{\circ}$F.)
d	differential operator
E	internal energy, (ft.)(lb.)/lb.
f	Fanning friction factor, $0.0008-0.0553\ \mathcal{R}e^{-0.237}$
g	gravitational constant, ft./sec.^{2}
H	enthalpy, (ft.)(lb.)/lb.
k	thermal conductivity, (ft.)(lb.)/(sec.)(ft.^{2})($^{\circ}$F./ft.)
L	relative position with respect to the plane of symmetry, ℓ/ℓ_o
ℓ	position with respect to the plane of symmetry, ft.
ℓn	natural logarithm
P	pressure, lb./ft.^{2}
$\mathcal{P}r$	Prandtl number
$\mathcal{P}r$	total Prandtl number, ϵ_m/ϵ_c
$\mathring{Q}$	thermal flux, (ft.)(lb.)/(ft.^{2})(sec.)
R	relative radial position with respect to the axis of symmetry, r/r_o
$\mathcal{R}e$	Reynolds number
r	radial position with respect to the axis of symmetry, ft.
r'	recovery factor
T	temperature, $^{\circ}$R.
$\tanh$	hyperbolic tangent
U	bulk velocity, ft./sec.
u	point velocity, ft./sec.
u^+	dimensionless velocity parameter

u_* friction velocity, $U\sqrt{\frac{f}{2}} = \sqrt{\frac{\tau_0 g}{\sigma}}$ ft./sec.

x position along the direction of flow, ft.

y position with respect to the solid boundary of the conduit, ft.

y^+ dimensionless position parameter

Δ difference in

ϵ_c eddy conductivity, $ft.^2/sec.$

$\underline{\epsilon}_c$ total conductivity, $ft.^2/sec.$

ϵ_m eddy viscosity, $ft.^2/sec.$

$\underline{\epsilon}_m$ total viscosity, $ft.^2/sec.$

η absolute viscosity, $\nu\sigma/g$, (lb.)(sec.)/$ft.^2$

K thermometric conductivity, $ft.^2/sec.$

ν kinematic viscosity, $ft.^2/sec.$

σ specific weight of fluid, $lb./ft.^3$

τ stress, $lb./ft.^2$

∂ partial differential operator

Superscripts

x,y denote the component of the stress

τ^{xy} is the component of viscous force in the x direction associated with a plane lying perpendicular to the y direction

Subscripts

a evaluated at the axis or plane of symmetry

b bulk average value

cc circular conduits

o evaluated at the solid boundary

p	isobaric
pp	parallel plates
s	stagnation
x	in the x direction
y	in the y direction

LITERATURE CITED

1. American Institute of Physics, "Temperature, Its Measurement and Control," New York, Reinhold Publishing Corp., 1941.

2. Bakhmeteff, B. A., "The Mechanics of Turbulent Flow," Princeton, Princeton University Press, 1941.

3. Batho, C., J. Inst. Civil Engrs. (London), 174, 317 (1907-8).

4. Bridgman, P. W., "The Logic of Modern Physics," New York, MacMillan Co., 1938, pp. 117-18.

5. Brun, E., and Vernotte, P., Compt. rend., 194, 594 (1932).

6. DeLauer, R. D., and Nagamatsu, H. T., Memo. No. 14, Guggenheim Aeronautical Laboratory, California Institute of Technology, April 15, 1953.

7. Eber, G. R., J. Aeronaut. Sci., 19, 1 (1952).

8. Eckert, E., Z. Ver. deut. Ing., 84, 813 (1940); Nat. Advisory Comm. Aeronaut., Tech. Mem. 983 (1941).

9. Eckert, E., and Weise, W., Forsch. Gebiete Ingenieurw. 12, 40 (1941); Nat. Advisory Comm. Aeronaut., Tech. Mem. 1000 (1941).

10. Emmons, H. W., and Brainerd, J. L., Trans. Am. Inst. Mining Met. Engrs., 63, A105 (1941).

11. Franz, A., Jahrbuch 1938, Deutschen Luftfahrforschung, 2, 215; Nat. Advisory Comm. Aeronaut., Tech. Mem. 953 (1940).

12. Goranson, R. W., "Thermodynamic Relations in Multicomponent Systems," Washington, D. C., Carnegie Institution of Washington, 1930, p. 9.

13. Hartmann, W., Forsch. Gebiete Ingenieurw. 10, Supplement, Forschungsheft 397 (1939).

14. Hartree, D. R., Proc. Cambridge Phil. Soc., 33, 223 (1937).

15. Hottel, H. C., and Kalitinsky, A., J. Applied Mechanics, 12, A25 (1945).

16. Kaye, J., Keenan, J. H., Klingensmith, K. K., Ketchum, G. M., and Toong, T. Y., ASME Paper 160, 51-A-29 (a).

17. Kirkwood, J. G., and Crawford, B., Jr., J. Phys. Chem., 56, 1048 (1952).

18. Lamb, H., "Hydrodynamics," Cambridge University Press, 1932.

19. Levy, S., and Seban, R. A., J. Aeronaut. Sci., 19, 355 (1952).

20. McAdams, W. H., "Heat Transmission," New York, McGraw-Hill Book Co., 1942.

21. McAdams, W. H., Nicolai, L. A., and Keenan, J. H., Trans. Am. Inst. Chem. Engrs., 42, 907 (1946).

22. Meissner, W., Forsch. Gebiete Ingenieurw., 9, 213 (1938).

23. Pohlhausen, E., Z. angew. Math. u. Mech., 9, 115 (1921).

24. Probstein, R. F., and Lees, L., J. Aeronaut. Sci., 20, 291 (1953).

25. Rouse, H., "Fluid Mechanics for Hydraulic Engineers," New York, McGraw-Hill Book Co., 1938.

26. Schlinger, W. G., Hsu, N. T., Cavers, S. D., and Sage, B. H., IND. ENG. CHEM., 45, 864 (1953).

27. Schlinger, W. G., and Sage, B. H., Ibid., 45, 2636 (1953).

28. Tifford, A. N., and Chu, S. T., J. Aeronaut. Sci., 19, 787 (1952).

29. Wilson, W. E., and Mitchell, W. I., in Proc. First U. S. Nat'l. Congress of Appl. Mechanics, ASME (1952), p. 789.

LIST OF FIGURES

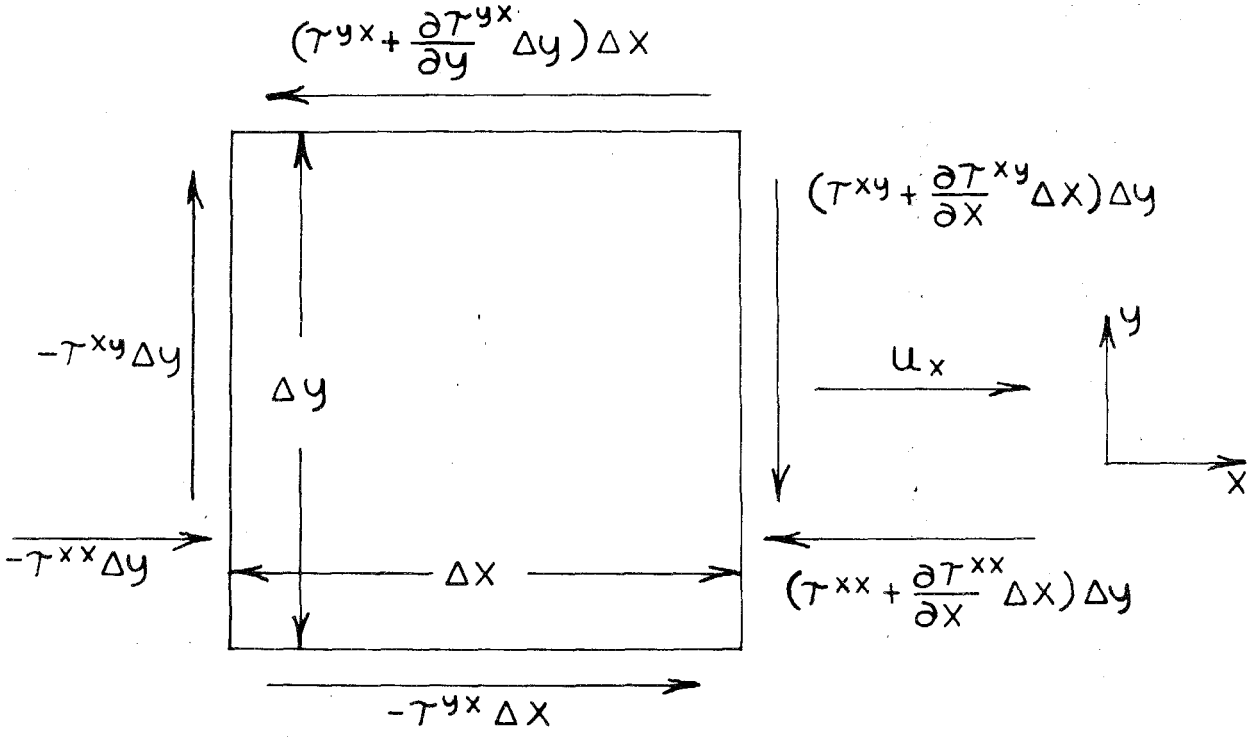

Fig. 1. Shear on an Element of Volume

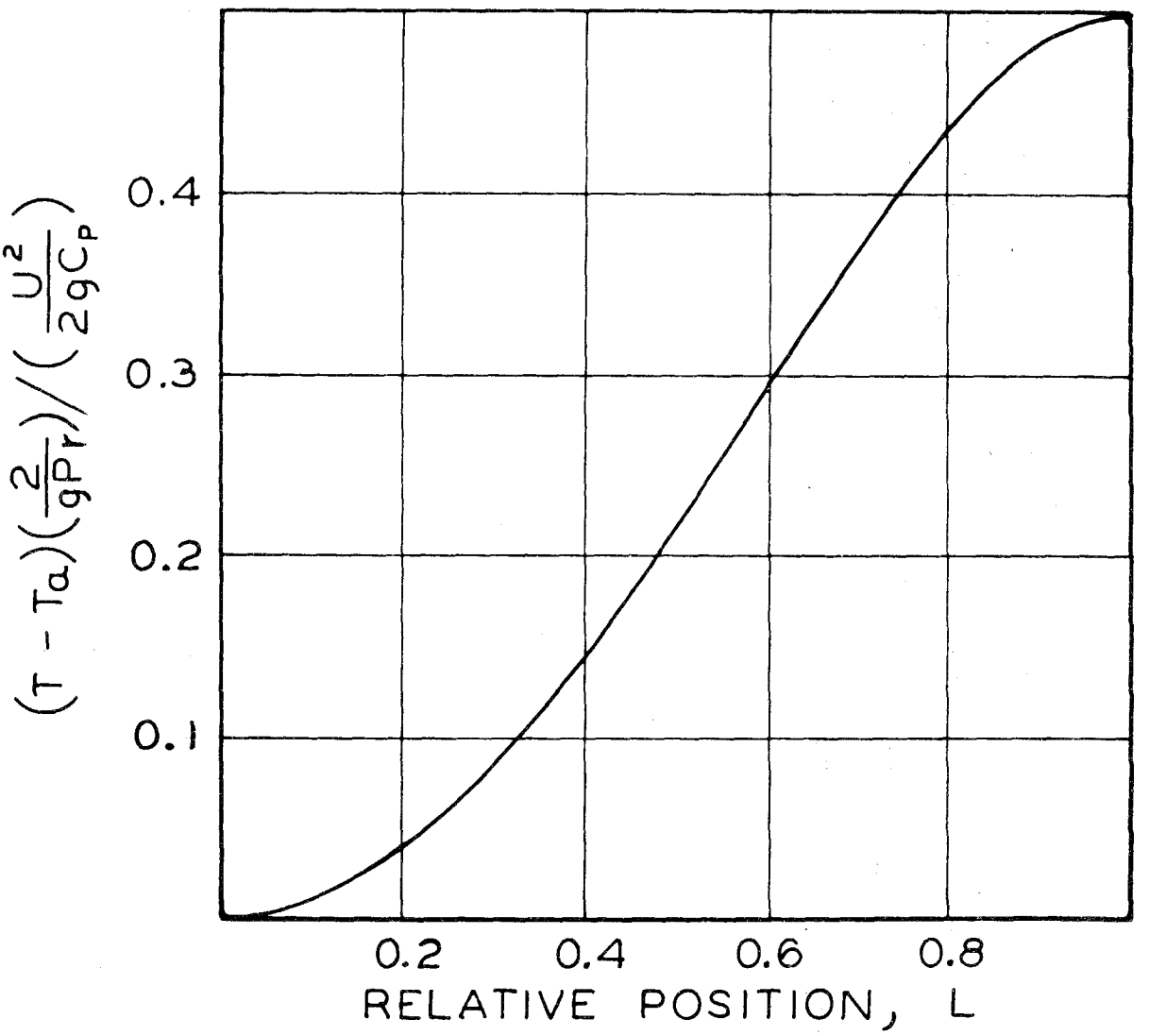

Fig. 2. Temperature Distribution in Adiabatic Laminar Flow

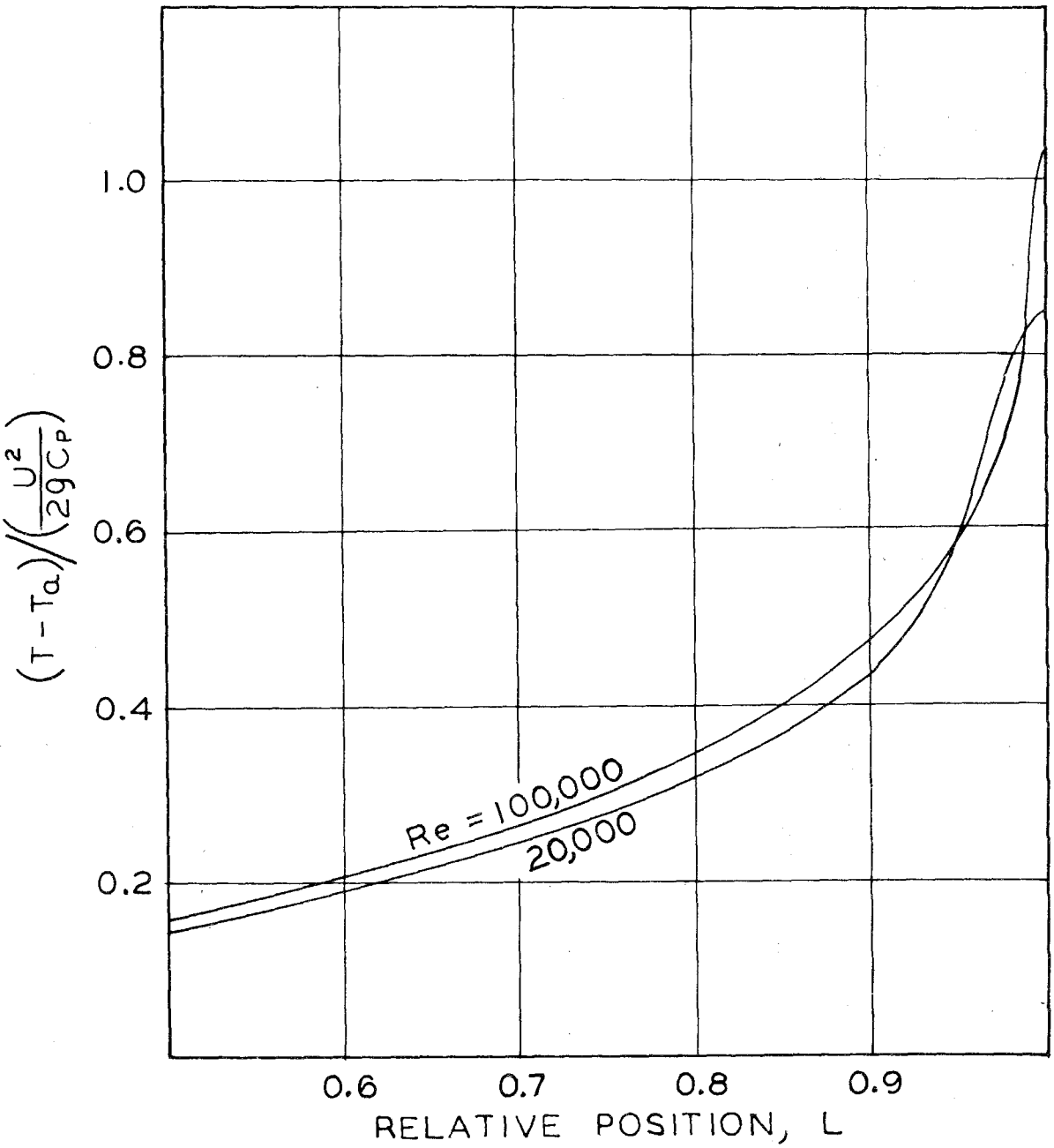

Fig. 3. Temperature Distribution in Adiabatic Turbulent Flow of Air

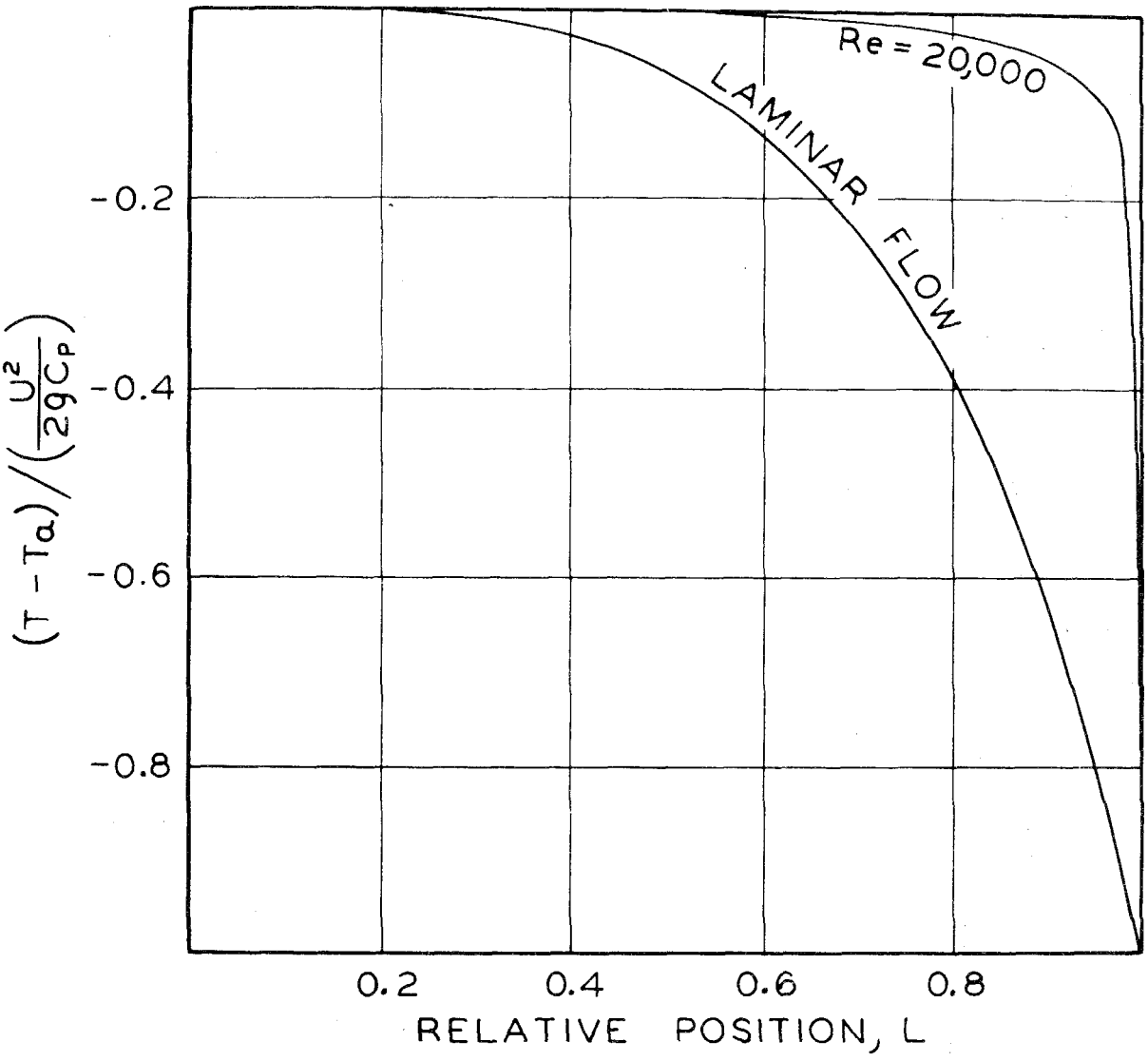

Fig. 4. Typical Temperature Profiles in Isothermal Flow between Parallel Plates

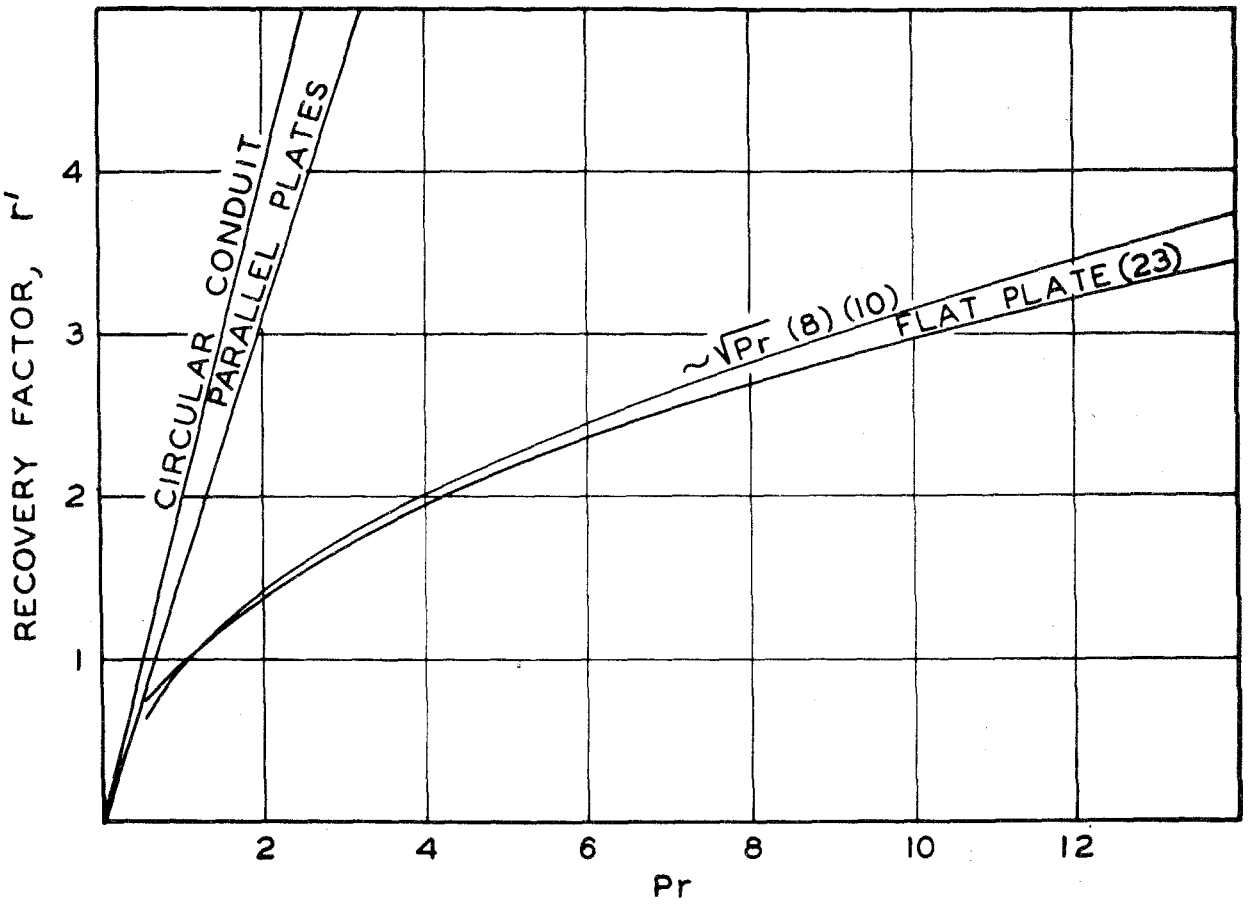

Fig. 5. Effect of Prandtl Number upon Recovery Factor in Adiabatic Laminar Flow

TABLE

1. Wall Temperatures for a Turbulently Flowing Air Stream

TABLE I

TEMPERATURES FOR A TURBULENTLY FLOWING AIR STREAM[a]

Adiabatic Flow

Parallel Plates				Circular Conduit			
Reynolds Number	Wall Temperature	Bulk Temperature	Recovery Factor	Reynolds Number	Wall Temperature	Bulk Temperature	Recovery Factor
$\mathcal{R}_\ell$	$\frac{T_{wall} - T_a}{U^2/2gC_p}$	$\frac{T_{bulk} - T_a}{U^2/2gC_p}$	r'	$\mathcal{R}_\ell$	$\frac{T_{wall} - T_a}{U^2/2gC_p}$	$\frac{T_{bulk} - T_a}{U^2/2gC_p}$	r'
100,000	1.030	0.186	0.844	46,350	1.030	0.277	0.753
50,000	0.958	0.180	0.778	23,120	0.958	0.268	0.690
20,000	0.850	0.166	0.684	9,230	0.850	0.245	0.605
			Isothermal Flow				
100,000	-0.738	-0.013	-0.725	46,350	-0.806	-0.026	-0.780
50,000	-0.731	-0.015	-0.716	23,120	-0.792	-0.028	-0.764
20,000	-0.704	-0.017	-0.687	9,230	-0.754	-0.020	-0.734

a The following data were employed:
$\nu = 1.892 \times 10^{-4}$ sq. ft./sec.
$K = 2.70 \times 10^{-4}$ sq. ft./sec.
$\epsilon_m/\epsilon_c = 0.922$ at $\mathcal{R}_{\ell\,pp} = 100{,}000$ or $\mathcal{R}_{\ell\,cc} = 46{,}350$
$\epsilon_m/\epsilon_c = 0.851$ at $\mathcal{R}_{\ell\,pp} = 50{,}000$ or $\mathcal{R}_{\ell\,cc} = 23{,}120$
$\epsilon_m/\epsilon_c = 0.744$ at $\mathcal{R}_{\ell\,pp} = 20{,}000$ or $\mathcal{R}_{\ell\,cc} = 9{,}230$

PROPOSITIONS

Oral Ph.D. Examination -- Kazuhiko Sato
Thursday, May 26, 1955 -- 1:30 P.M., Crellin Conference Room
Committee: Professors Sage (Ch.), Corcoran, Lacey, Niemann and Wulf

PROPOSITIONS

1. The viscosity of suspensions of small glass spheres has been investigated in liquids having a viscosity of 1.5 to 2 poise. The high viscosity was necessary to prevent appreciable settling of the spheres during the experiment. The study of viscosity of suspensions may be extended to liquids with a lower viscosity by employing liquids having the same specific gravity as the spheres. This will allow the behavior of suspensions to be determined over a wider range of conditions. (Robinson, J. V., J. of P. Chem., 55, 455 (1951).)

2. The occurrence of destructive pressure oscillations in rocket combustion chambers may be due to transient heat transfer phenomena.

3. There may exist an optimum operating temperature for a specific eluent in achieving the best resolution of components in chromatographic separation.

4. The installation of thermocouples at critical points in machinery would allow detection of overheating at locations which are not being properly lubricated. The voltages

of the thermocouples can be used by appropriate circuits to reduce the power input to the machinery when the temperature exceeds the safe limit.

5. The overvoltage for a platinum-hydrogen electrode was found to be substantially decreased by the use of ultrasonic agitation. The application of ultrasonic agitation to electroplating processes may prove to be useful. (Yeager, E., Oey, T. S., and Hovorka, F., J. of P. Chem., 57, 268 (1953).)

6. Study of homogeneous reactions in fluid streams as a function of turbulence level would be a valuable addition to the available information on non-turbulent fluid streams.

7. The material balance of an elementary section per unit time in a homogeneous reactor is expressed as

$$rdV_r = FdX_A$$

where r = rate of reaction, moles of A converted per unit volume of reacting system

V_r = reactor volume occupied by reacting fluid system

F = reactor feed rate, mass per unit time

X_A = moles of A converted per unit mass of reactor feed

Integration of the equation for a constant feed rate yields

$$\frac{V_r}{F} = \int_0^{X_A} \frac{dX_A}{r}$$

This procedure assumes that the fluid in the reactor is nonviscous. A better value of the reactor volume required for a reaction may be obtained by taking into consideration that a velocity profile does exist in the reactor. (Hougen, O. A. and Watson, K. M., "Chemical Process Principles", Part III, p. 832, New York, John Wiley and Sons, Inc., 1949.)

8. The coefficient α in the equation

$$\alpha \, dH = T \, dS$$

where T = thermodynamic temperature, ^{o}R.
S = specific entropy, Btu./lb. ^{o}R.
α = dimensionless
H = specific enthalpy, Btu./lb.

is useful in computing performances of compressors. The addition of this coefficient to the conventional specifications of commercial compressors for fluids normally encountered in use would aid materially in the selection of the proper equipment.

9. The installation of alternating current generators on automobiles is proposed. Substantial savings may be realized when the number of electrically powered appliances are large.

10. Specifying the turbulence level of a flowing fluid stream by the conventional hot wire equation is not always sufficient to relate the change of the transfer coefficient due to turbulence level.

11. In order to obtain information on the mechanism of turbulence and its effect on heat transfer from wires, the study of heat transfer from vibrating wires as a function of frequency and amplitude in a flowing stream would be useful.